

AFFDL-TR-75-78

12

ADA U27422

**LANDING GEAR/SOIL INTERACTION
DEVELOPMENT OF CRITERIA FOR AIRCRAFT
OPERATION ON SOIL DURING TURNING
AND MULTIPASS OPERATIONS**

*UNIVERSITY OF DAYTON
SCHOOL OF ENGINEERING
DAYTON, OHIO*

OCTOBER 1975

TECHNICAL REPORT AFFDL-TR-75-78
FINAL REPORT FOR PERIOD JANUARY 1974 - MAY 1975

DDC
RECEIVED
26 1976
REGISTERED

Approved for public release; distribution unlimited

AIR FORCE FLIGHT DYNAMICS LABORATORY
AIR FORCE WRIGHT AERONAUTICAL LABORATORIES
Air Force Systems Command
Wright-Patterson Air Force Base, Ohio 45433


NOTICE

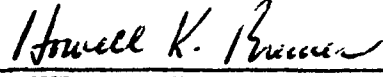
When Government drawings, specifications, or other data are used for any purpose other than in connection with a definitely related Government procurement operation, the United States Government thereby incurs no responsibility nor any obligation whatsoever; and the fact that the Government may have formulated, furnished or in any way supplied the said drawings, specifications, or other data, is not to be regarded by implication or otherwise as in any manner licensing the holder or any other person or corporation, or conveying any rights or permission to manufacture, use or sell any patented invention that may in any way be related thereto.

This report has been received by the Information Office (OI) and is releasable to the National Technical Information Service (NTIS). At NTIS, it will be available to the general public, including foreign nations.

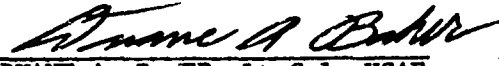
This final report was submitted by The University of Dayton, School of Engineering, 300 College Park Avenue, Dayton, Ohio 45469, under Contract F33615-73-C-3023, Work Unit Number 13690117, with the Air Force Flight Dynamics Laboratory, Vehicle Equipment Division, Mechanical Branch, Wright-Patterson Air Force Base, Ohio 45433. George J. Sperry, AFFDL/FEM, was the Project Engineer for this effort.

This report has been reviewed and is approved for publication.


GEORGE J. SPERRY,
Project Engineer
Mechanical Branch


HOWELL K. BREWER
Acting Chief, Mechanical Branch
Vehicle Equipment Division

FOR THE COMMANDER


DUANE A. BAKER, Lt Col, USAF
Acting Chief
Vehicle Equipment Division

APPROVED BY	White Section	<input type="checkbox"/>
NTIS	Ball Section	<input type="checkbox"/>
C.G.		<input type="checkbox"/>
UNCLASSIFIED		
DECLASSIFICATION		
BY	DISTRIBUTION/AVAILABILITY CODES	
	Dist. Avail. Div. #	
	SP-2141	
		A

Copies of this report should not be returned unless return is required by security considerations, contractual obligations, or notice on a specific document.

UNCLASSIFIED

SECURITY CLASSIFICATION OF THIS PAGE (When Data Entered)

REPORT DOCUMENTATION PAGE		READ INSTRUCTIONS BEFORE COMPLETING FORM	
1. REPORT NUMBER AFFDL TR-75-78	2. GOVT ACCESSION NO	3. RECIPIENT'S CATALOG NUMBER	
4. TITLE (and Subtitle) LANDING GEAR/SOIL INTERACTION DEVELOPMENT OF CRITERIA FOR AIRCRAFT OPERATION ON SOIL DURING TURNING AND MULTIPASS OPERATIONS.		5. TYPE OF REPORT & PERIOD COVERED Final Report 1 Jan 74-15 May 75	6. PERFORMING ORG. REPORT NUMBER
7. AUTHOR David C. Kraft Norman S. Phillips		8. CONTRACT OR GRANT NUMBER(s) F33615-73-C-3023	
9. PERFORMING ORGANIZATION NAME AND ADDRESS University of Dayton, School of Engineering 300 College Park Avenue Dayton, Ohio 45469		10. PROGRAM ELEMENT, PROJECT, TASK AREA & WORK UNIT NUMBERS Project No. 1369 Task No. 136901 Work Unit No. 13690117	
11. CONTROLLING OFFICE NAME AND ADDRESS United States Air Force, Air Force Systems Command, ASD/PPMNA Wright-Patterson Air Force Base, Ohio 45433		12. REPORT DATE October 1975	
14. MONITORING AGENCY NAME & ADDRESS (if different from Controlling Office) Air Force Flight Dynamics Laboratory (FY1456) Wright-Patterson AFB, Ohio 45433 Attn: Mr. George J. Sperry, AFFDL/FEM		13. NUMBER OF PAGES 157	
		15. SECURITY CLASS. of this report Unclassified	
		15a. DECLASSIFICATION/DOWNGRADING SCHEDULE	
16. DISTRIBUTION STATEMENT (of this Report) Approved for public release; distribution unlimited.			
17. DISTRIBUTION STATEMENT (of the abstract entered in Block 20, if different from Report)			
18. SUPPLEMENTARY NOTES			
19. KEY WORDS (Continue on reverse side if necessary and identify by block number) Aircraft flotation Aircraft tire drag Aircraft high speed ground surface drag Soil mechanics Aircraft turning operations Landing Gear Aircraft tire turning side loads Digital Computer Programs Aircraft tire sinkage			
20. ABSTRACT (Continue on reverse side if necessary and identify by block number) The continuing design and operational requirements for military aircraft to operate on unimproved runways has led to the need to investigate those landing gear/soil runway parameters which most significantly influence performance. This report summarized those activities accomplished during the second year of a two-year research effort concerned with the development of criteria for turning, operation at high speed, and multipass operation.			

DDC
 REPRODUCED
 JUL 26 1976
 REQUESTED

DD FORM 1 JAN 73 1473

EDITION OF 1 NOV 65 IS OBSOLETE

UNCLASSIFIED

SECURITY CLASSIFICATION OF THIS PAGE (When Data Entered)

407 377

next page mt

UNCLASSIFIED

SECURITY CLASSIFICATION OF THIS PAGE(When Data Entered)

The work reported was conducted in several areas. The turned tire test data was completely analyzed and predictive equations incorporated into the turning program. A limited parametric study was conducted for three classes of vehicles to calculate wheel force ratios as functions of runway width required. A multipass test program was conducted at the Army Engineers Waterways Experiment Station to measure the response of rolling and braked tires in alternating paths. The data was reduced and predictive equations evolved from rut depths as a function of first pass response and subsequent path and braking.

Limited start-up force data were examined to determine a preliminary estimate of start-up drag ratios. A soft tire/soil computer program was developed to study roughness effects. The program was compiled and run but not with coefficients obtained from test data. A training session was held at the University of Dayton, a Test Plan developed for full-scale test planning, and a "Master" program constructed which permits calculation of takeoff distance, landing rollout, turning performance, and number of allowable passes for a particular vehicle and selected soil.

UNCLASSIFIED

SECURITY CLASSIFICATION OF THIS PAGE(When Data Entered)

FOREWORD

This report was prepared by personnel of the School of Engineering of the University of Dayton, under USAF Contract F33615-73-C-3023, Project 1369, Task 01, Work Unit 17. This work was accomplished under the direction of the Vehicle Equipment Division, Air Force Flight Dynamics Laboratory, Air Force Wright Aeronautical Laboratories, Wright-Patterson Air Force Base, Ohio, Mr. George J. Sperry, AFFDL/FEM, Project Engineer. ASD/PPMNA was the controlling procurement office.

This report covers work conducted from 1 January 1974 to 15 May 1975. A prior report, AFFDL-TR-74-6, entitled "Landing Gear/Soil Interaction Development of Criteria for Aircraft Operation on Soil During Turning and High Speed Straight Roll," was also developed under this contract and released January 1974. The first report discusses a turned tire test program, initial work on a digital program for turning prediction, high speed drag prediction and a takeoff program development. The second year's effort, reported herein, discusses the use of the turned tire data, use of multipass data, roughness analysis through a digital program, and development of improved predictive digital programs for takeoff, landing, turning and taxi performance. The authors' submittal date was 1 October 1975.

The authors wish to thank Mr. Sperry for his support and assistance in the accomplishment of the research activities and in the successful conduction of these training sessions.

TABLE OF CONTENTS

Section		Page
I	INTRODUCTION AND SUMMARY	1
II	TURNTD TIRE/SOIL INTERACTION ANALYSIS AND APPLICATION	4
	A. INTRODUCTION	4
	B. TURNTD TIRE TEST PROGRAMS	6
	C. TEST RESULTS	11
	D. AN AIRCRAFT TURNING MANEUVER	17
	E. SAMPLE CALCULATIONS	33
	F. TURNING OPERATIONS PARAMETRIC STUDY	35
	G. AIRCRAFT TURNING SUMMARY	49
III	MULTIPASS TIRE/SOIL INTERACTION ANALYSIS	51
	A. GENERAL AND DEFINITIONS	51
	B. TEST PROGRAM AT AEWS	52
	C. SINGLE WHEEL FREE ROLLING TESTS	58
	D. SINGLE WHEEL, RANDOM BRAKING AND PATH	70
	E. MULTIPASS PREDICTIVE PROCEDURES	79
	F. DISCUSSION	82
IV	STATIC START-UP FORCE ANALYSIS	89
	A. INTRODUCTION	89
	B. DATA AVAILABLE	89
	C. DATA PRESENTATION	89
	D. SUMMARY	95
V	TIRE/SOIL ROUGHNESS INTERACTION STUDIES	96
	A. INTRODUCTION	96
	B. BACKGROUND	96
	C. ROLLING TIRE COMPUTER PROGRAM AND SAMPLE RESULTS	110
	D. ROUGHNESS INTERACTION STUDIES SUMMARY	111
VI	ADDITIONAL EFFORT IN TIRE/SOIL INTERACTION	114
	A. TRAINING SESSION - SHORT COURSE ON LANDING GEAR/SOIL INTERACTION AND FLOTATION SYSTEM DESIGN	114

TABLE OF CONTENTS (Continued)

Section		Page
VII	DEVELOPMENT OF A FULL SCALE TEST PROGRAM	115
	A. INTRODUCTION	115
	B. PURPOSE	115
	C. TEST PROGRAM	116
VIII	MASTER PREDICTIVE COMPUTER PROGRAM	131
IX	APPLICATION TO CURRENT SPECIFICATIONS	135
	A. TURNING	135
	B. MULTIPASS	138
	C. TAKEOFF AND LANDING	140
X	CONCLUSIONS AND RECOMMENDATIONS	141
	A. CONCLUSIONS	141
	B. RECOMMENDATIONS	142
APPENDICES		
A	CHARACTERISTICS OF AIRCRAFT USED FOR TURNING PARAMETRIC STUDY	144
B	PROGRAM LISTING FOR ROLLING TIRE ON TIRE ON SOFT SOIL	148
REFERENCES		156

LIST OF ILLUSTRATIONS

Figure		Page
1	Aircraft Turning Geometry	5
2	Test Program using University of Dayton Linear Tire Soil Test Track	7
3	Test Program Conducted at the Army Engineers Waterways Experiment Station	8
4	Turned Tire Geometry and Loads	9
5	UD Test Results for Sand	12
6	UD Test Results for Clay	12
7	AEWES Test Results for Sand	13
8	AEWES Test Results for Clay	13
9	Turned Tire Rut Profile, Clay, (AEWES)	15
10	Turned Tire Rut Profile, Sand, (AEWES)	15
11	Lateral Load versus Turn Angle for Two Sinkage Ratios	16
12	Aircraft Geometry During a Turn	18
13	Nose Wheel Steering at 60°	22
14	Nose Wheel Steering at 60° with Differential Braking	24
15	Pneumatic Trail Parameter Versus Turn Angle for Cohesive Soil	26
16	Pneumatic Trail Parameter Versus Turn Angle for Cohesionless Soil	26
17	Side Force Ratio versus Turn Angle in Cohesive Soil	28
18	Side Force Ratio versus Turn Angle in Cohesionless Soil	28

LIST OF ILLUSTRATIONS (Continued)

Figure		Page
19	Free Rolling Slip versus Turn Angle in Cohesive Soil	30
20	Free Rolling Slip versus Turn Angle in Cohesionless Soil	30
21	In-Line Drag Ratio versus Turn Angle in Cohesionless Soil	31
22	In-Line Drag Ratio versus Turn Angle in Cohesive Soil	31
23	Input Data for Sample Calculation	34
24	Output Data for Sample Calculations	36
25	C-130 Configuration Performance in Cohesive Soil of CBR 6 at 5 Knots and Gross Weight of 133,000 Pounds with Symmetrical Thrust	38
26	C-130 Configuration Performance in Cohesive Soil of CBR 6 at 5 Knots and Gross Weight of 133,000 Pounds with 50 Percent Thrust Differential	39
27	C-130 Configuration Performance Composite for Cohesive Soil of CBR 6 at 5 Knots and Gross Weight of 133,000 Pounds	40
28	Advanced Transport Configuration Performance in Cohesive Soil of CBR 6 at 5 Knots and Gross Weight of 216,000 Pounds with Symmetrical Thrust	41
29	Advanced Transport Configuration Performance in Cohesive Soil of CBR 6 at 5 Knots and Gross Weight of 216,000 Pounds with 50 Percent Thrust Differential	42
30	Advanced Transport Configuration Performance Composite for Cohesive Soil of CBR 6 at 5 Knots and Gross Weight of 216,000 Pounds	43
31	Attack Vehicle Performance in Cohesive Soil of CBR 6 at 5 Knots and Gross Weight of 31,000 Pounds with Symmetrical Thrust	44

LIST OF ILLUSTRATIONS (Continued)

Figure		Page
32	Attack Vehicle Performance in Cohesive Soil of CBR 6 at 5 Knots and Gross Weight of 31,000 Pounds with 50 Percent Thrust Differential	45
33	Attack Vehicle Performance Composite for Cohesive Soil of CBR 6 at 5 Knots and Gross Weight of 31,000 Pounds	46
34	Multipass Tire Test Outline	53
35	Passes Distribution for Test Part 2 and Test Part 3	54
36	Test Matrix Format	55
37	Drag Ratio-Sinkage Ratio, Single Wheels on Soil	57
38	Raw Data of Single Wheel Multipass Data	59
39	Nomograph for Calculation of Instantaneous Sinkage and Drag	61
40	AEWES Data Relating Sinkage to Axle Movement	62
41	Relation Between Instantaneous Sinkage, Z, and Rut Depth -UD Data	63
42	Variation of Cumulative Rut Depth, Z_R , Divided by First Pass Calculated Rut Depth $Z_{R_{CI}}$	67
43	Cumulative Rut Depth Calculated versus Measured for 7:00-6 and 8:50-10 Tires at 35% Deflection with CI Ranges of 37 to 55 in Clay	69
44	Deformation History of Center Lane (Path # 1) Tire Passed Over Path # 1 on Passes 1, 4, 5, 6, 9, 10, 15, 16; Hence Z_A are Available	75
45	Cumulative Rut Depth and Axle Motion versus Number of Passes for Center Lane	76
46	Cumulative Rut Depth and Axle Motion versus Number of Passes for Center Lane	77

LIST OF ILLUSTRATIONS (Concluded)

Figure		Page
47	Cumulative Rut Depth and Axle Motion versus Number of Passes for Center Lane	78
48	Deformation History of Center Lane (Path # 1). Tire Passed Over Path # 1 on Passes 1, 4, 5, 6, 9, 10, 15, 16; Hence, Z_A Available Rut Depth Versus Predicted Using Coefficients of Page 85.	80
49	Sample Cumulative Rut Calculations	88
50	Drag Ratio Comparisons versus Load Strength Ratio	91
51	"Peak" Rolling and Free Rolling Drag Ratio versus Load Strength Ratio	93
52	Start-Up Predicted Drag Ratio versus Comparable Measured Data	94
53	Tire/Soil/Roughness Model	98
54	Schematic of Eleven Elements Rotating at Angular Velocity $\dot{\theta}$.	99
55	Free Body Diagram of Complete Wheel	100
56	Transient Response of Theoretical Soft Tire in Soft Soil	112
57	Master Program Input Requirements	129
58	Master Program Input Printout	132
59	Input Data Cards for Master Program	134

LIST OF SYMBOLS

Symbol	Definition	Page Defined
A	Rigid surface contact area	11
A_B	Applied braked motion	72
A_R	Applied rolling motion	72
A_Z	Tread area	105
ACVS	Vehicle side acceleration	125
AL	Nose gear center of gravity to vehicle average center of gravity	19
AVM	Main gear center of gravity to vehicle average center of gravity	19
B, b	Tire section width	54
B_D	Direct braked pass effect	78
B_I	Indirect braked pass effect	78
B_T	Tire width	105
BETA	Nose wheel steering angle	124
BP	Nose wheel steering angle	124
C	Soil cohesion	105
C. G. (c. g.)	Center of gravity	5
C_S	Damping coefficient of soil surface	102
C_{SS}	Damping coefficient of soil subsurface	102

LIST OF SYMBOLS (Continued)

Symbol	Definition	Page Defined
C_T	Damping coefficient of tire element	107
CI	Cone index reading	124
CI_{avg}	Average cone index reading	11
D	Tire outside diameter	10
DE	Nose tire deflection in percent	123
DM	Main tire diameter	124
DN	Nose tire diameter	123
DEM	Main tire deflection	124
DFN	Nose tire flange diameter	123
d	Tire deflection in percent	11
E	Distance between main mounts	19
EE	Engine spacing	123
F	Applied force	102
F	Nose gear center of gravity to main gear center of gravity	123
F_B	Far field braked effect	72
F_S	Soil force	104
F_T	Tread force	107
g	Gravitational constant	19
I_{zz}	Yawing mass moment of inertia	123

LIST OF SYMBOLS (Continued)

Symbol	Definition	Page Defined
K	Constant in pneumatic trail equation	27
K_S	Soil stiffness	102
K_T	Tire stiffness	107
L	Lateral load	10
L	Nose gear center of gravity to vehicle forward center of gravity	123
LL	Nose gear center of gravity to vehicle aft center of gravity	123
L/P	Lateral load ratio	14
l	Tire footprint length	25
M_B	Applied torque	108
M_S	Soil mass	102
M_T	Tread mass	103
N	Normal force	104
NM	Total number of main tires	124
NN	Total number of nose tires	123
NTYP	Soil type	124
NM1	Number of tires in tandem	124
NNT	Number of tires in twin configuration	124
N1	Number of tires per side	124

LIST OF SYMBOLS (Continued)

Symbol	Definition	Page Defined
N_B	Near field braked effect	72
N_L	Longitudinal load factor	137
N_R	Near field rolling effect	72
N_S	Side load factor	137
O	Instantaneous center of rotation	5
P	Tire vertical load	10
PML	Left wheel vertical force	125
PMR	Right wheel vertical force	125
PN	Nose wheel vertical force	124
PR	Tire ply rating	53
R	Drag force (in-line)	10
RML	Left wheel drag force	124
PMR	Right wheel drag force	124
RN	Nose wheel drag force	124
RW	Tire radius	105
R/P	Rolling drag ratio	12
$(R/P)_t$	Rolling drag ratio -turned	32
R_B/P	Braked drag ratio	83
R_S/P	Static start-up drag ratio	89

LIST OF SYMBOLS (Continued)

Symbol	Definition	Page Defined
R_I	Indirect rolling effect	78
R_D	Direct rolling effect	78
r	Pneumatic trail	25
S	Side load for turned tire	10
SFML	Side force left main gear	124
SFMR	Side force right main gear	124
SFN	Side force nose gear	124
SL	Slip in percent	29
SM	Twin spacing of main gear	123
SN	Twin spacing of nose gear	123
S/P	Side force ratio for turned tire	28
T	Traction	104
THRT	Thrust	125
TMML	Left wheel torque	124
TMMR	Right wheel torque	124
TMN	Nose wheel torque	124
UE	Ground label to thrust line	123
V	Aircraft velocity	17
V_a	Wheel horizontal speed	105

LIST OF SYMBOLS (Continued)

Symbol	Definition	Page Defined
V_w	Wheel peripheral speed	105
W	Gross weight	123
W_P	Payload weight	108
W_T	Tread weight	103
W_W	Wheel segment weight	108
x_c	Distance for main gear y-axis to the instantaneous center of rotation	5
X_T	Horizontal displacement of the tread element	103
y_c	Distance from aircraft (x-axis) to the	5
Z	Instantaneous soil sinkage	25
Z_A	Axle vertical movement	59
Z_R	Rut depth	59
Z_S	Vertical movement of soil element	102
Z_T	Vertical movement of tread element	103
Z_{max}	Maximum fully braked instantaneous sinkage	82
Z/D	Sinkage ratio	14
Z/l	Sinkage characteristic	82
Z_{10}	Tenth pass rut depth	66

LIST OF SYMBOLS (Concluded)

Symbol	Definition	Page Defined
α / CI	Load strength ratio	82
β	Nose wheel steering angle	19
θ	Wheel rotational displacement	103
$\mu(s)$	Coefficient of surface friction	105
ζ	Instantaneous radius of turn	9
ϕ	Tire turn angle - the angle between the direction of motion and tire longitudinal axis	10
ϕ	Internal friction angle	105
ϕ_n	Nose wheel turn angle	17
ϕ_{ml}	Left main gear wheel turn angle	17
ϕ_{mr}	Right main gear wheel turn angle	17
σ	Normal stress	105

SECTION 1

INTRODUCTION AND SUMMARY

The continuing design and operational requirement for aircraft to operate on unimproved runways, as evidenced by the current design requirements on the MSTOL aircraft currently under development, has resulted in continuing efforts to identify and analyze the primary and secondary variables which influence aircraft flotation/operation performance on soil runways. These flotation/operation variables have been defined previously ⁽¹⁻⁵⁾. These variables include drag, sinkage, braking, turning, multipass, high speed, soil strength, etc.

The current research effort is a part of a long range research program sponsored by the United States Air Force Flight Dynamics Laboratory. The objective of this continuing research program is: (1) to identify and analytically define landing gear/soil interaction; (2) to develop criteria for establishing working range conditions for aircraft in their landing, takeoff, braking, and turning modes of operation; (3) to develop systematic design procedures for optimizing the flotation and surface operations capability of existing and future aircraft. Phase I ⁽⁵⁾ of this program included a survey of the flotation problem, establishment of the critical parameters, and an investigation of available flotation data leading to the development of a flotation analysis equation. Phase II ⁽⁴⁾ included the development of an empirical sinkage prediction equation, development of a lumped parameter simulation prediction technique, conducting the Rolling Single Wheel Verification Tests, and the development of the Single Wheel Relative Merit Index (RMI) system for defining comparative flotation capacity. Phase III - Part I ⁽³⁾ consisted of the development of the multiwheel sinkage-drag analysis equations, conducting the Multiwheel Verification Tests, and the development of a lumped parameter iteration technique for simulating the interaction of dual tires on soil.

Phase III - Part II ⁽¹⁾ included the Braked Wheel Verification Tests, the development of a lumped parameter braking simulation technique computer program, the development of the braking analysis equations for defining braking drag ratios, and preliminary studies of multipass and high speed effects of aircraft tire operation on soil.

The current two-year effort was aimed at developing analysis techniques, conducting verification tests, and developing predictive equations for landing gear/soil interaction as necessary to estimate vehicle performance during turning, high speed and multipass operations. During the first year the following tasks were completed.

- 1) A turned tire test program was conducted at UD and AEWES to provide measured data.
- 2) An Aircraft Turning Operation Predictive Computer Program was evolved.
- 3) High speed drag ratio analysis and predictive techniques were generated.
- 4) An existing takeoff length program was modified.
- 5) A Landing Gear/Soil Interaction Training Session was conducted.

During the second year the following have been accomplished.

- 1) The Aircraft Turning Program was completed and had incorporated into it the complete results of the turned tire test data. Additionally, the routine now has the capability to accept thrust differential as well as differential braking and nose wheel steering. Examples of the response of three vehicles are presented.
- 2) Multipass data were collected at UD and AEWES to provide measured data for single wheels, rolling and braked, over alternating paths.

- 3) Predictive equations were evolved for single wheel multipass operations.
- 4) A landing length program was developed by modifying an existing routine.
- 5) Existing tire/soil/roughness data were reviewed and an analytical model developed to predict soft tire/soft soil response. The digital program was completed but not verified using test data.
- 6) Existing start-up force data were examined to establish preliminary criteria for estimating start-up forces in relation to free rolling drag.
- 7) A master program was developed to permit a user to calculate takeoff distance, landing distance, turning response, and multipass performance for one set of data.
- 8) A test plan was developed to indicate how testing could be conducted to verify the computer generated data of the developed digital programs.
- 9) A second Landing Gear/Soil Interaction Training Session was conducted.

The research conducted has provided additional capability in determining tire/soil performance for all aspects of unprepared runway operations. For a particular mission, the vehicle lands, rolls out, turns, taxiis, on-loads or off-loads, taxiis back out, turns, and then takes off perhaps to repeat the cycle. The results of this program and others ⁽¹⁻¹⁰⁾, provide data to estimate the landing gear performance for these mission segments in terms of drag, sinkage and rut depth.

SECTION II

TURNED TIRE/SOIL INTERACTION ANALYSIS AND APPLICATION

A. INTRODUCTION

Aircraft turning operation is an important consideration in the flotation analysis of aircraft operating on unprepared runways. Landing gear failures due to high side loads brought about by turning either in a high sinkage condition or out of accumulated ruts are possible. The forces developed can create large steering torque requirements. Additionally, the turning process, whether by steering or braking, contributes to the increased deterioration of the runway surface making further operations questionable.

The uncertainty associated with a turning operation is reflected in current design and analysis criteria. The C-130 operations manual indicates that there are restrictions on the steering angle as a function of taxi speed, but not soil type, or steering rate. Military Specification MIL-A-008862A, Airplane Strength and Rigidity, indicates that there are side force, drag force and lateral force ratios applicable to operations in soils, but does not mention the effects of steering angle, steering rate, velocity, soil type or braking upon turning.

There are several means available to turn an aircraft. The nose wheel can be turned at an angle relative to the aircraft plane of symmetry and the side forces developed at the nose tire will turn the aircraft. The engines can be used to turn the vehicle by using differential thrust. Asymmetrical braking creates a moment that turns the vehicle. Any combination of the nose wheel steering, braking and thrust differential can also be used. Regardless of the means used, all tires will have some turn angle which generates a side force. This is shown in Figure 1 which represents the geometry of a vehicle turning due to some applied moment. Notice that all wheels have some turn angle. Frequently in calculations of turn radii figures will be drawn showing the turning axis as the intercept of a line through the main gear and one perpendicular to the plane of the nose wheel. This is obviously erroneous

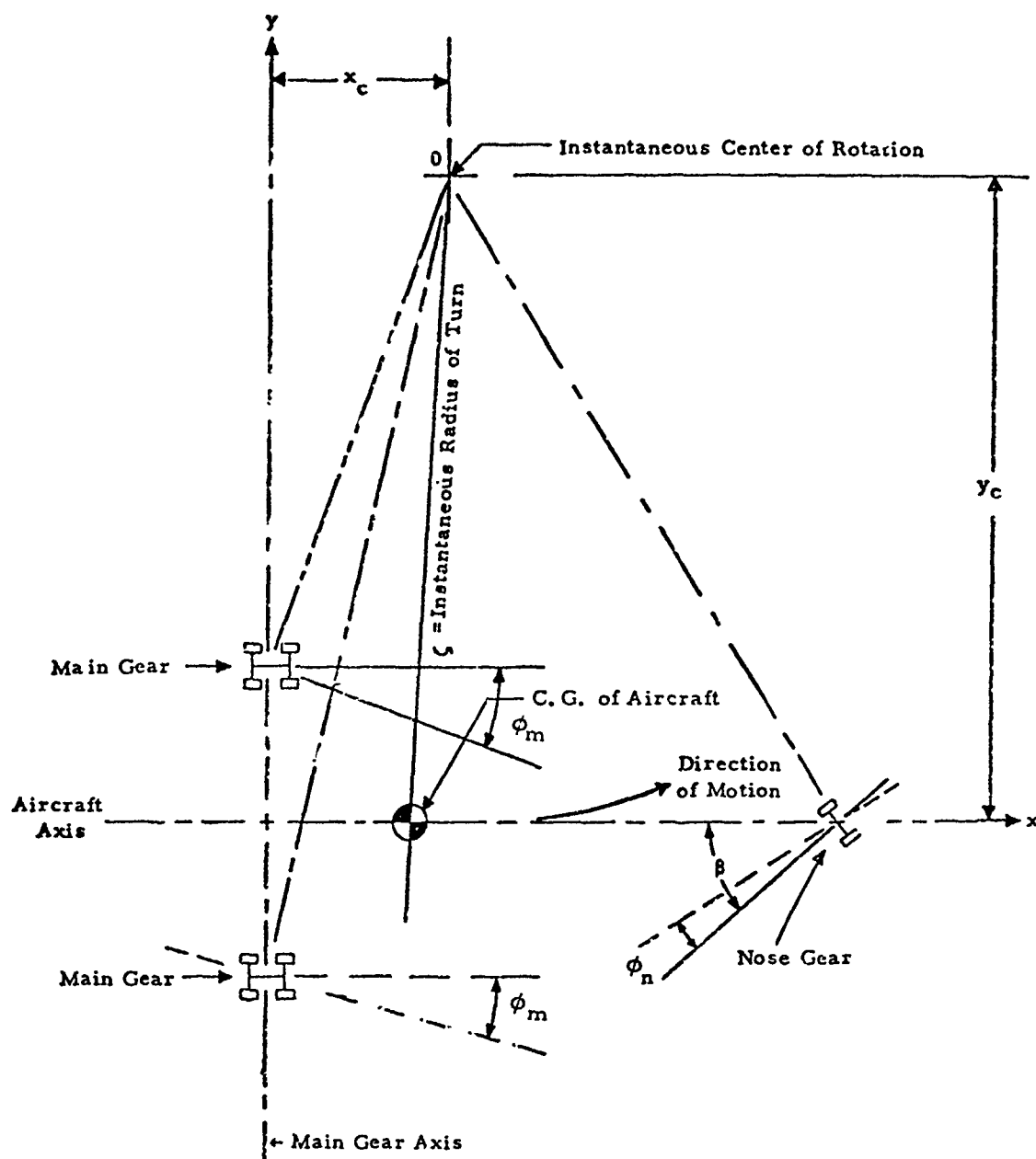


Figure 1. Aircraft Turning Geometry.

for nose wheel steering only turns, since if all three wheels have zero turn angle, there is no applied moment to turn the vehicle. As will be discussed later, the true turning of the vehicle requires an equilibrium condition of side and drag forces at the wheels, all at different turn angles, with the centrifugal forces in the turn. Simultaneously the moments generated by these factors, brakes and engines must be properly accounted for.

For computation of the turning response it is necessary to know how the side and drag forces of the tire are influenced by the turn angle. A review of the existing literature indicated very little was known analytically or experimentally about side loads on aircraft tires turning on pavement, with less known about turning in soils. And yet, Figure 1 indicates that each wheel will have a turn angle whether dictated by the turning radius, as for the main gear, or as by the difference between steering angle and turning angle at the nose. The information required was found by conducting turned tire tests with aircraft tires towed at a constant turn angle, ϕ , down a test track.

B. TURNED TIRE TEST PROGRAMS

Two series of turned tire/soil interaction tests were conducted. The purpose of both test programs was to obtain experimental data to permit further studies of the variables that influence the performance of aircraft tires while operating in a turned (yawed) mode. The test program using the University of Dayton Linear Tire/Soil Test Track (see Figure 2) was conducted first (March 1973) and the results were used primarily to design the test program conducted at the Army Engineers Waterways Experiment Station (AEWES) (see Figure 3) small scale facility during June and July 1973. The specific objectives of the turned tire tests included:

1. Establishment of relationships between in-line drag (see Figure 4) side load, and lateral load as a function of turn angle.



Figure 2. Test Program using University of Dayton Linear Tire/Soil Test Track.

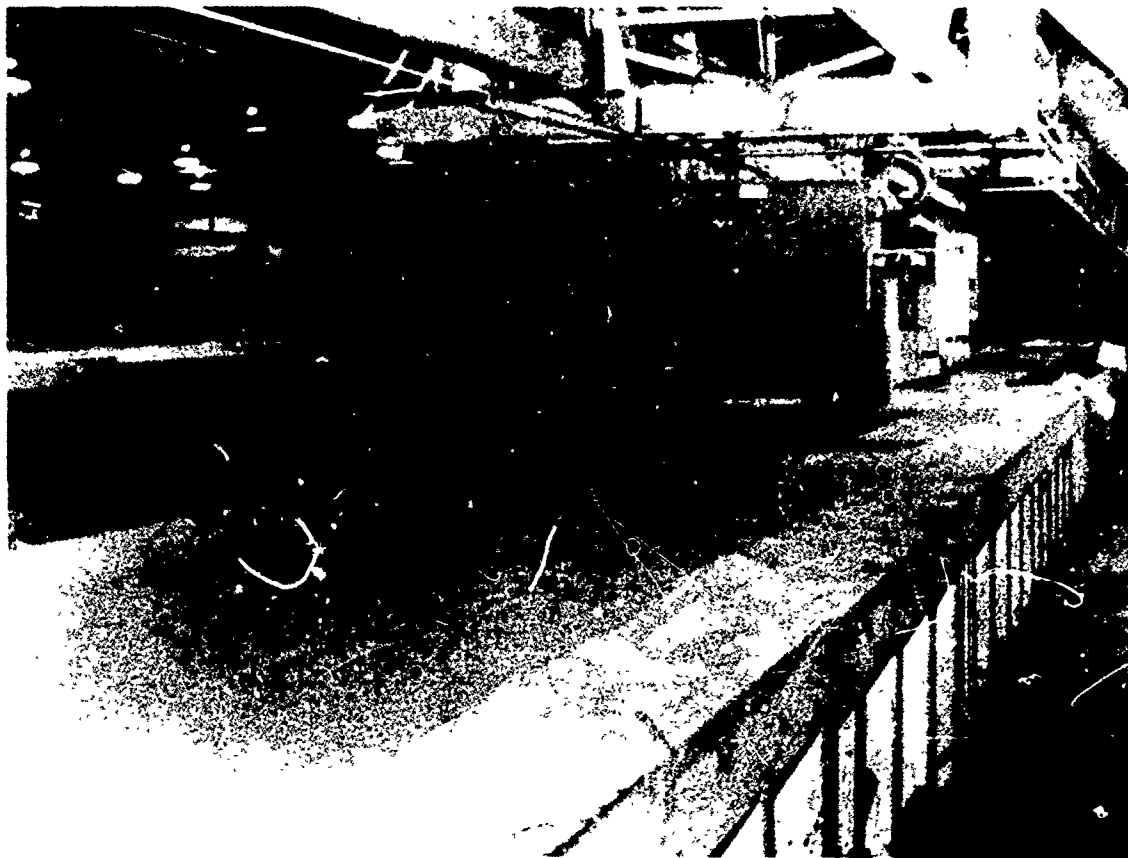


Figure 3. Test Program Conducted at the Army Engineers Waterways Experiment Station.

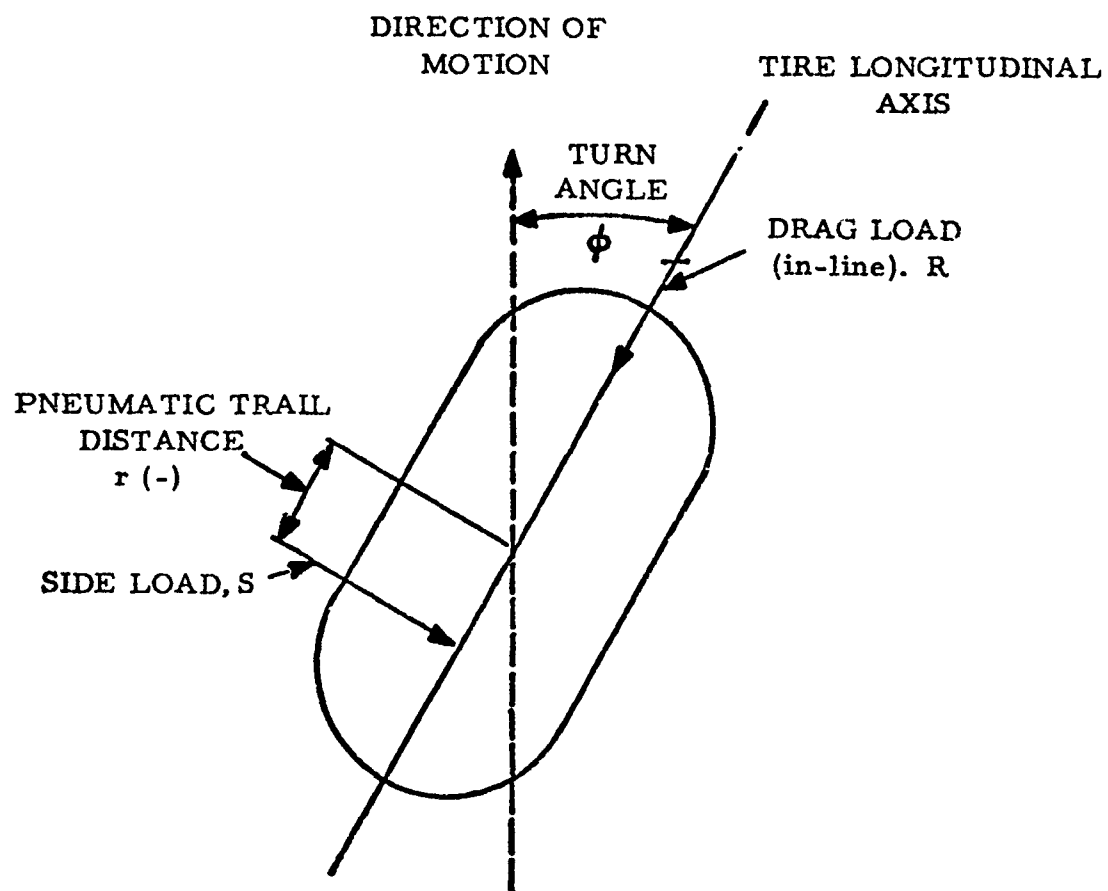


Figure 4. Turned Tire Geometry and Loads.

2. Determination of the variations in percent slip (negative) with increasing turn angle.
3. Establishment of the influence of increasing turn angle on the resultant sinkage and rut depth.

The specific test results discussed below are contained in detail in References 13 and 14.

Soil Type, Test Equipment and Sinkage Ranges

The AEWES tests were conducted in mortar sand and buckshot clay. The soil strength varied from cone index readings of approximately 35 to nearly 45 in sand, and 37 to 74 in clay. Applied vertical loads varied from 550 to 1,030 pounds for the sand, and 1,310 to 1,580 pounds for the clay. These values, along with 35 to 40 percent deflections on 8:50-10 tires and 7:00-6 tires; provide a 0° turn sinkage ratio of 0.03 to 0.04. The sinkage ratio is defined as the ratio of sinkage Z , to tire diameter D , and the values selected are indicative of operational conditions on soil runways.

The University of Dayton tests were conducted on riverwash sand and clayey silt. Soil strengths of 30 to 46 cone index values for clayey silt and 70 to 80 for riverwash sand were selected. These, with applied loads of 115 to 145 pounds on a 5:00-5 Type III tire at 17 percent deflection, generate the desired sinkage ratio.

Test Parameters Measured

For both series the following were measured.

vertical load, P

drag load (in-line drag), R

side load (perpendicular to plane of wheel), S

resultant lateral force (determined from R and S above), L

horizontal carriage velocity

turn angle, ϕ

tire deflection, d

tire contact geometry (rigid surface contact area), A

soil properties (moisture, density, classification properties,

Cone index, CI_{avg})

permanent rut depth (instantaneous sinkages were determined from
rut depth and rebound measurements)

All University of Dayton tests were conducted at six feet per second.
All AEWES data were collected at ten feet per second.

C. TEST RESULTS

Riverwash Sand

The curves shown in Figure 5 summarize a total of 22 tests conducted on riverwash sand. The buildup of side load and resultant lateral load with increased turn angle is evident.

Clayey Silt

The results of 23 tests in clayey silt are shown in Figure 6 and indicate the significant increase in side force with increasing turn angle. The in-line drag is relatively constant over the turn angles measured.

Mortar Sand

Twenty-one tests in mortar sand generated curves very similar to those of riverwash sand as shown in Figure 7 . Very little difference exists between the two sand test series although two different size tires were used.

Buckshot Clay

The results of 23 tests in buckshot clay are shown in Figure 8 . The tests conducted with larger tires in buckshot clay indicate less side force for a given turn angle than that measured in riverwash sand using a smaller tire.

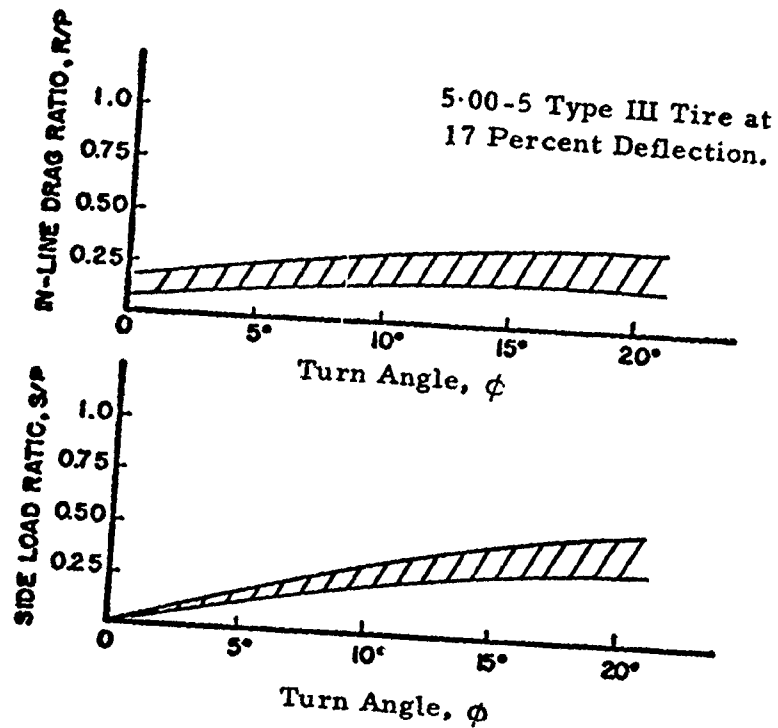


Figure 5. UD Test Results for Sand.

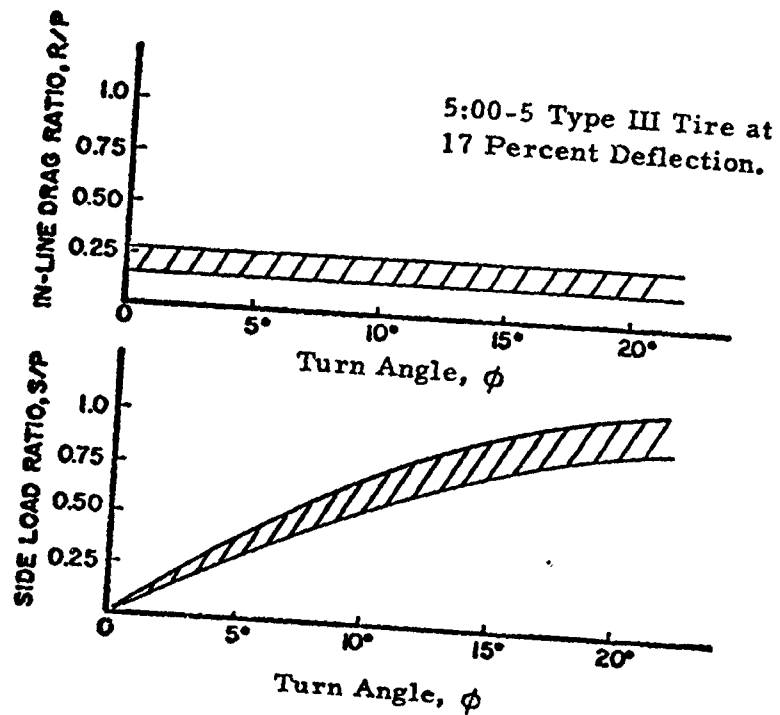


Figure 6. UD Test Results for Clay.

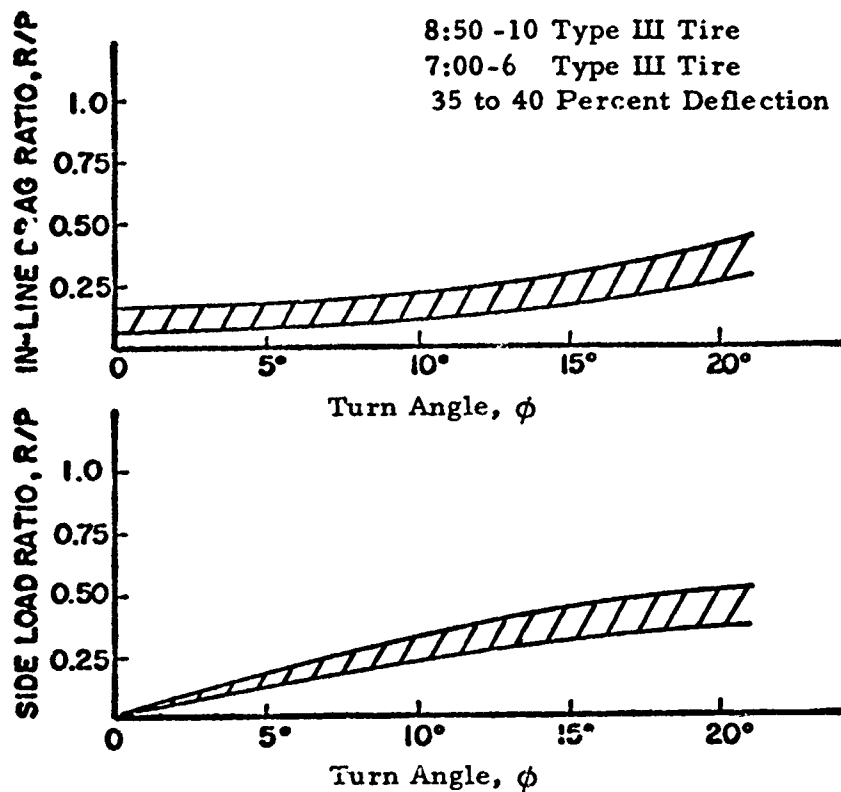


Figure 7. AEWES Test Results for Sand.

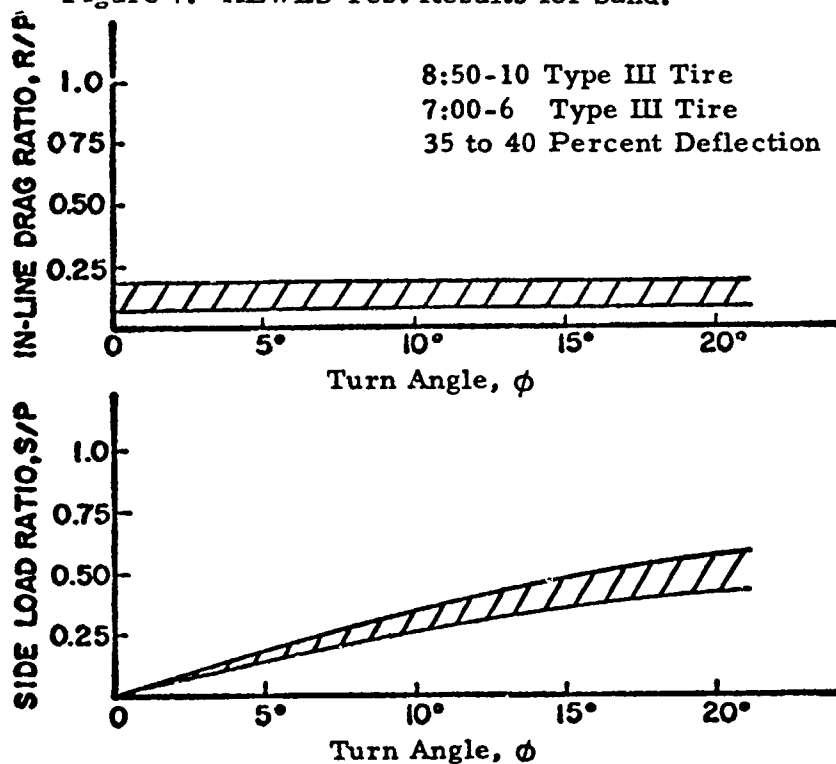


Figure 8. AEWES Test Results for Clay.

Comparative Summary Analysis of Turned Tire Tests

The results of both turned tire test programs were analyzed and compared. The results of this comparison indicated the following points of similarity.

1. Sinkage and rut depth increase markedly with increasing turn angle for aircraft tires operating on sand (frictional) type soils, but only moderate increases in sinkage occur on clay type soils. See Figures 9 and 10.
2. The in-line drag ratio remains relatively constant over the 0° to 20° turn angle range for aircraft tires on clay type soils.
3. Significant amounts of soil buildup, opposite to the direction of turn, occur for turning tires in both sand and clay types of soil.

Perhaps the most significant result of the turned tire tests is some preliminary indication of the magnitudes of side load buildup on a turned tire operating on a soil runway. Figure 11 presents this type of result as related to the nonturned tire sinkage ratio (Z, D). Reference to Figure 11 shows that the magnitude of this sinkage has a considerable influence on the resulting lateral loads. Lateral load ratios may very well exceed one-half in situations of tight turn angles and high sinkage conditions. Some of the general conclusions as to turned tire performance on soil runways would include:

1. The lateral load ratio (L/P) very likely will approach and in some cases exceed one-half for aircraft operating on moderate strength soil runways (rolling drag ratios greater than 0.10) where tight turning situations are encountered.
2. The tire negative slip will increase throughout the entire turn angle range of 0° to 20° . Negative slips approached 25% in sand and 15% for clay in the 20° turn situation.

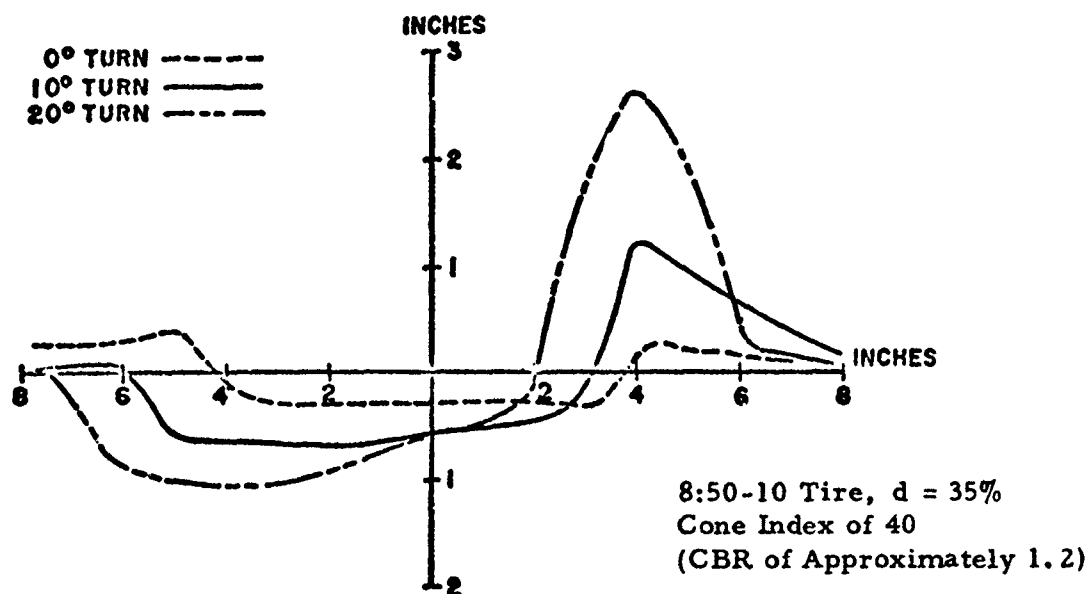


Figure 9. Turned Tire Rut Profile, Clay, (AEWES).

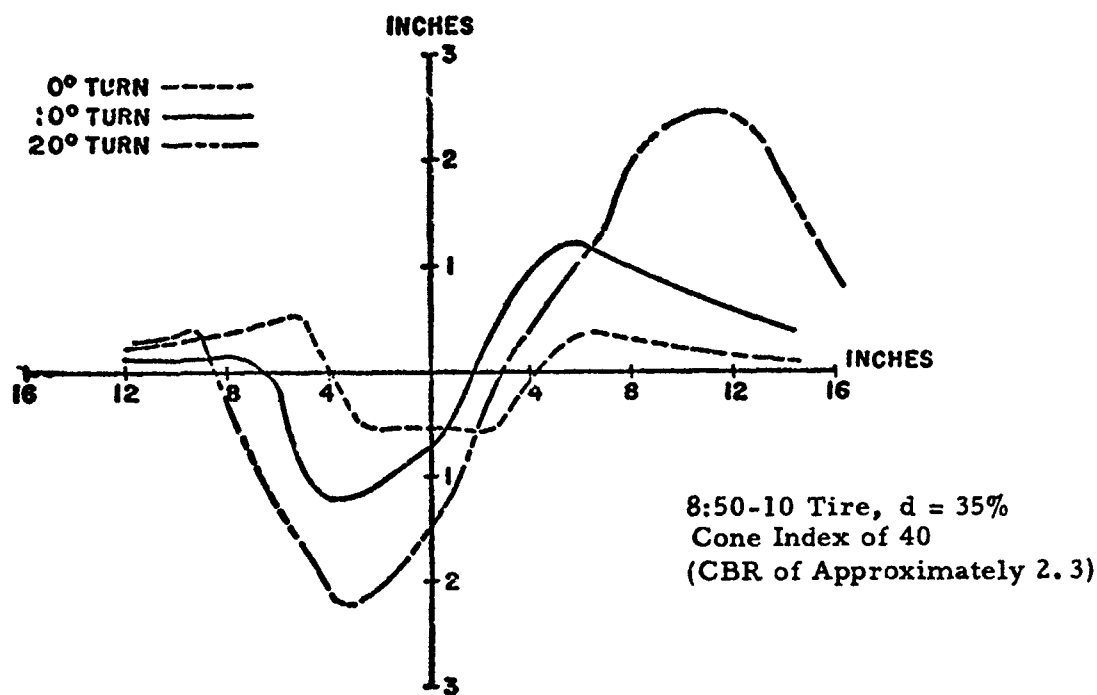


Figure 10. Turned Tire Rut Profile, Sand, (AEWES).

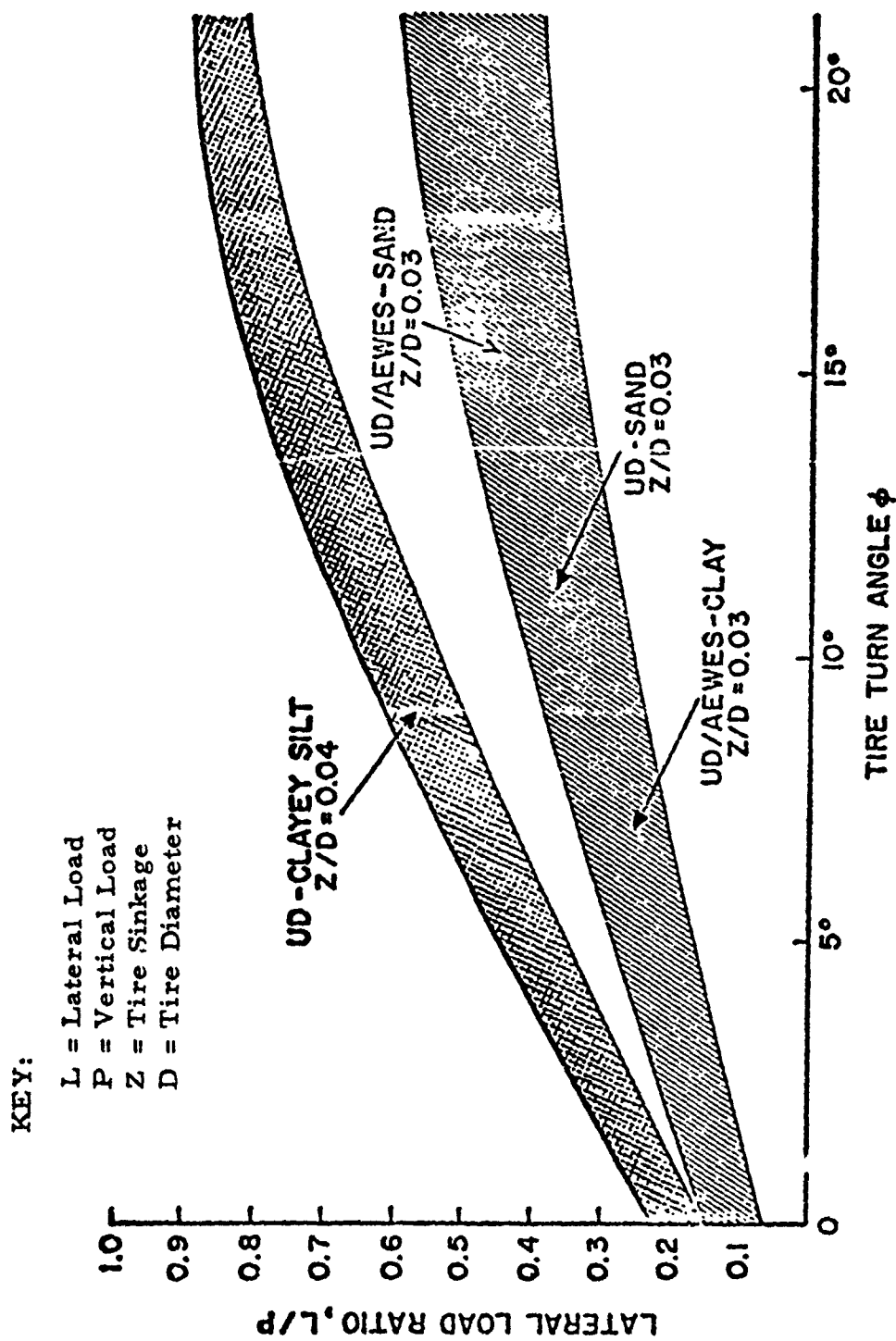


Figure 11. Lateral Load versus Turn Angle for Two Sinkage Ratios.

3. Unlike the behavior of turned tires on rigid pavement, the percent tire deflection had little influence on the lateral load ratio for either sand or clay operation.
4. More severe rutting will occur for aircraft turning operations on frictional type soils (sand) than on cohesive (clay) type soils.
5. No clear trend existed in the variation of pneumatic trail (r) with turn angle. The pneumatic trail increased with increasing turn angle in sand but decreased with increasing turn angle in clay.

Although sufficient turned tire tests were not conducted to encompass a broad range of sinkage ratios (Z/D), the results do indicate that an increase in the sinkage ratio will result in an increased lateral load ratio for a turned tire for all other conditions being constant.

D. AN AIRCRAFT TURNING MANEUVER

The side force data collected were incorporated within a digital program to compute the turning performance of a tricycle landing gear aircraft. The physical description of the vehicle in a turn is shown in Figure 12. The symbols are defined as:

- ϕ_n = nose wheel turning angle
- ϕ_{ml} = left main gear wheel turning angle
- ϕ_{mr} = right main gear wheel turning angle
- W = weight of aircraft
- R = drag loads (braking or driving) in longitudinal wheel direction ($R_{n1}, R_{n2}, R_{m1}, R_{m2}, R_{m3}, R_{m4}$)
- S = side load perpendicular to wheel longitudinal direction ($S_{n1}, S_{m1}, S_{m2}, S_{m3},$ and S_{m4})
- V = aircraft forward velocity

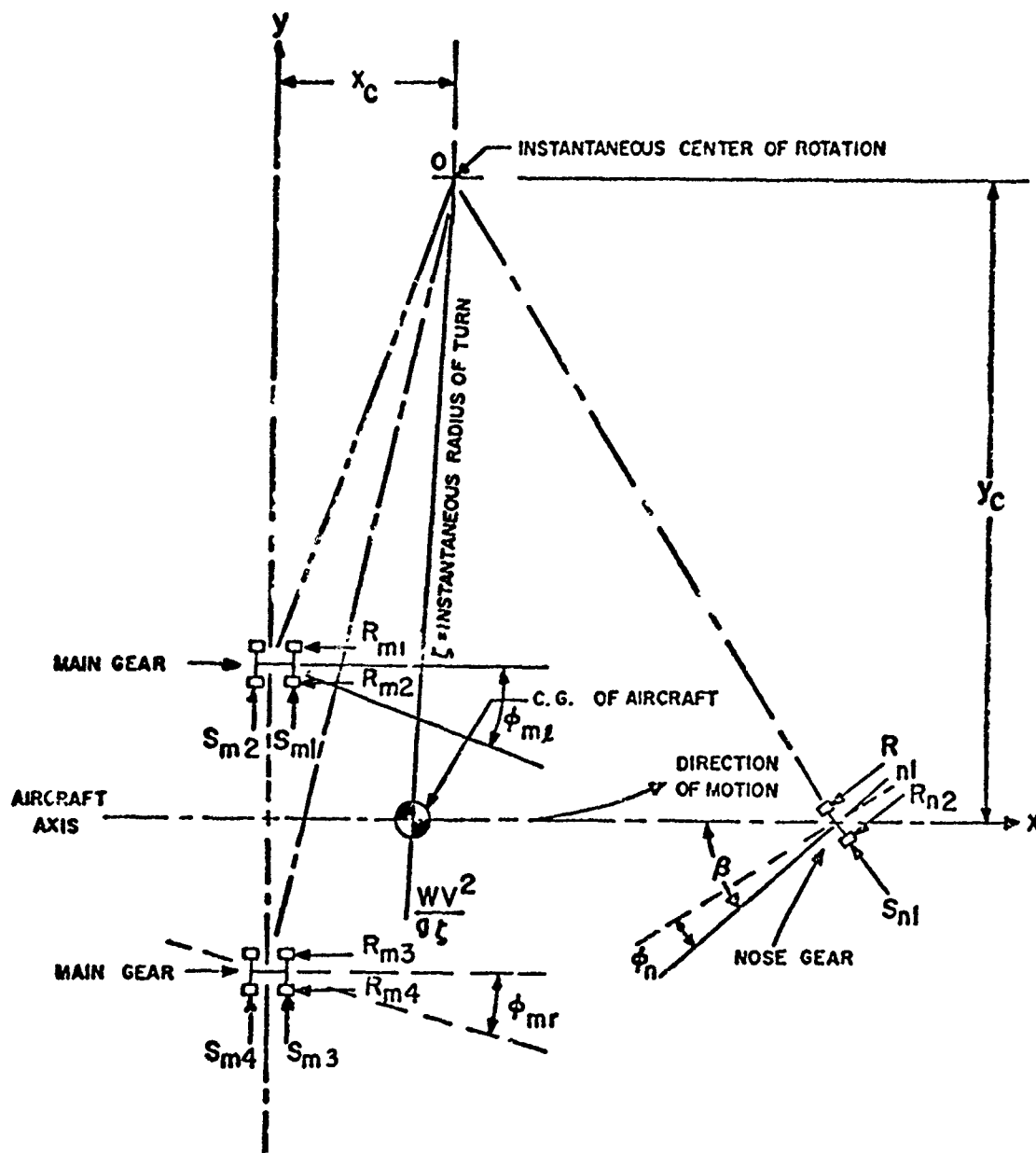


Figure 12. Aircraft Geometry During A Turn.

- ζ = instantaneous radius of turn
 β = caster angle of nose wheel
 E = distance between main mounts
 AVM = main gear center of gravity to average vehicle center of gravity
 AL = nose gear center of gravity to average vehicle center of gravity
 g = gravitational constant

The aircraft at any instant is turning about some instantaneous center of rotation. The side forces are generated by wheels being forced to follow a circular arc not in line with the plane of the tire. The main wheels do so because of the radius of curvature generated by all forces, whereas the nose wheel side force is generated by both the radius of turn and the steering angle. As the vehicle travels about the turn at a given velocity, the summation of side and drag forces create the net force which generates a centripetal acceleration. The forces generate moments about the center of gravity of the vehicle which must be proportional to the angular acceleration.

A summation of forces and moment about the center of gravity yields:

$$\sum F_y = M\ddot{y} = \sum S_m + S_n \cos\beta + R_n \sin\beta$$

$$\sum M_{CG} = I_{\theta} \ddot{\theta} = ((R_{m1} + R_{m2}) (R_{m3} + R_{m4})) \frac{E}{2} - ((S_{m1} + S_{m2}) - (S_{m3} + S_{m4})) \times AVM + S_n (\cos\beta) AL - R_n (\sin\beta) AL.$$

Over a small increment of time if constant velocity motion is about a fixed radius, the radial acceleration of the body is that of centripetal acceleration, and the angular acceleration is dictated by the change in angular velocity from one radius to the next.

Since the centrifugal force is known for any assumed radius,

centrifugal force = $\frac{mV^2}{R}$. The inertial force and moments can be placed on the right side of the equation and then both the equations are of the form,

$$\Sigma F = 0$$

$$\Sigma M = 0 .$$

The problem is to find forces which will simultaneously satisfy both equations.

A Newton-Raphson technique is used to iterate from an assumed radius of curvature to one that provides equilibrium of applied and inertial forces and moments. Other subroutines calculate the weight distribution, sinkage, drag, turn angles, multiwheel effects, and thrust required.

The program accepts nose wheel steering angle as a function of time along with wheel slip as a function of time. These, along with a complete description of the vehicle, landing gear and tire configurations, are required as input. The program then calculates the path over the ground, the tire/soil interaction forces, and the vehicle acceleration.

A complete description of the routine developed during the first year of the research program is available in Reference 15. All subroutines were fully discussed and sample results presented. At the time the digital program had several short-comings and these were mentioned in the conclusions of the referenced report. Specifically,

1. The braked drag equation was an approximation to other equations that were available.
2. Pneumatic trail data were not included.
3. Throttle controls were not possible.
4. Corrections were not included for "driven" and "pulled" wheel.
5. Direction reversals were not possible.

Additionally, the program was restricted to CBR 6 clay soil. Sample computations were made using the initial turning program. The C-130E was chosen as a vehicle that could be analyzed by the developed program. Most of the aircraft input data required were available and some information from the pilots handbook provided an insight into how the aircraft is turned. Specifically, the pilots handbook states that 60° nose wheel steering is permitted up to 5 knots. Nose wheel steering of 20° is permitted at taxi speeds of up to 20 knots. For these conditions, what are the turn radii, side forces and drag forces, and how do they compare with the criteria of existing military standards?

The first case, 60° nose wheel steering at 5 knots, was examined by assuming a time-steering angle relation. It was assumed that it would take 10 seconds to reach a 60° steering angle. The vehicle will turn at an equilibrium radius of 51 feet and require a minimum runway width of 106 feet. The width includes the entry transient as well as the landing gear width. The centrifugal force generates an aircraft side load factor of 0.054, and thrust required reaches a maximum of 23,000 pounds, which is a significant portion of the 40,000 pounds available. The response is shown in Figure 13.

The force ratios developed during the turn indicate that while the main gear develops very little side force, the nose wheel reaches the maximum permissible. Therefore, the 60° nose wheel steering maneuver would appear to be that which is limited by the side force capability of the nose gear.

The second case, that of 20° nose wheel steering is examined by beginning with a 5 knot taxi speed and then increasing it to 10 and 20 knots. For these turns it was assumed that 3-1/2 seconds were required to turn the nose wheel to 20° . The computed results indicate that in going from 5 knots to 20 knots, the minimum runway width goes from 214 to 394 feet, and the aircraft side load factor from 0.22 to 0.40. The force ratios indicate that again the main gear does not develop the allowable levels but that the nose wheel does.

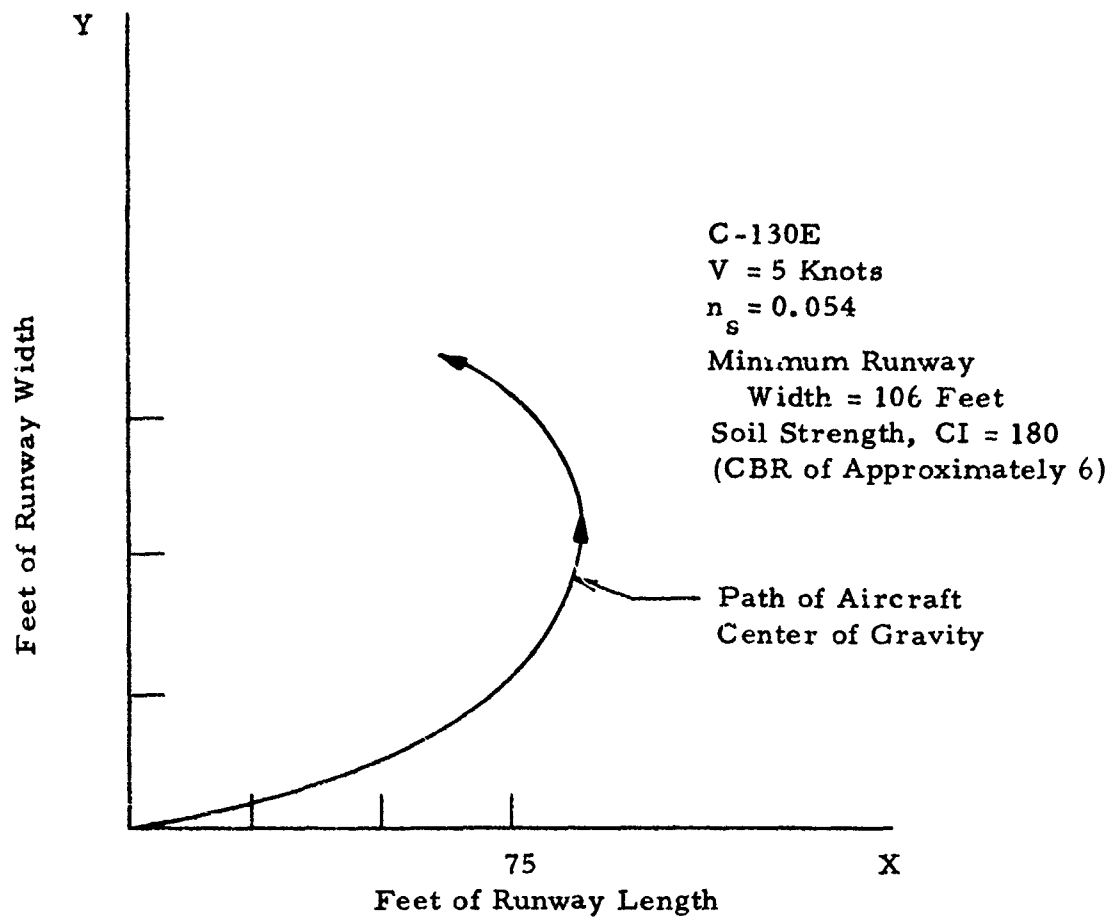


Figure 13. Nose Wheel Steering at 60° .

As another case to be examined, it was assumed that both braking and nose wheel steering would be used. Braking at 32 percent slip on the inboard gear and sufficient nose wheel steering to "trail" the turn were used. The braked turn at 5 knots generates an 85 foot minimum runway width with a vehicle side force ratio of 0.062. The landing gear side force ratios are again quite small although the drag forces developed were limiting. It is interesting to note that the turn computed is barely possible, since the thrust required, 37,700 pounds, approaches that available for the C-130E aircraft. See Figure 14 .

Improved Turning Program

During the second year several goals were established to improve the existing routine. These were:

- 1) Incorporate sinkage and drag relations from sand and clay soil,
- 2) Incorporate new braked drag relations,
- 3) Utilize turned tire test results to incorporate
 - a) pneumatic trail for sand and clay
 - b) side force ratios for sand and clay
 - c) slip for sand and clay as a function of turn angle
 - d) in-line drag modifications for sand and clay
- 4) Add thrust variations with time,
- 5) Add the longitudinal degree of freedom.

All of these were not achieved, but significant advancements were made. In the following paragraphs the raw data from which the equations were evolved may not be presented. The complete information if required is contained in Reference 13.

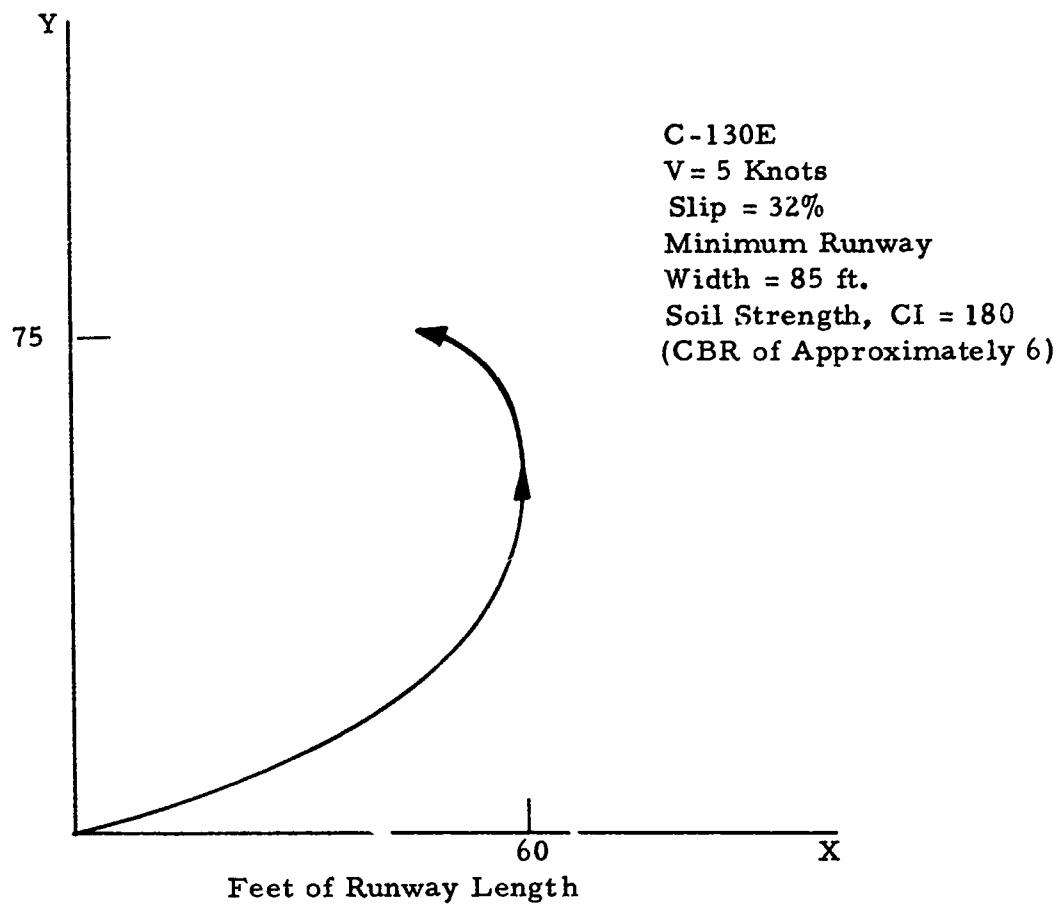


Figure 14. Nose Wheel Steering at 60° with Differential Braking.

Pneumatic Trail

Pneumatic trail (r) data were plotted for the 8:50 and 7:00 tire for both clay and sand. For clay the trail versus turn angle was plotted, then trail over footprint length (l) versus turn angle to be consistent with published literature (16). The wide scatter in the data indicated that some other term would be necessary to combine the data into some easily usable form. Not surprisingly, instantaneous sinkage (Z) was found to pull the data together in terms of tire deflections as shown in Figure 15 for clay soil.

From the figure it is seen that pneumatic trail is behind the axis of the tire by the negative of $\frac{r}{l} \cdot Z$, and that the trail decreases with increased turn angle. Secondly, the curves are grouped according to tire deflection with the 40 percent deflection tires having greater trail values for a given turn angle.

Several approximate expressions for the trail were attempted. Finally, the simplest expression evolved was

$$r \times \frac{Z}{l} = \frac{0.00675}{\sin \beta} (2.0) \left(\frac{DE - 30}{5} \right)$$

where r is the trail (inches)
 Z is the instantaneous sinkage (inches)
 l is the footprint length (inches)
 β is the turn angle
 DE is the deflection in percent.

The equation provides a smooth transition from 30 to 40 percent deflection which was assumed to be sufficient for most tires of interest. The equations specifically "fits" the 35 percent and 40 percent deflection data measured.

Similar procedures were followed for sand. The data are shown in Figure 16. The curves are entirely different in that the trail is positive, ahead of the tire axis, and increases with turn angle. The curves are

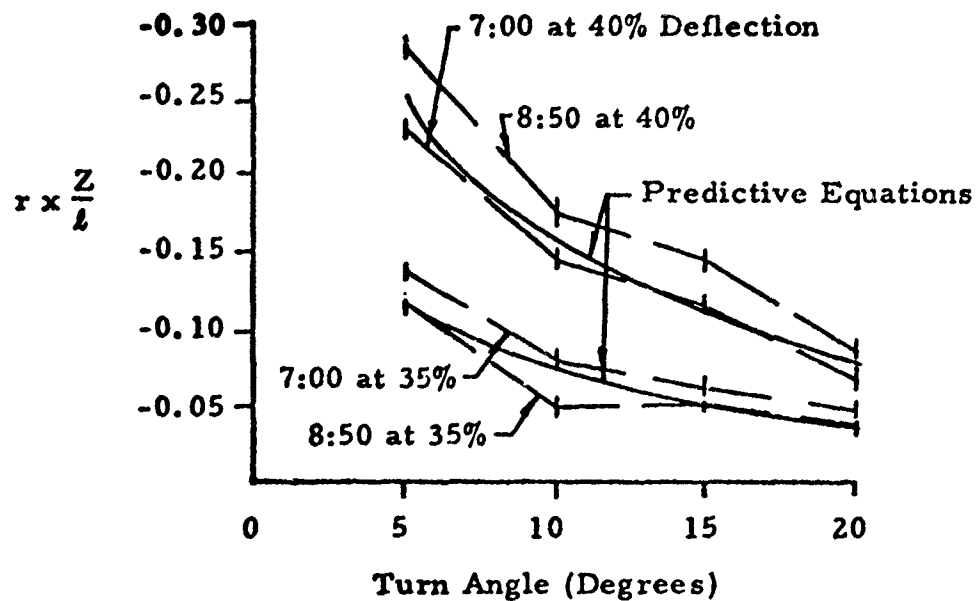


Figure 15. Pneumatic Trail Parameter versus Turn Angle for Cohesive Soil.

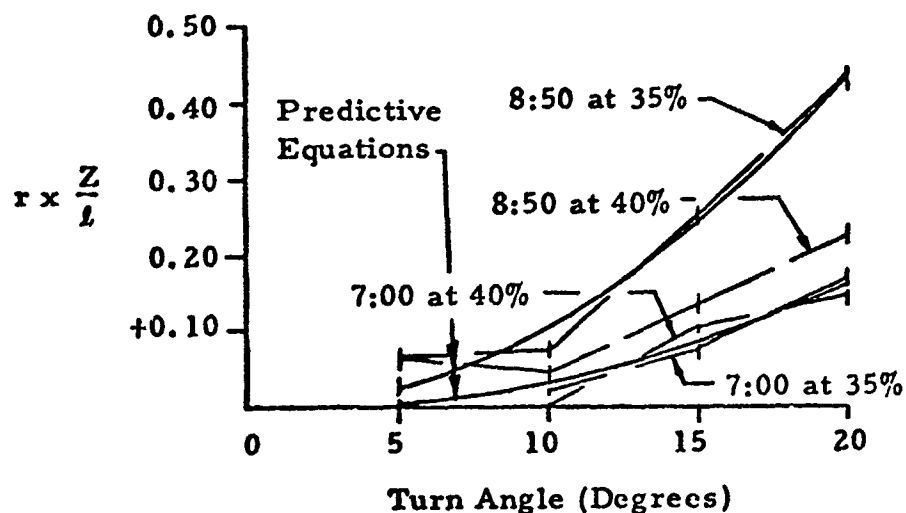


Figure 16. Pneumatic Trail Parameter versus Turn Angle for Cohesionless Soil.

functions of both deflection and sinkage. Equations developed were:

$$r \times \frac{Z}{l} = 0.0375 \cdot 10^{-2} \beta^2 \quad Z \leq 0.6''$$

where β is the turn angle in degrees, and

$$r \times \frac{Z}{l} = 0.1075 \cdot 10^{-2} \beta^2 \cdot K \quad Z > 0.6'',$$

where $K = 4.5 - \frac{DE}{10}$ in order to correct for the influence of deflection at greater sinkages.

The equations listed above were incorporated into the turning program.

During the incorporation of the pneumatic trail into the program, calculations were made for a small fighter type aircraft of approximately 30,000 pounds. For single wheel landing gear in sand and clay it was found that the pneumatic trail made negligible difference in the path over the ground or thrust required. This seems reasonable in that the torque generated at the tire is very small in proportion to the moment generated by the side force about the aircraft center of gravity. Therefore, the torque generated by the inclusion of pneumatic trail is important from the standpoint of steering control torque values, but unimportant in trajectory calculations. Since the torque for one tire is always the side force times the trail and the rigid body moment is always the side force times the distance to the center of gravity of the vehicle; it seems reasonable to assume the relative importance of the trail established would be the same for multiple wheel configurations.

Side Force Ratios

Side force ratio data for sand and clay are shown plotted in Figures 17 and 18. The curves show little dependence upon tire deflection or size and hence two equations were found to fit the data. These were:

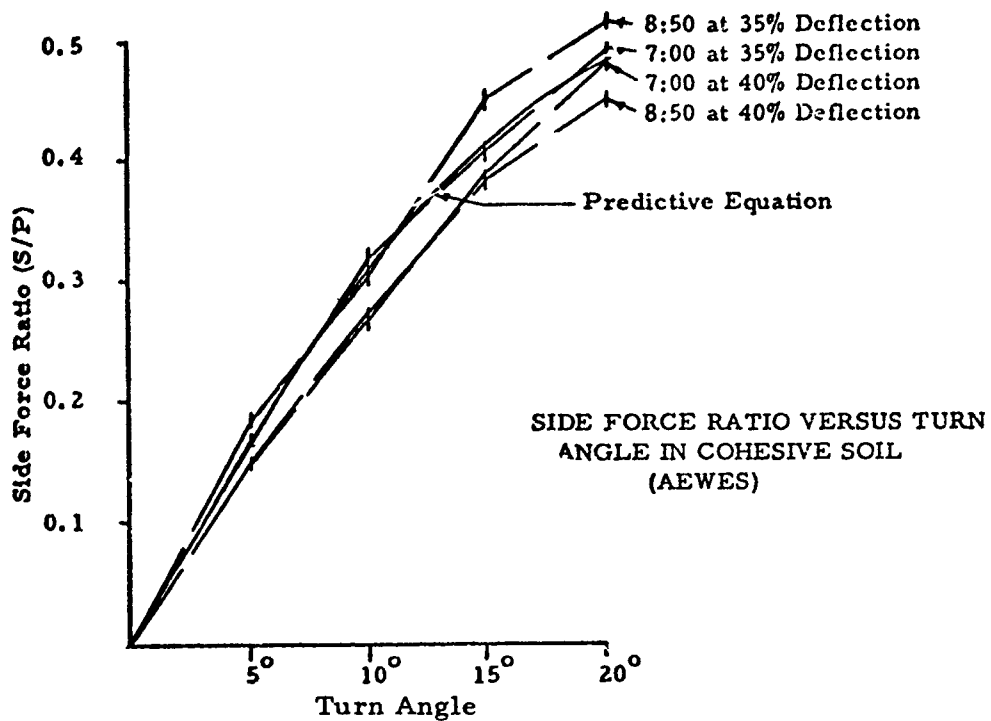


Figure 17. Side Force Ratio versus Turn Angle in Cohesive Soil.

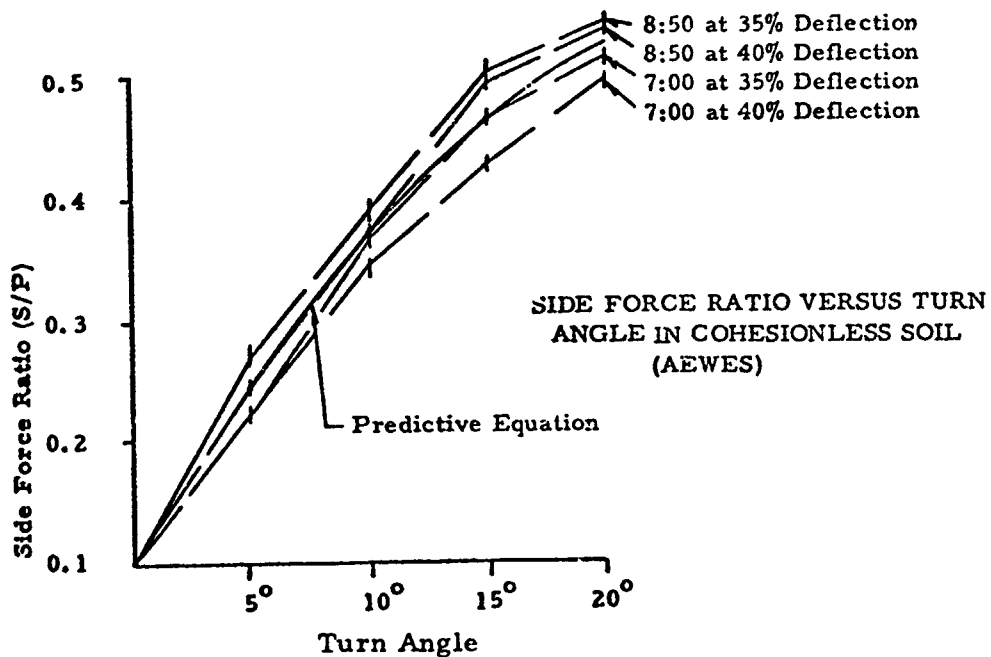


Figure 18. Side Force Ratio versus Turn Angle in Cohesionless Soil.

$$\frac{S}{P} = 0.438 \sin(4\beta) \text{ for clay and}$$

$$\frac{S}{P} = 0.432 \sin(4\beta) \text{ for sand}$$

Slip Data

Free rolling slip generated by the turned tire is plotted in Figures 19 and 20. No attempt was made to establish sinkage or tire deflection of tire size dependence. Approximate curves evolved were:

$$S = 5.00 + 0.0425 \beta^2 \text{ for sand and}$$

$$S = 3.00 + 0.0325 \beta \text{ for clay}$$

where β is in degrees.

The slip measured was used in the braked drag equation to determine whether or not drag as only a function of slip could be computed properly. This did not work. Drag created by braking in terms of slip can be calculated from a braked drag relation. Drag increases with turn angle are apparently not functions of the slip due to the turn angle. It was found, however, that calculated instantaneous sinkage for a turn angle can be computed using the relation

$$Z_{\beta} = Z_M \sqrt[3]{S}$$

which is similar to a portion of the braked drag equation. In this equation the turned instantaneous sinkage, Z_{β} , is calculated using the slip, S , due to the turn angle and the maximum fully braked sinkage Z_M . The instantaneous sinkage is then used in calculating rut depth.

In-Line Drag

As mentioned above, the in-line drag does not change with slip as originally hoped. Consequently, the in-line drag ratios were plotted as shown in Figures 21 and 22. For each curve it was realized that we need not meet

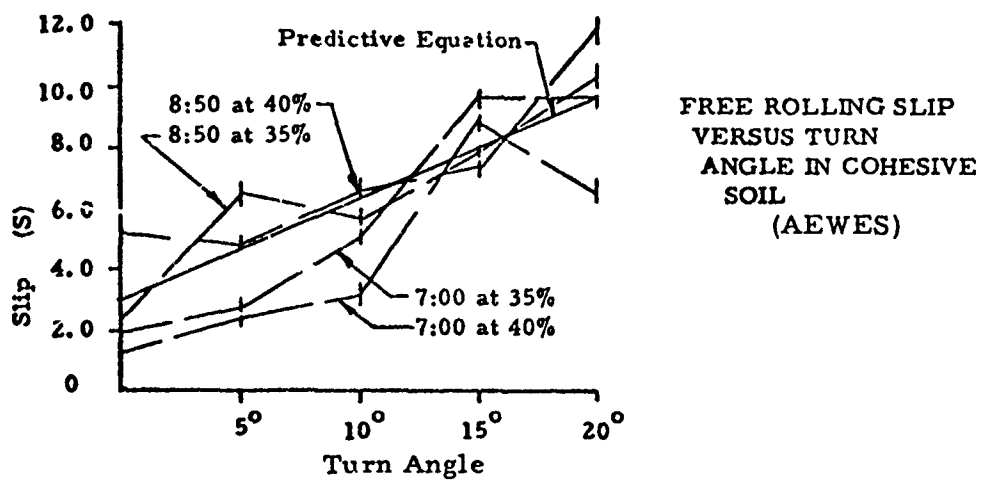


Figure 19. Free Rolling Slip versus Turn Angle in Cohesive Soil.

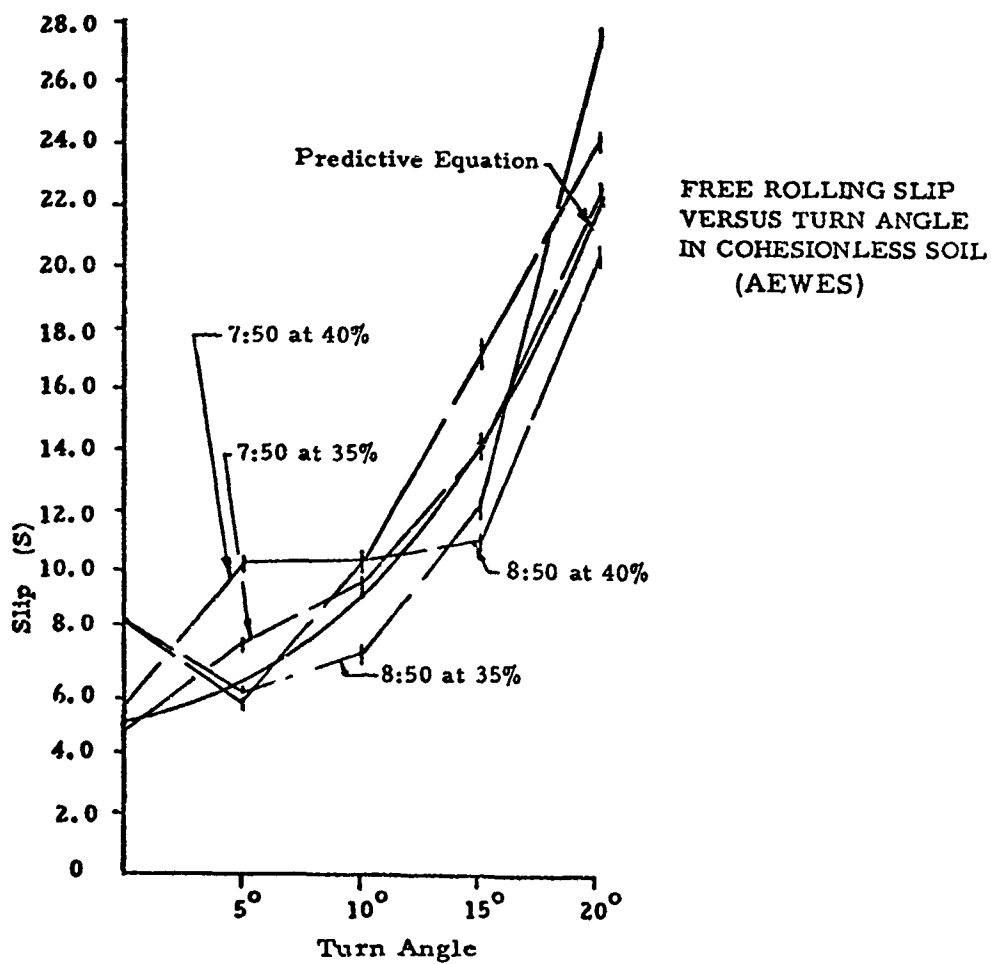


Figure 20. Free Rolling slip versus Turn Angle in Cohesionless Soil.

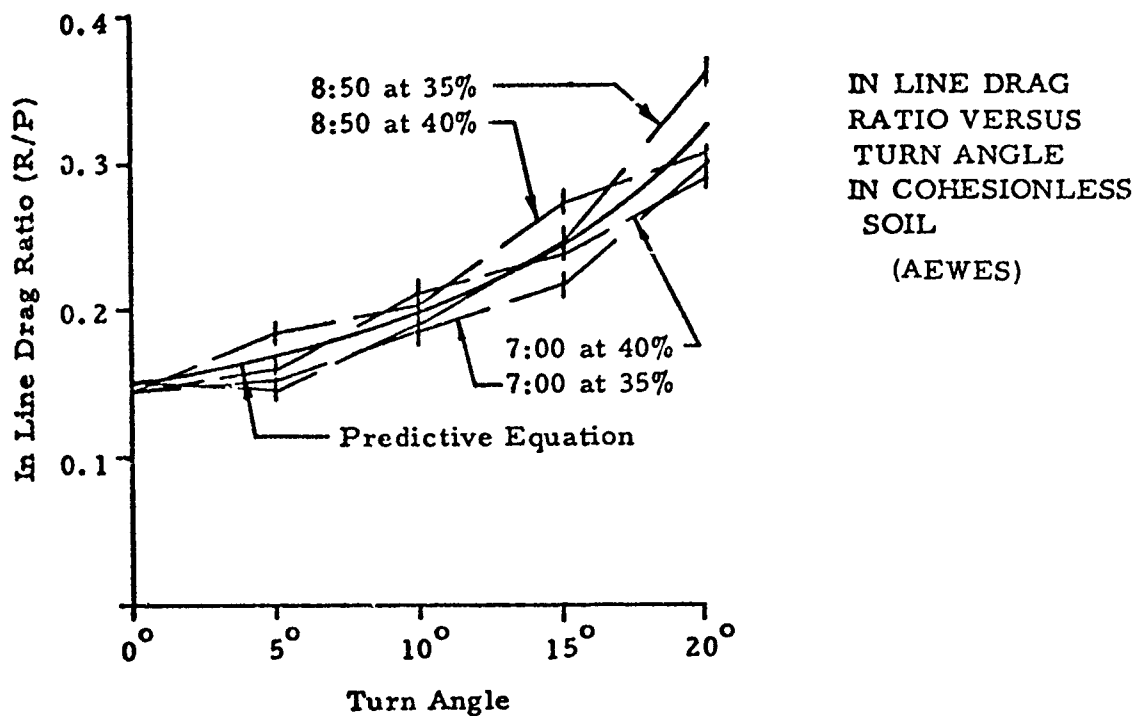


Figure 21. In-Line Drag Ratio versus Turn Angle in Cohesionless Soil.

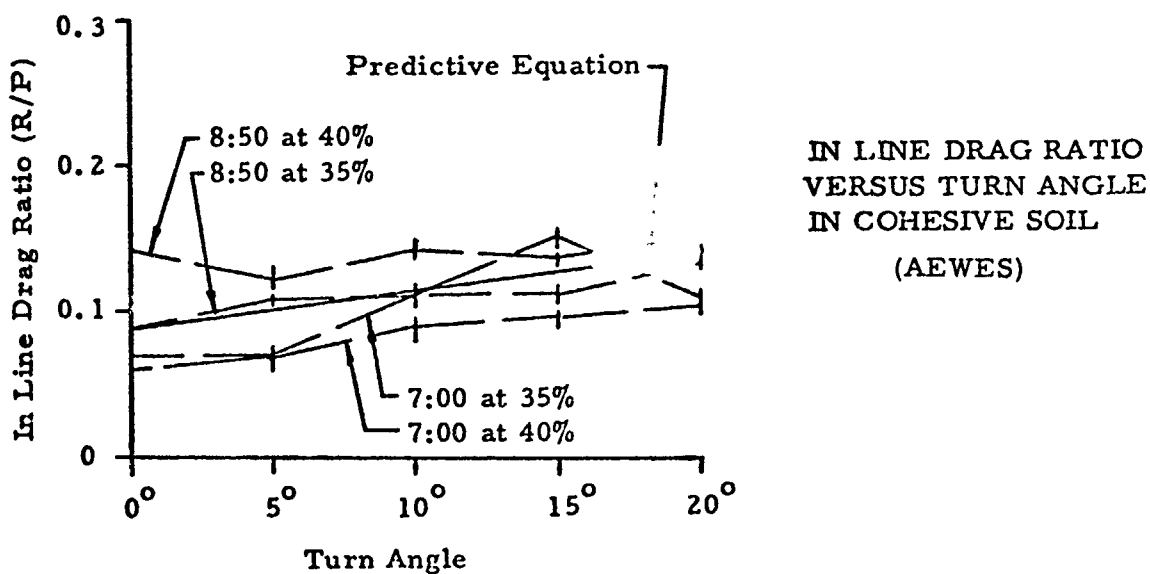


Figure 22. In-Line Drag Ratio versus Turn Angle In Cohesive Soil.

the magnitudes shown, but relations that establish changes from a zero turn condition. These relations were found and were:

$$\left(\frac{R}{P}\right)_t = \left(\frac{R}{P}\right)_o (1 + 0.27 \cdot 10^{-2} \beta^2) \text{ for sand}$$

$$\left(\frac{R}{P}\right)_t = \left(\frac{R}{P}\right)_o (1 + 0.25 \cdot 10^{-1} \beta) \text{ for clay}$$

where $\left(\frac{R}{P}\right)_t$ is the turned drag ratio

$\left(\frac{R}{P}\right)_o$ is the rolling drag ratio at zero turn angle,

and β is the turn angle in degrees.

By defining the turned drag ratio in this manner it is possible to calculate the free rolling drag ratio as previously found and correct for the given turn angle.

Thrust Control

Thrust control was included by incorporating a constant thrust differential in order to maintain a specified taxi speed. If thrust is controlled on both engines as a function of time, what are the relations used as input? This type of question was similar to that asked for steering and braking control. Given that the program user wants to vary the thrust or the braking, what time relation is used? In order to eliminate some of this problem and yet provide useful data, it was decided that a specified differential of power would be used. That is, if a differential of 1.00 is specified, the left engine is 1.00 times the right engine for a symmetrical thrust condition. If 0.50 is specified, the left engine/engines generate one-half that of the outboard engine. The program calculates the thrust required to maintain a given taxi speed. This value is then used to calculate the thrust on each side and a

calculated moment applied to the summation of moments equation. The generation of differential thrust in this manner is hoped to simulate the response of a pilot who when entering a turn wants thrust differential while maintaining the same taxi speed.

Braking and Rolling Drag Relations

The braked and free rolling drag and sinkage equations of Reference 17 were included in the digital program. Therefore, the drag subroutines were updated to permit the drag to be calculated for both cohesive and cohesionless soils defined in terms of their cone index values. Braked drag relations, as well as free rolling drag, were available for both soil types.

Additional Revisions Possible

Corrections for "driven" and "pulled" wheels on the same axle were not incorporated. The possibility of a turning reversal is not available. Lastly, rotating effects of wheels and engines were not included. All three aspects can be incorporated later.

E. SAMPLE CALCULATIONS

The resulting improved digital program can best be described by presenting some sample calculations. The C-130 was again used as a representative vehicle. The input required is presented in Figure 23 in which a computer generated list appears as the heading of each complete turn calculation.

Most of the data listing are self explanatory. All dimensions not specifically mentioned are in inches. The cone index value shown, 192.00, corresponds to a CBR value of 6 since 32 to 1 was used for cohesive soil. Cohesive soil is specified by NTYP equal 1. The engine thrust parameter of 1.00 indicates that the left engine develops 1.00 times the right engine for symmetrical thrust distribution. Maximum steering angle for the nose wheel is specified at 60.00 degrees and the maximum slip is 0.00 percent.

AIRCRAFT PARAMETERS

GROSS WEIGHT

GW = 133000.0 LBS.

INITIAL GROUND VEL.

VO = 5.0 KNOTS

TIRE DATA--

NOSE

MAIN

TIRE DEFLECTION(%)	DE = 35.00	DEM = 35.00
TIRE DIAMETER (IN.)	DN = 38.00	DM = 55.20
FLANGE DIAM. (IN.)	DFN = 18.50	DFM = 24.00
TOTAL NO. OF TIRES	NN = 2	NM = 4
NO. OF TIRES/BOGIE		N1 = 2
NO. OF TIRES--TANDEM		NM1 = 2
NO. OF TIRES--TWIN		NN1 = 0
TIRE TYPE	TYPE 3	TYPE 3

TYPE AND C.G. DISTANCES--(IN INCHES)

NOSE GEAR C.G. TO FWD C.G.	L = 346.33
NOSE GEAR C.G. TO AVE C.G.	AL = 358.80
NOSE GEAR C.G. TO AFT C.G.	LL = 371.30
NOSE GEAR C.G. TO MAIN GEAR C.G.	F = 388.00
MAIN GEAR C.G. TO FWD C.G.	M = 41.70
MAIN GEAR C.G. TO AVE C.G.	AVM = 29.20
GROUND LEVEL TO FWD C.G.	U = 150.00
GROUND LEVEL TO ENGINE	UE = 153.00
BETWEEN C.G.'S OF LEFT & RIGHT MAIN	E = 172.00
TWIN SPACING OF NOSE TIRES	SN = 22.00
TWIN SPACING OF MAIN TIRES	SM = 0.00
TANDEM SPACING OF MAIN TIRES	SNM = 60.00

SOIL PARAMETERS

COPE INDEX

CI= 192.00

SOIL TYPE

NTYP= 1

ENGINE PARAMETER

THRUST DIFFERENTIAL PE= 1.00

MAX STEERING = 60.00 MAX SLIP = 0.00

Figure 23. Input Data for Sample Calculation.

In the original program, specific values of steering and slip were entered as half second functions of time, with many runs required, and since specific values were not really known, it was decided to use 40 time pairs which would have fractional values up to unity. In this manner a waveform could be entered and the maximum value entered with one card. Thereafter all inputs could have the same waveform, and changes could be made with only one card.

Sample output data for the inputs of Figure 23 are shown in Figure 24. As listed, the equilibrium runway width required will be 75.8 feet. The results shown in Figure 13 indicated that for the same vehicle with 60° of nose wheel steering the field width would be 106 feet. This difference is not due entirely to the subroutine changes, but more because of the time to enter the turn. The previous run was for a 10 second entry into the turn whereas the revised data are for a 2.5 second entry.

The output shown reflects several changes made to improve the output for the analyst. The pneumatic trail information was incorporated by presenting the torque generated at each landing gear. For example, the turning torque listed for the left main gear reflects the total torque generated for all wheels at that mount. Because of the use of lateral force ratio in the military standard, it has been generated for each gear mount. Lastly, because of the need to recognize the soil surface damage that might occur, instantaneous sinkage, and rut depth are computed.

F. TURNING OPERATIONS PARAMETRIC STUDY

The digital program evolved reflected nearly all aspects of the tire/soil interaction that could be analytically incorporated. At this stage it was desirable to use the program and compute some qualitative results as a means of inferring the effects of the many parameters that influence turning response. The number of parameters is considerable when we consider, aircraft type, landing gear configuration, tire types, soil strength, soil

TIME= 3.00 X= 295.2 Y= 52.7 THRUST= 20345.3

NOSE GEAR DATA

TURN ANGLE= .21519 STEERING ANGLE= 1.04716

DRAG FORCE = 1538.0 SIDE FORCE = 6675.6

DRAG FORCE RATIO= .094 SIDE RATIO = .366

TURNING TORQUE =12548.6 LATERAL RATIO= .376

Z= .621 Z TURNED= 1.034 RUT= .574

LEFT MAIN GEAR DATA

TURN ANGLE= .04905 BRAKED SLIP PERCENT= 0.00

DRAG FORCE = 4742.0 SIDE FORCE = 4557.5

DRAG FORCE RATIO= .098 SIDE RATIO = .094

TURNING TORQUE =31260.8 LATERAL RATIO= .136

Z= 1.125 Z BRAKED= 2.359 RUT= 1.310

RIGHT MAIN GEAR DATA

TURN ANGLE= .02935

DRAG FORCE = 9554.0 SIDE FORCE = 3755.0

DRAG FORCE RATIO= .144 SIDE RATIO = .057

TURNING TORQUE =11841.8 LATERAL RATIO= .155

Z= 1.854 Z TURNED= 2.050 RUT= 1.139

AIRCRAFT SIDE FORCE RATIO = .077

SUM OF FORCES= -.00 SUM OF MOMENTS= .00

CENTER OF CURVATURE AT X= 12.57 Y= 340.97 RADIUS 342.40

EQUILIBRIUM REACHED, RUNWAY WIDTH 75.8

Figure 24. Output Data for Sample Calculations.

type, gross weight, speed, thrust and braking; to mention a few of the input parameters. Similarly, the number of possible outputs are considerable. Consequently, it was decided to examine specific types of vehicles for fixed configurations. The three types selected were an attack aircraft, a C-130 configuration, and an advanced transport configuration. The dimensional data used are shown in Appendix A. These were selected because the attack vehicle has a smaller gross weight with all single wheel landing gear, the C-130 has a middle gross weight with twin nose gear and tandem main gear; and the advanced transport has a greater weight with twin and tandem main mounts.

The time restraints of the research program required careful selection of the number of parameters and parameter variations to be studied. It was decided that each vehicle would be examined for a fixed gross weight, one taxi speed, one tire deflection, one soil type and strength. This permits then, evaluation of the effects of steering angle, thrust differential and braking. Steering angles of 20, 40, and 60 degrees were selected to provide data indicative of current nose wheel steering limits. Thrust differentials of unity and one-half were used. Inboard braking of 0, 15, 30, and 45 percent slip were used to generate drag ratios up to 0.5.

Several outputs are possible from the tabulated data. Those most applicable to current specifications would be side force ratio on any tire and lateral force ratio on any braked tire. Other values thought to be critical were runway width and thrust required since these are measured of how well the vehicle performs or can perform. These data are all plotted on one figure to show the effects of selected inputs on desired outputs.

The results for the three vehicles are shown in Figures 25 through 33.

All vehicles have similar performance in terms of the apparent curvature of the presented lines of constant parameter values. However, each covers a different range of runway width and force ratio magnitude. The

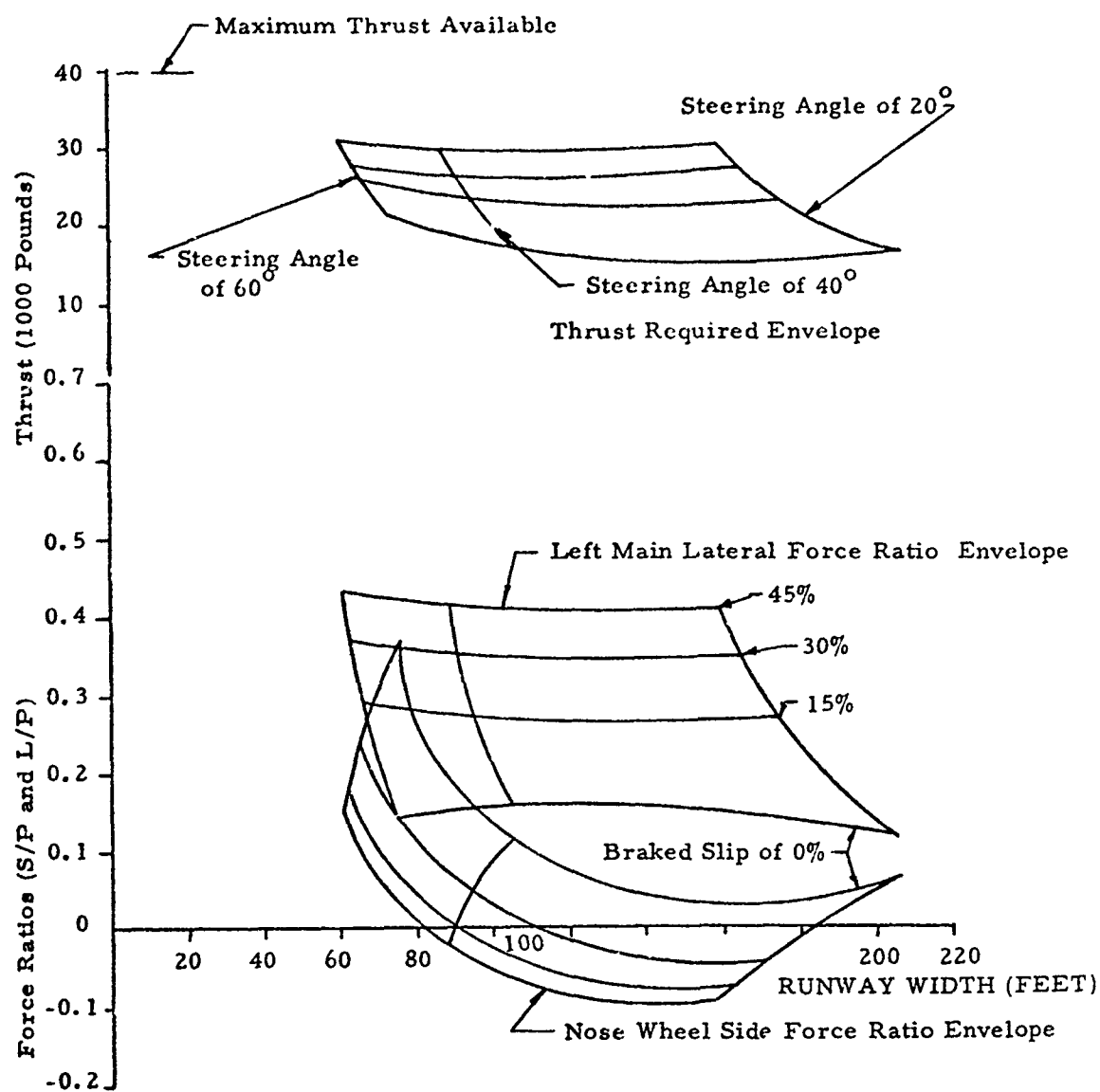


Figure 25. C-130 Configuration Performance in Cohesive Soil of CBR 6 at 5 Knots and Gross Weight of 133,000 Pounds with Symmetrical Thrust.

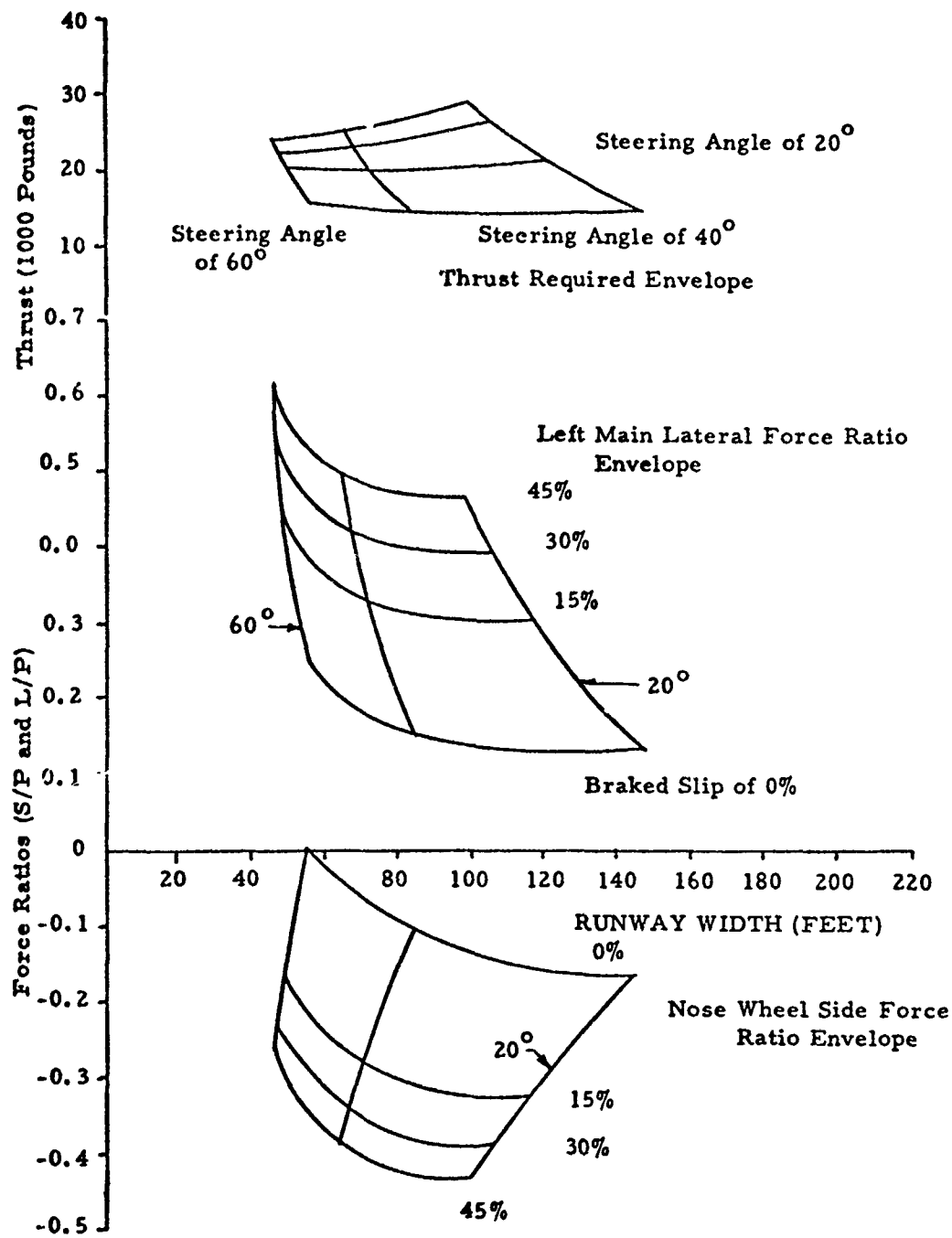


Figure 26. C-130 Configuration Performance in Cohesive Soil of CBR 6 at 5 Knots and Gross Weight of 133,000 Pounds with 50 Percent Thrust Differential.

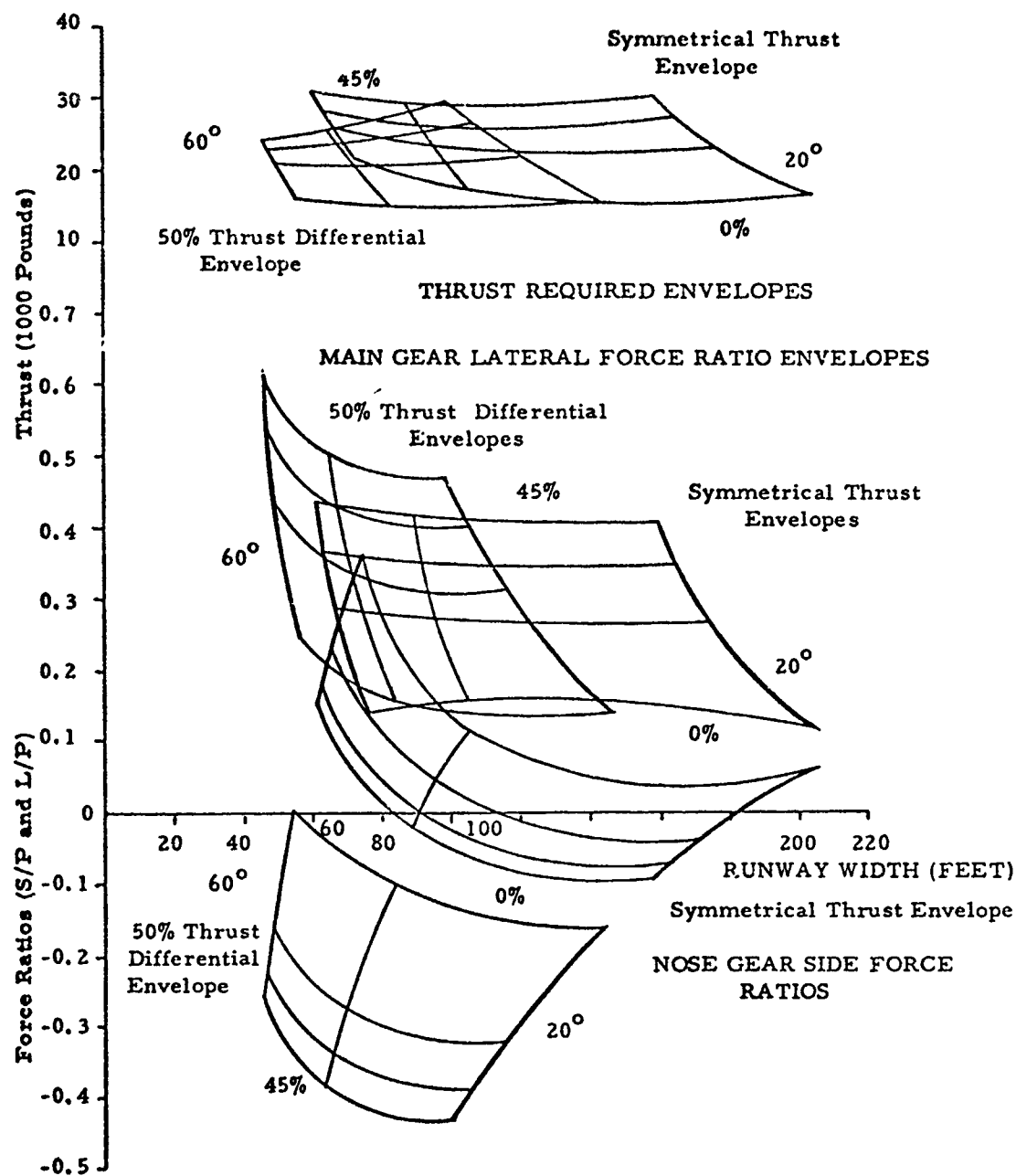


Figure 27. C-130 Configuration Performance Composite for Cohesive Soil of CBR 6 at 5 Knots and Gross Weight of 133,000 Pounds.

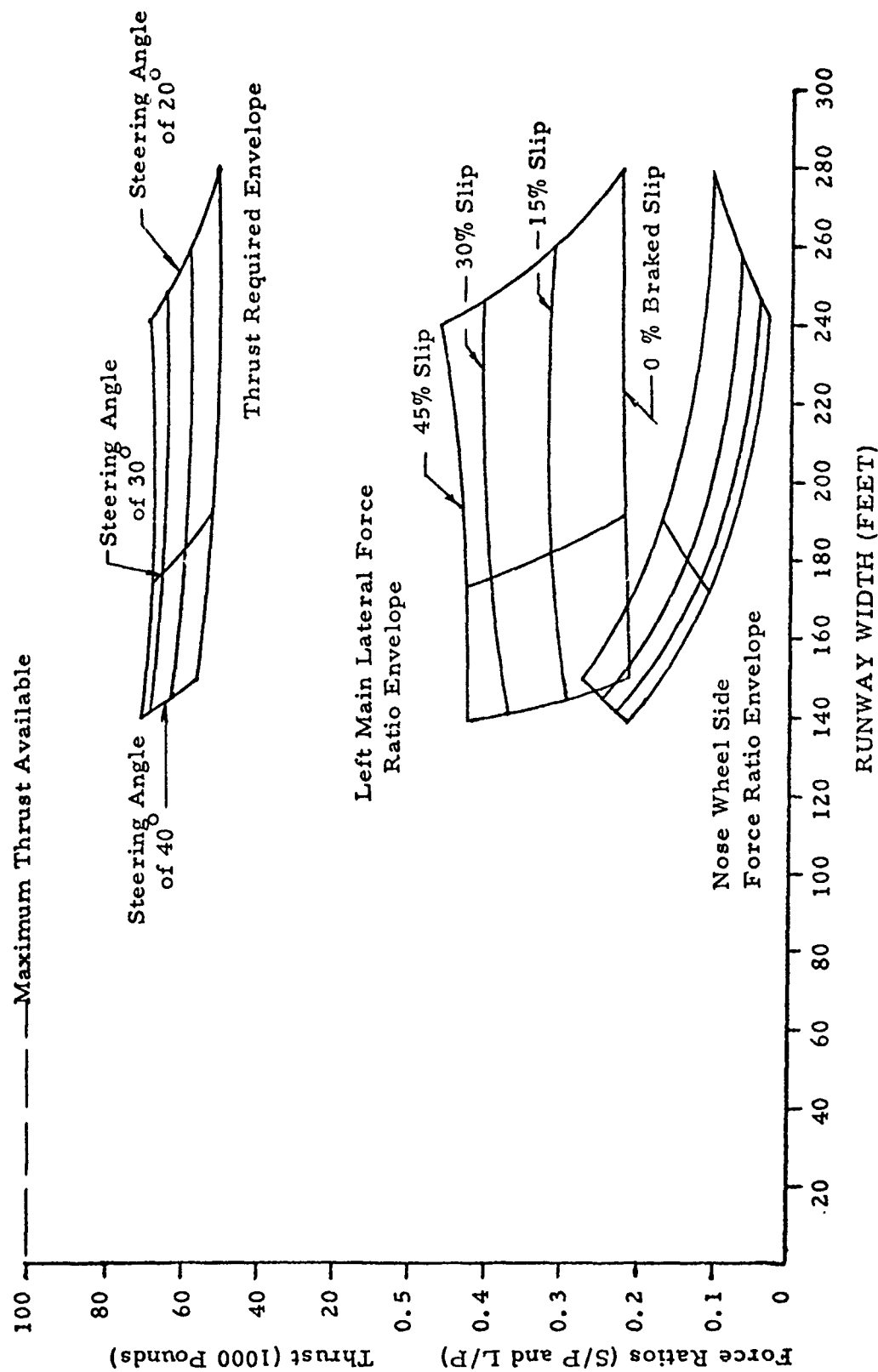


Figure 28. Advanced Transport Configuration Performance in Cohesive Soil of CBR 6 at 5 Knots and Gross Weight of 216,000 Pounds with Symmetrical Thrust.

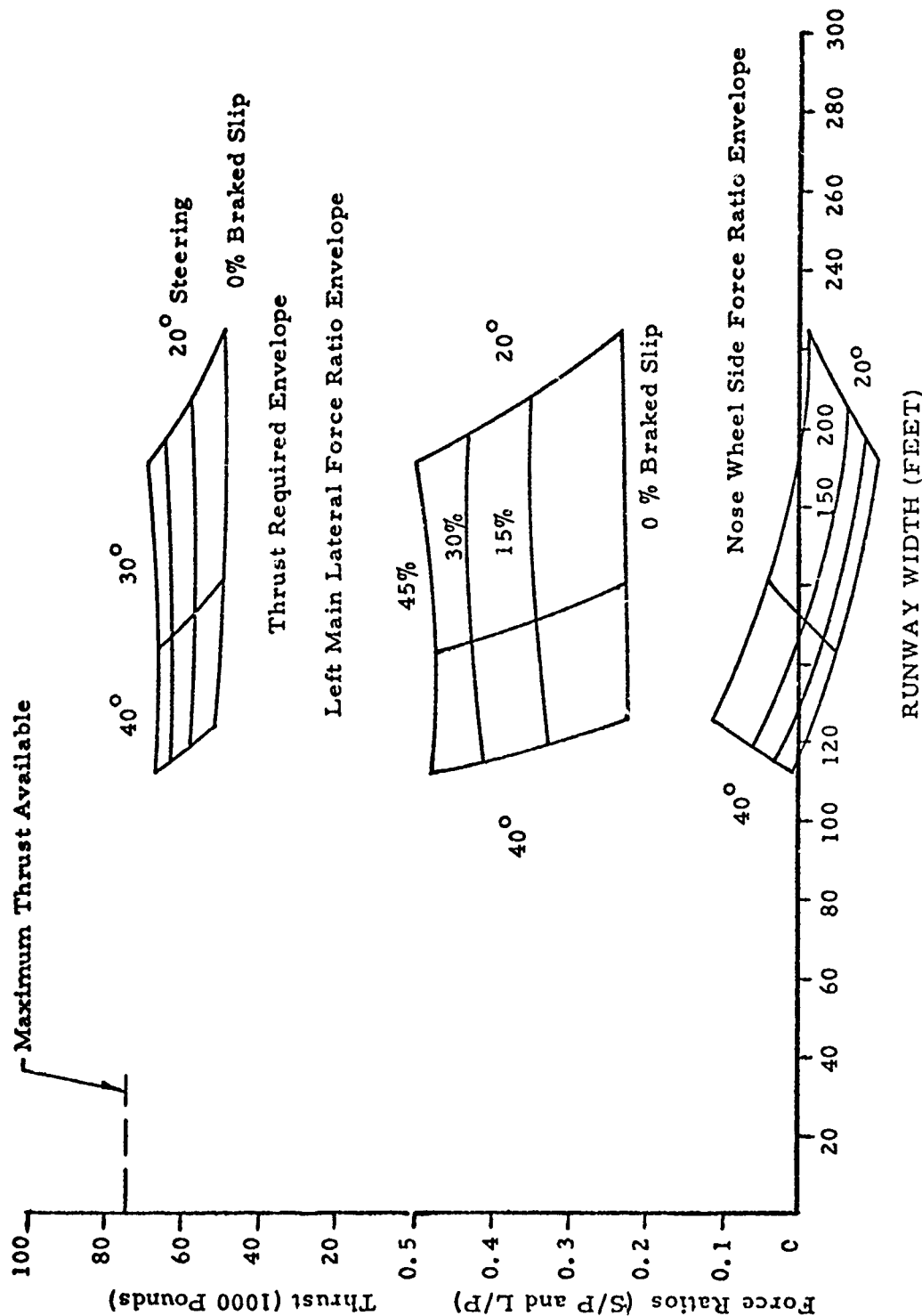


Figure 29. Advanced Transport Configuration Performance in Cohesive Soil of CBR 6 at 5 Knots and Gross Weight of 216,000 Pounds with 50 Percent Thrust Differential.

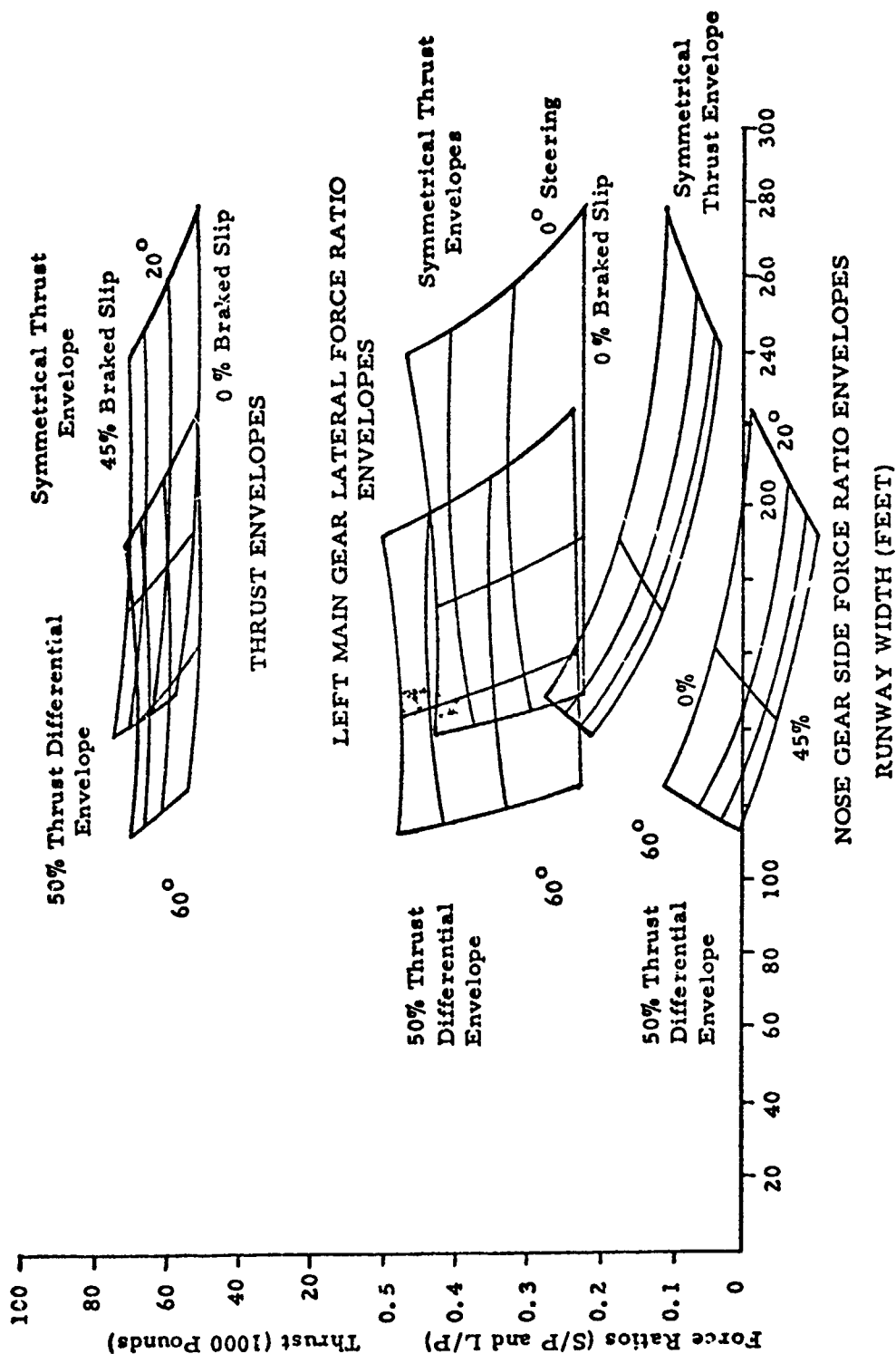


Figure 30. Advanced Transport Configuration Performance Composite for Cohesive Soil of CBR 6 at 5 Knots and Gross Weight of 216,000 Pounds.

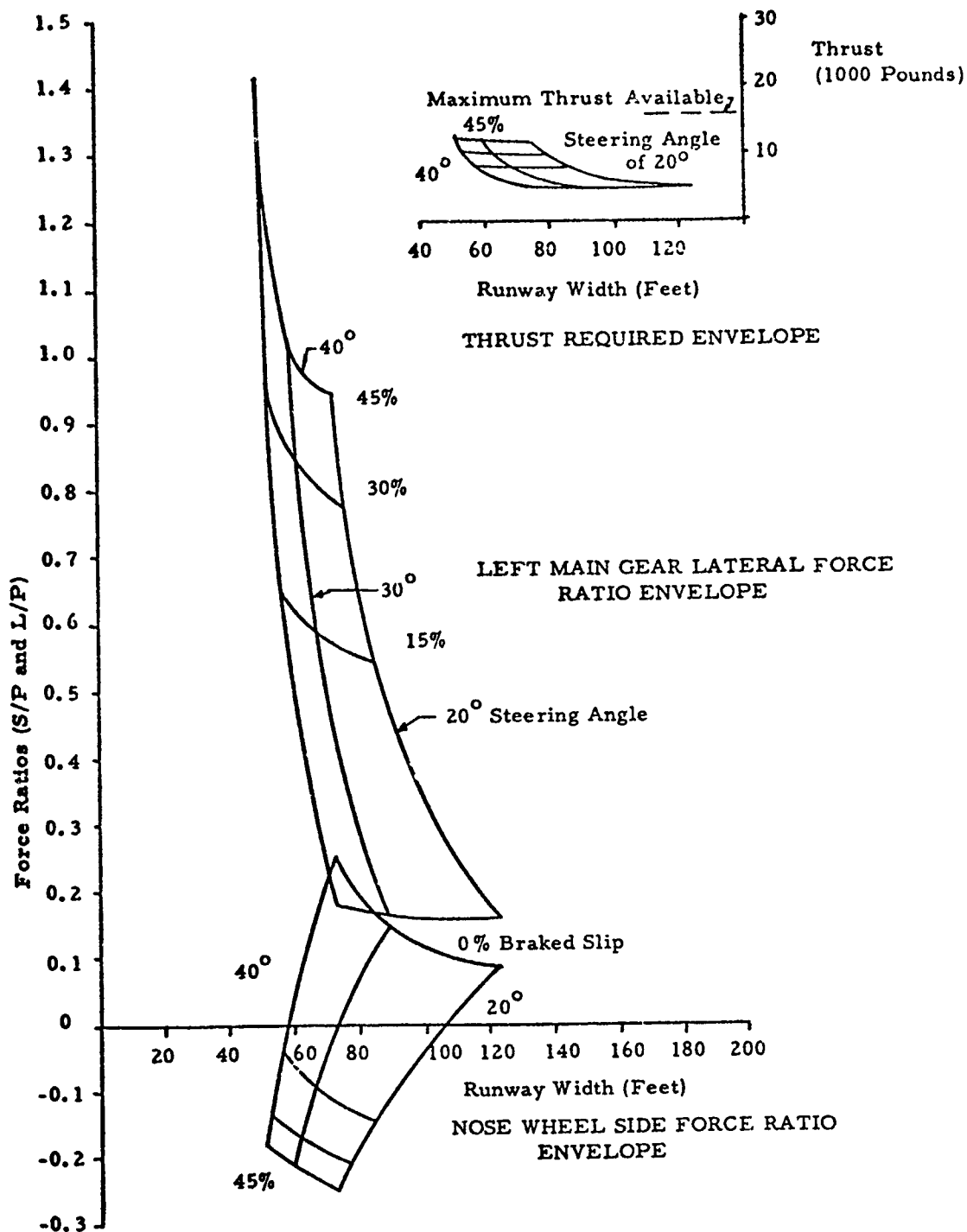


Figure 31. Attack Vehicle Performance in Cohesive Soil of CBR 6 at 5 Knots and Gross Weight of 31,000 Pounds with Symmetrical Thrust.

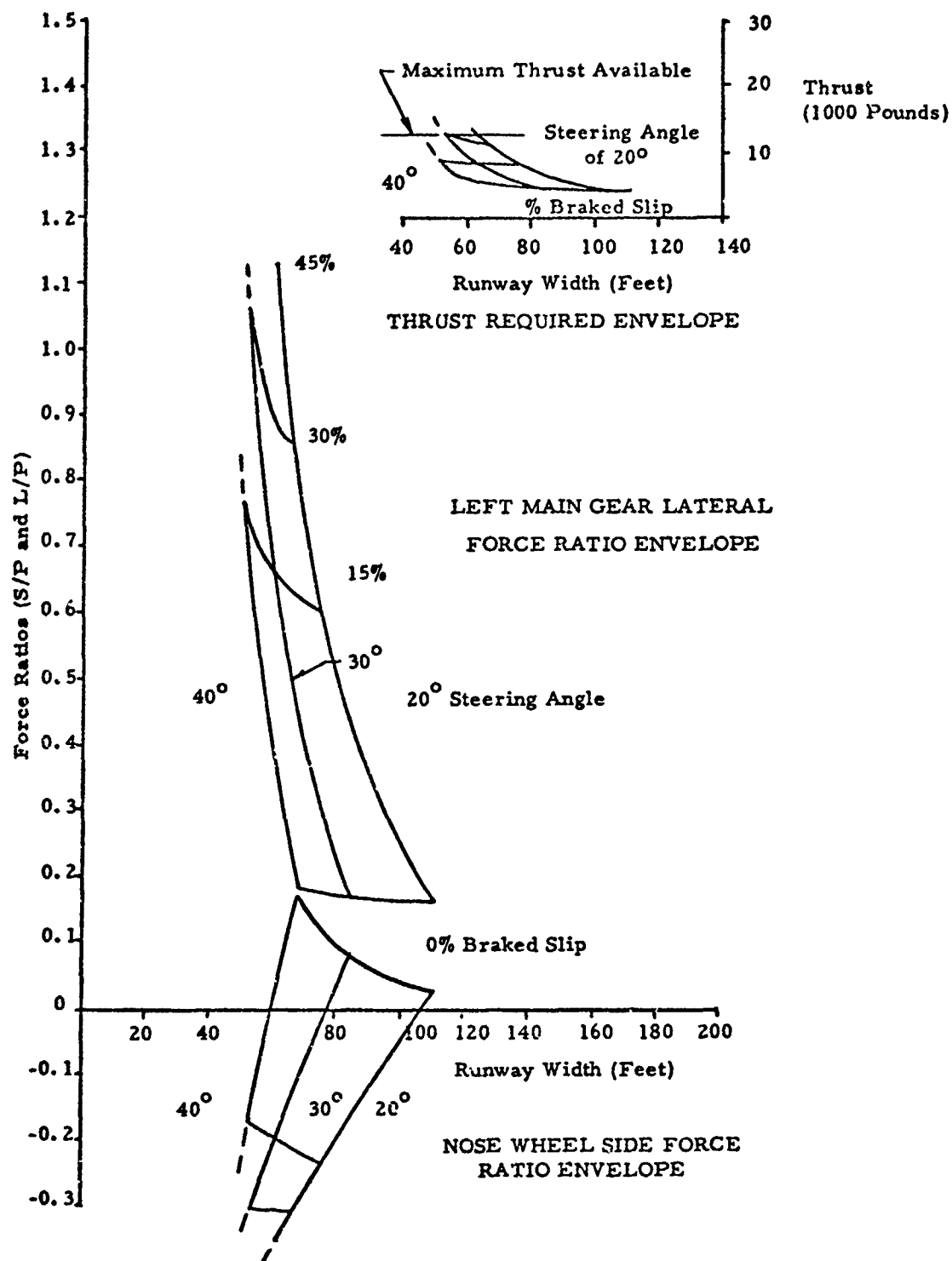


Figure 32. Attack Vehicle Performance in Cohesive Soil of CBR 6 at 5 Knots and Gross Weight of 31,000 Pounds with 50 Percent Thrust Differential.

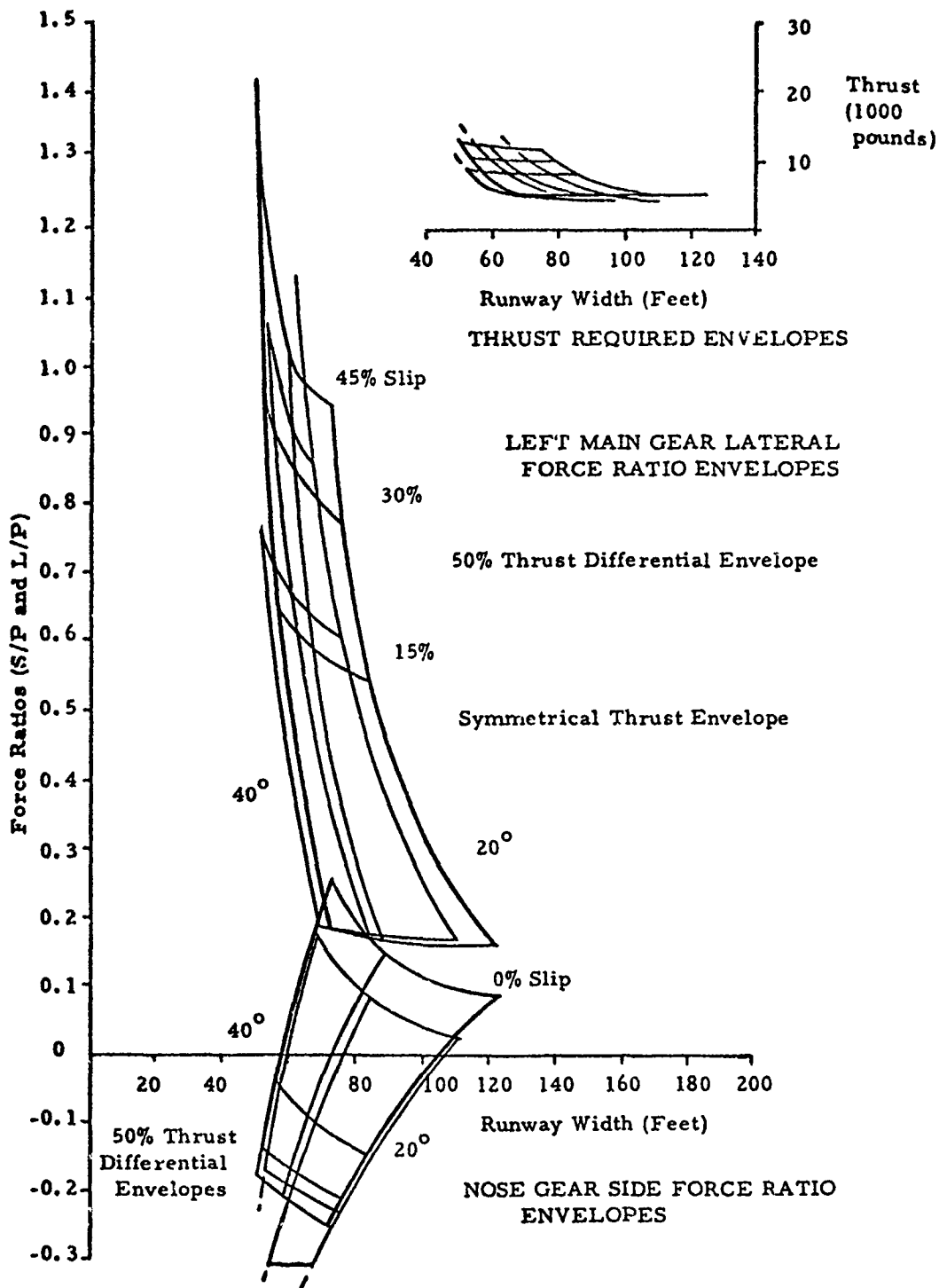


Figure 33. Attack Vehicle Performance Composite for Cohesive Soil of CBR 6 at 5 Knots and Gross Weight of 31,000 Pounds.

attack vehicle data presented are for 20, 30, and 40 degree nose wheel steering angles because the 60 degree variation could not be calculated. The program prints out diagnostics that indicate when the load strength ratios exceed predictive equation limits, turn angles are too great, or the iteration cannot converge to a solution. For the attack vehicle all occurred at 60 degree nose wheel steering. These types of diagnostics were not included in the original program and it was then necessary to look at the specific values printed out. A similar response was calculated for the advanced transport configuration. Consequently, it was also examined for 20, 30, and 40 degree nose wheel steering. One known reason for the difficulty in computing large steering angle response is that the turn angle enters into the calculation of turned sinkage as indicated by measured data. This is then used in the calculation of braked drag for the inboard gear and is reflected in the large drag force generated at relatively low slip values. The relation between turned sinkage and braked slip is neither known nor measured. However, from previous works it was assumed that braked response would be calculated from instantaneous sinkage regardless of whether due to straight ahead or turned rolling.

The C-130 configuration did permit calculations over the desired range of parameter values. Whether this can be attributed to wheel base, track, weight or tire configuration is not really known at present. There are just too many variables that influence the response that have not been examined. The C-130 plots indicate several aspects which are in general true for the other two. Starting from a nose wheel steering only configuration, inboard braking naturally decreases the runway width required. However, the change of 45 percent slip is not as significant as that gained by a 10 degree increase in steering angle. However, the 10 degree change causes a more significant change than a 50 percent thrust differential. Since the main gear lateral force ratio is primarily dictated by the braking, it appears that the best method of achieving reduced structural loads into the gear is that of not using the brakes unless necessary.

The one aspect that is difficult to generalize is that of the nose wheel side force ratio. The curves that are plotted above the abscissa are positive side forces indicating that the nose wheel helps to turn the vehicle. Those below the abscissa indicate that the nose wheel steering angle is insufficient for the equilibrium turn generated. The nose wheel that generates a negative side force ratio is being plowed through the soil. Therefore, the plot for a 50 percent thrust differential indicates that there is only one point where the steering is sufficient, at 60 degrees with no braking. All other points have insufficient turning for a 50 percent thrust differential.

The thrust curves indicate that differential thrust not only decreases the runway width required but does so at reduced thrust required. The danger in going too far with that relation is that as the thrust required goes down, so too does the available thrust. The C-130 has roughly 40,000 pounds of thrust available. At a minimum radius turn the thrust required is 24,000 pounds. However, in order to get a differential of 50 percent, the outboard engines must develop two-thirds of that required, 16,000 pounds which is 80 percent of that available from the two engines. If no thrust differential exists for the same steering and braking, the thrust required is about 30,000 pounds or 75 percent of the thrust available on both sides.

The plots for both the C-130 and the advanced transport indicate that turning is best accomplished, in terms of lateral forces on the main gear, by using nose wheel steering, then differential thrust, and lastly braking. This is particularly true for the advanced transport configuration shown where a thrust differential essentially translates the lateral forces ratio curves without increasing them. Therefore, the paragraph of MIL-A-00862A pertaining to turning has the means of turning the aircraft listed in the optimum manner by stating "unsymmetrical thrust or nose gear steering" first, and "differential braking" last.

It is difficult to discuss at length any additional parameter variations since comparison between thrust, braking, and steering response can be seen from the plots for the specific values of input used. What happens when the gross weight changes, soil type and cone index changes, or velocity increases is not known exactly although other sample turns have provided some insight into what would happen qualitatively. This suggests also the fact that the results shown are indeed qualitative. Although the drags, sinkages, side forces, etc., are all calculated from predictive equations, these were developed from laboratory tests of wheels not complete vehicles. Therefore, the shift due to a given braking or thrust is probably reasonably correct for a percentage change, but may not create exactly 27.4 feet of runway width change. Similarly, the C-130 will for given conditions have a smaller field width required, but not necessarily 50.0 feet.

G. AIRCRAFT TURNING SUMMARY

Turned tire test results have been incorporated into a digital program containing drag and sinkage prediction equations previously evolved. The equations reflected free rolling and braked drag as well as multiple wheel effects for aircraft tires operating in cohesive and cohesionless soils. The turned tire data were used to add side force curves, pneumatic trail, in-line drag modifications, slip due to turn angle, sinkage due to turn angle, and rut depth prediction. The equations of motion for a rigid vehicle turning at a constant velocity are solved for given conditions of braking, nose wheel steering and thrust differential. The program generates performance data in terms of path over the ground, side and drag force ratios, lateral force ratios, turn angles, torque due to pneumatic trail, instantaneous sinkage, braked sinkage and rut depths.

Several plots for representative aircraft have been presented to indicate the nature of the turning phenomena in terms of runway width required, force ratios, and thrust required. Some information computed

was consistent with the current turning criteria. That is, the C-130 representation generated performance curves for the range of steering angles permitted by the pilot's handbook. However, the others could not be taken to their limit steering angle because the computed turn angles, load strength ratios, or other internal parameters, were outside of the range of the predictive equations. When attempting to compute minimum runway width, the existing test data is insufficient and the program has difficulty in iterating to convergent solution. Practically this infers that it is difficult to predict what a tire does at a turn angle of 70 degrees, or, what really happens when a landing gear nearly pivots about a point?

SECTION III

MULTIPASS TIRE/SOIL INTERACTION ANALYSIS

A. GENERAL AND DEFINITIONS

Multipass criteria for the operation of aircraft over remote soil runways have been previously established. The Military Vehicle/Aircraft Rut Depth Method has been proposed and published criteria and procedures for calculating flotation are available in "Aircraft Ground Flotation Investigation, Part I, "AFFDL-TR-66-43 or AFSCM 80-1 "Handbook of Instructions for Aircraft Design. "

The current research program was designed to determine whether or not new criteria could be developed from multipass test data which would be an extension of the previously developed predictive equations. Equations and nomograms are available to calculate instantaneous sinkage and drag for a rolling single wheel. This can be adjusted to reflect twin and tandem configurations as well as braked effects. The next logical steps were then to determine how multiple passes of the rolling or braked tire over alternating but adjacent paths could influence sinkage, drag and rut depth. If trends could be established as functions of the number of the pass, where it occurred, and whether or not it were braked; relative to first pass calculated response; then predictive equations would be available to better establish "failure criteria".

Current multipass criteria are functions of drag developed and cumulative rut depth. Will the drag exceed the capability of the vehicle to maneuver over the soil? Will the cumulative rut depth cause excessive drag or interference between vehicle structure and the soil surface? If the data permits reasonable prediction of cumulative rut depth and drag as a function of the multipass history (rolling, braked, same lane, adjacent lane), then it would be possible to better relate the physical characteristics of the vehicle, its mission, and flotation criteria.

In the following sections it is well to remember that the predictive equations that are available are based upon instantaneous sinkage calculated for the tire type, applied load, cone index and soil type. Measured test data does not yield instantaneous sinkage and hence it is necessary to relate it to another parameter such as axle movement for the AEWES data. After instantaneous sinkage is found to relate to measured drag, then it is also correlated with rut depth, another measured parameter. Therefore, in the analysis of the data it will be shown that indeed sinkage, axle movement, and rut depth are different quantities which can be related not only for first pass, but multipass operations.

B. TEST PROGRAM AT AEWES

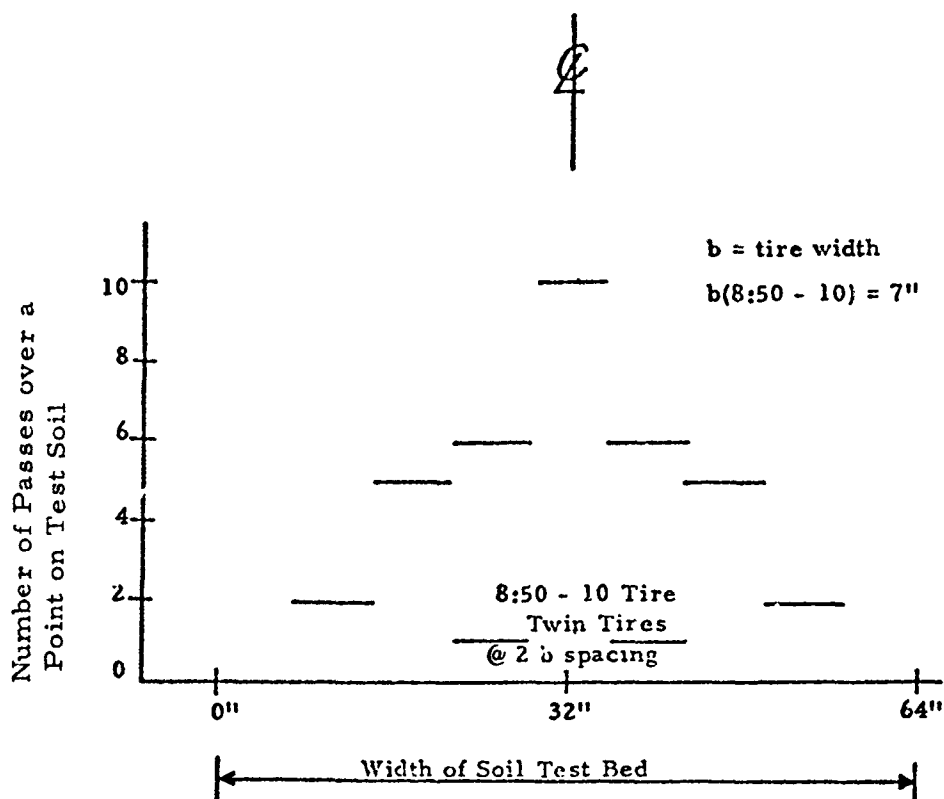
Test Matrix

A series of tests were conducted at the Army Engineers Waterways Experiment Station (AEWES) under the supervision of University of Dayton personnel. It was desirable to have three basic types of tests. These were free rolling single wheel over one lane, rolling and braked over alternating adjacent lanes, and twin tires free rolling over alternating adjacent lanes. The tests were to be conducted for at least two types of tires, two cone index values and two applied loads. The original test outline is shown in Figure 34. The pass distribution for alternating paths are shown in Figure 35.

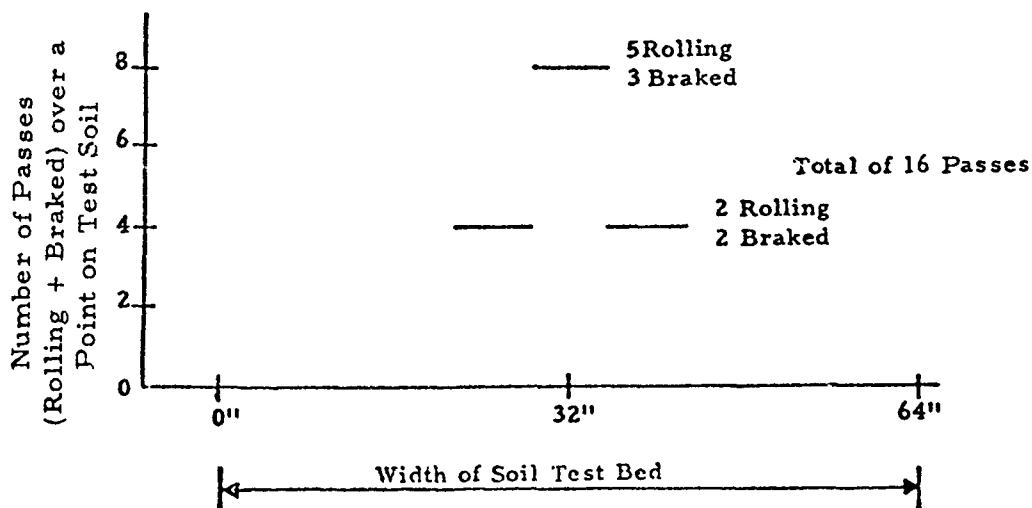
From these figures a test matrix was evolved to specify the testing to be accomplished. The first page of the matrix is shown in Figure 36. The variable of greatest importance was soil type. That is, the variable which could be changed least frequently. Hence, the test matrix was set up to run all high cone index soil tests first. Secondly, single tire tests of one tire type precedes a second tire type, with variable applied loads. Therefore, the test plan was to progress with minimal changes from one test to the next and one series to the next.

Test Part	Tire Designation	Tire Deflection d, %	Soil Type	Soil Strength CI Avg.	Vertical Load P, lbs.	Number of Passes	Pass Distribution
1	7:00-6, 6 PR	35%	Clay	55	1100 to 1200	10	Single Tire
	7:00-6, 6 PR	35%	Clay	55	800 to 900	10	All passes
	8:50-10, 8 PR	35%	Clay	40	1200 to 1300	10	conducted in
	8:50-10, 8 PR	35%	Clay	55	1200 to 1300	10	the rut of the previous path.
2	7:00-6, 6 PR	35%	Clay	55	1100 to 1200	15 to 20	Twin Tires
	7:00-6, 6 PR	35%	Clay	55	800 to 900	15 to 20	with 2 b
	8:50-10, 8 PR	35%	Clay	40	1200 to 1300	15 to 20	spacing -
	8:50-10, 8 PR	35%	Clay	55	1200 to 1300	15 to 20	distribution as shown in
							Figure 1
3	7:00-6, 6 PR	35%	Clay	55	1100 to 1200	up to 20	Singe Tire -
	7:00-6, 6 PR	35%	Clay	55	800 to 900	up to 20	alternating
	8:50-10, 8 PR	35%	Clay	40	1200 to 1300	up to 20	rolling and
	8:50-10, 8 PR	35%	Clay	55	1200 to 1300	up to 20	braked condi-
							tion. Braking condition always at 35% slip

Figure 34. Multipass Tire Test Outline.



Passes Distribution for Test Part 2, Twin Tire Configuration, for 18 Passes as Shown.



Passes Distribution for Test Part 3, Single Tire, Alternating Rolling and Braking.

Figure 35. Passes Distribution for Test Part 2 and Test Part 3.

MULTIPASS TIRE TEST PROGRAM TEST MATRIX

Test No.	Tire Designation	CI Avg	Vertical Load lbs	Number of Tires	Pass Configuration Path	Braking	Rut Depth and Conc Index
1	7:00-6, 6 PR	55	800 to 900	Single	All in Same Rut	Free Rolling	Yes
2							
3							
4							
5							Yes
6							
7							
8							
9							
10			800 to 900				Yes
11			1100 to 1200				Yes
12							
13							
14							
15							Yes
16							
17							
18					All in Same Rut	Free Rolling	
19							Yes
20							Yes
21					1	R	Yes
22					2	B	
23					3	B	
24					1	B	
25					1	B	Yes
26					1	R	
27					2	R	
28					2	B	
29					1	R	
30					1	R	Yes
31					3	B	
32					3	R	
33					3	R	
34					2	R	
35					1	R	Yes *
36	7:00-6, 6 PR	55	1100 to 1200	Single	1	B	

Notes:

CI of 55 = CBR of 1.7

See Figures

1 and 2 for Code to Particular Paths

Paths -1, 2, 3
Braking-0%, 35%

*Measured after the Numbered Test or When Failure Criteria Reached

Figure 36. Test Matrix Format.

The number of passes over a particular path had been selected as indicative of the distribution that would exist about the centerline. The number of rolling versus braked passes was selected to provide sufficient data indicative of the acceleration of "failure" due to both rolling and braking action. Once these were established, the selection of alternating rolling or braked, this path or that, were determined in a purely random selection process.

Failure Criteria

Prior to any testing it was necessary to establish failure criteria guidelines for the tests. Two criteria were established. Instantaneous sinkage divided by the tire diameter was restricted to 0.06. This was established by examining the drag ratio-sinkage ratio of a single wheel on soil shown in Figure 37. Assuming that most cargo aircraft have a thrust to weight ratio of 0.25 to 0.30, takeoff would be impossible if the R/P ratio were greater than approximately 0.25. This establishes 0.06 as the limiting value for Z/D. Hence, for a 8:50 tire the instantaneous sinkage would be approximately one and one-half inch.

Cumulative rut depth to tire diameter ratio, Z_R/D was restricted to 0.20. This approximates the value of one half to two thirds of the free height of the aircraft tire, or approximately five inches for the larger tire.

Test Measurements

Tests were conducted using Type III aircraft tires; 7:00-6, 6PR and 8:50-10, 8PR, both operating at deflections of 35%. All tests were conducted at forward speeds of 10 feet per second. The following measurements were taken:

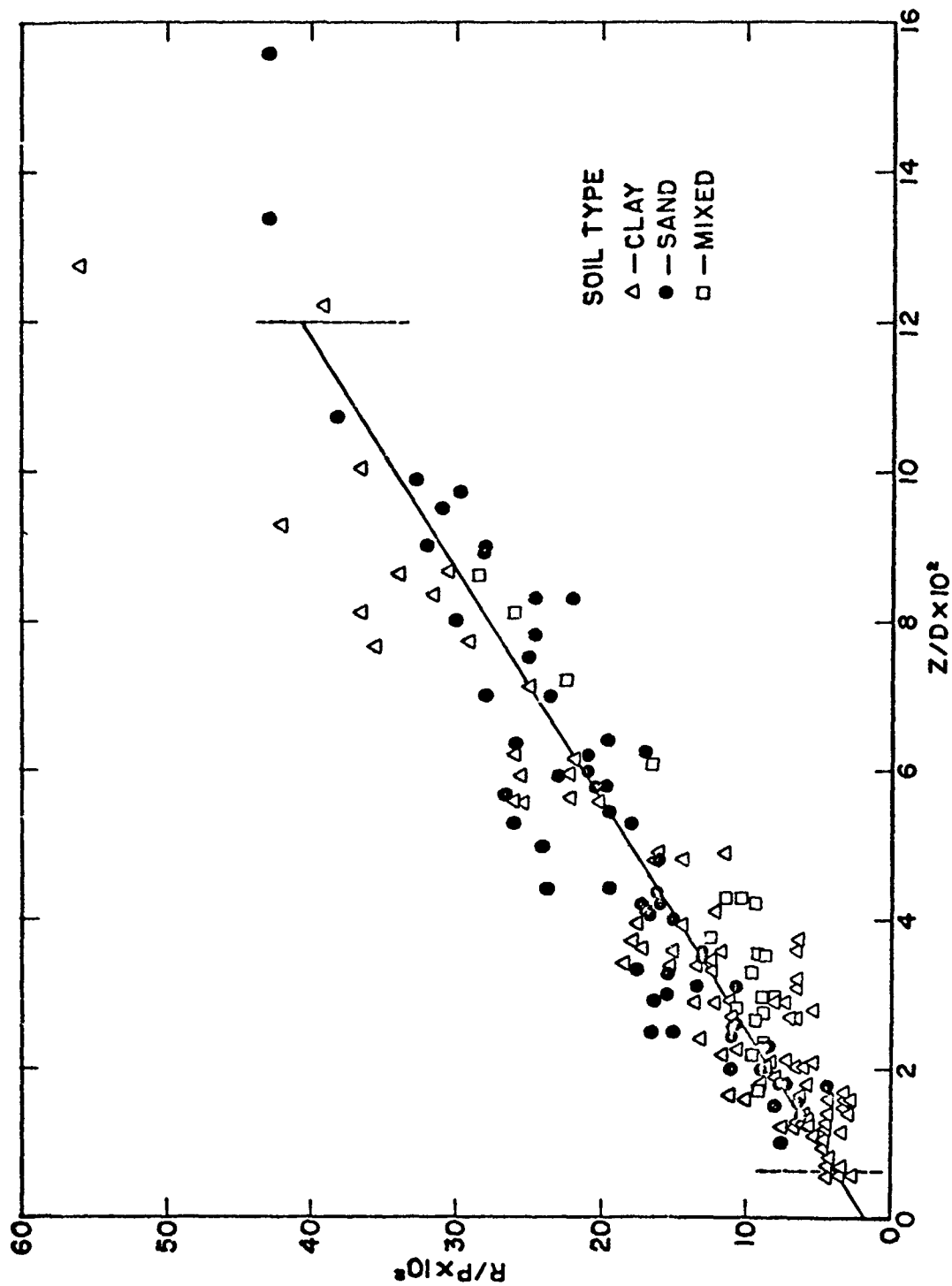


Figure 37. Drag Ratio-Sinkage Ratio, Single Wheels on Soil.

Vertical Load (each pass)

Drag Load (each pass)

Axle Movement (each pass)

Rut Depth (each pass)

Rut Profile (after test, 5th, 10th, and either last
or failure pass)

Velocity (each pass)

All data collected were reported in Reference 18. The following analyses
select typical test results from that report.

C. SINGLE WHEEL FREE ROLLING TESTS

Test Part 1 of the test matrix called for four series of tests to be
conducted using two tire types, two soil strengths, two load levels and ten
passes in the same rut. Each test was examined to determine how well the
first pass data matched existing techniques, and then to establish a relation
between drag and rut depth as a function of the pass number and first pass
calculated values.

Test series A74-0001-3 was conducted using a 7:00-6 tire at 35%
deflection. The raw data are plotted as shown in Figure 38, and as tabulated
below.

YEAR	74.	TEST	1.	SOIL	3.		
PASS NO.	DESIRED SLIP %	ACTUAL SLIP %	LOAD LBS	DRAG LBS	AXLE MOVEMENT IN.	AXLE VELOCITY FT/SEC	TORQUE FT-LB
1.		1.2	798.3	-64.7	0.48	10.219	0.0
2.		2.2	747.1	-66.3	0.34	10.208	0.0
3.		1.7	754.0	-66.0	0.55	10.240	0.0
4.		1.4	753.2	-70.0	0.59	10.230	0.0
5.		1.8	758.7	-70.6	0.71	10.298	0.0
6.		2.0	762.0	-75.3	0.79	10.185	0.0
7.		2.0	753.4	-76.5	0.86	10.301	0.0
8.		1.2	759.8	-77.9	0.92	10.346	0.0
9.		2.2	753.5	-78.2	0.99	10.354	0.0
10.		2.2	764.3	-77.2	1.08	10.408	0.0

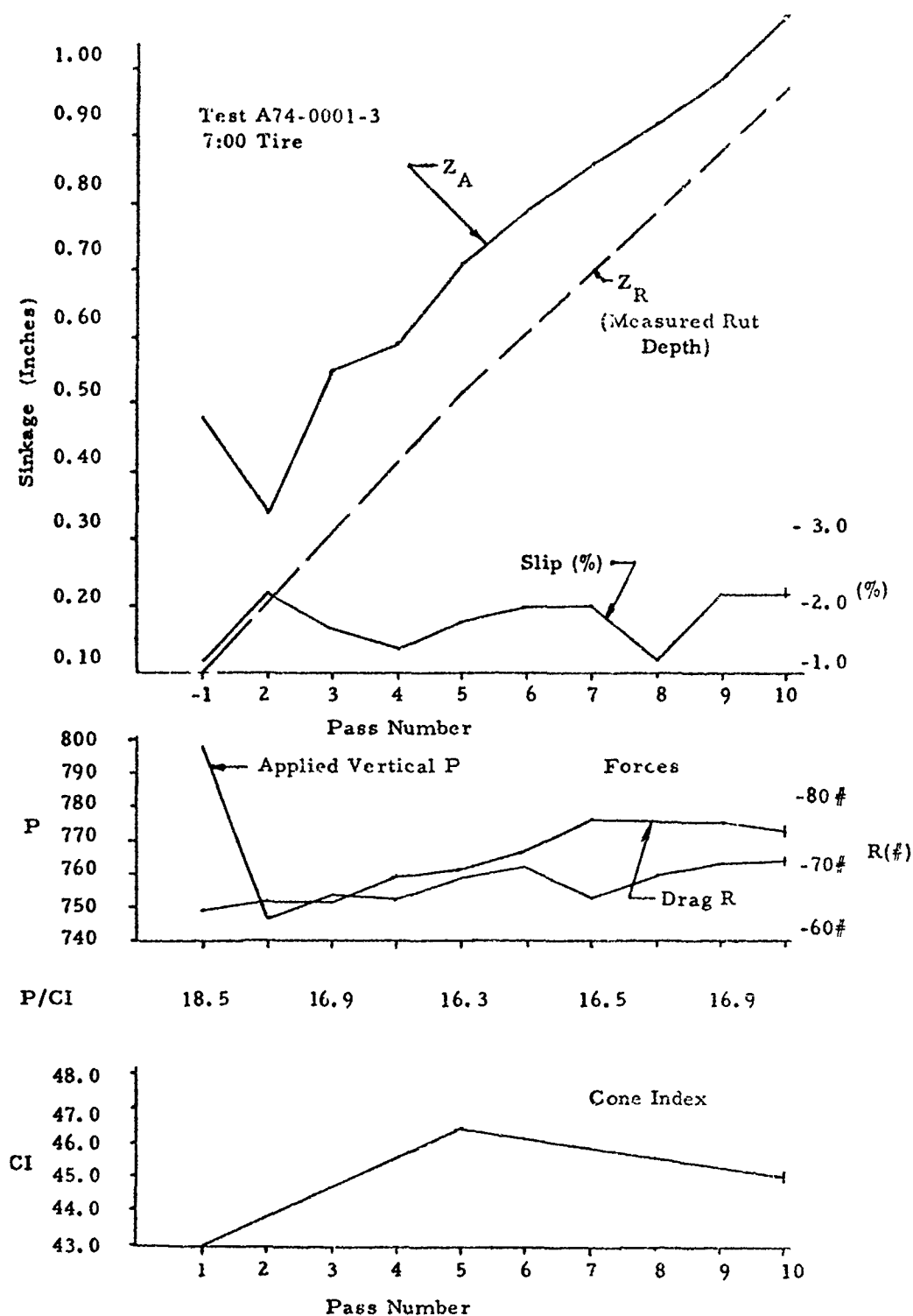


Figure 38. Raw Data of Single Wheel Multipass Data.

The cone index values were measured before the test began and after the first, fifth, and tenth pass.

The first pass generated an axle movement that appears to be above the general trend of the last eight passes. We would anticipate that first pass effects would differ from later pass effects, but not as drastically different as shown. Consequently, the first pass data was closely examined to determine how well it could be explained and understood.

For the 7:00 tires, the rigid surface contact area is calculated to be 43.4 square inches. Using the nomogram shown in Figure 39, the sinkage and drag were calculated for the first pass. An applied load of 798 pounds with a cone index of 43.0 generates a sinkage of 0.75 inches and an R/P of 0.157. Hence calculated drag would be 125 pounds as compared with 65 measured.

The rut profile data indicates that the rut depth measured after the first pass was 0.097 (average for three locations). The axle movement measurements show a motion of 0.48 inches. From AEWES data relating sinkage to axle movement (Figure 40), the relation

$$Z_a = 2/3 Z$$

was used for 35% tire deflection. The calculated axle motion would then have been 0.50 inches.

The relation between instantaneous sinkage, Z , and rut depth comes from Figure 41, data collected at the University of Dayton. The curve shown is:

$$Z = (2.4 Z_R)^{1/2}$$

The calculated rut depth would then be, $Z_R = 0.21$ inches, therefore:

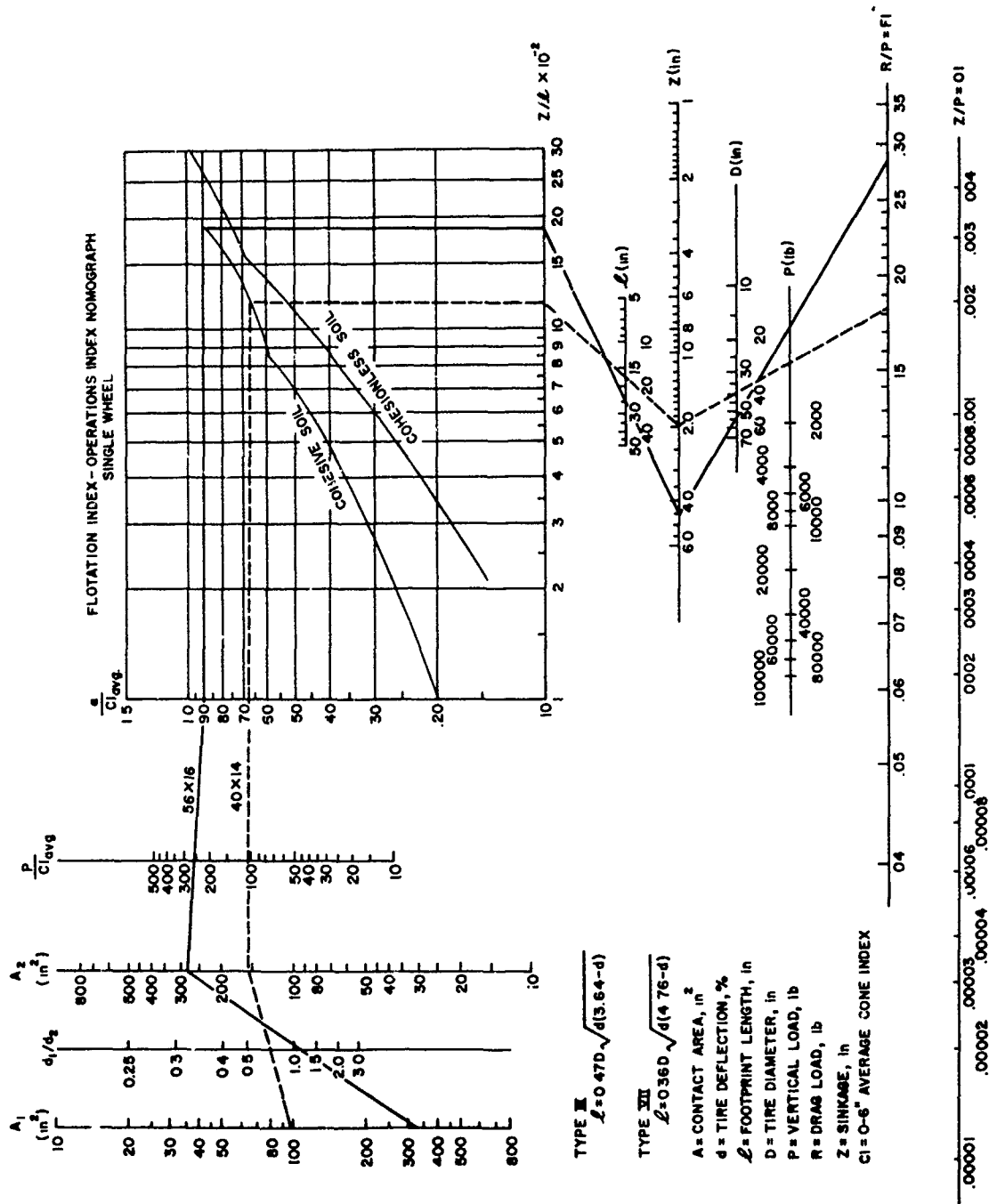


Figure 39. Nomograph for Calculation of Instantaneous Sinkage and Drag.

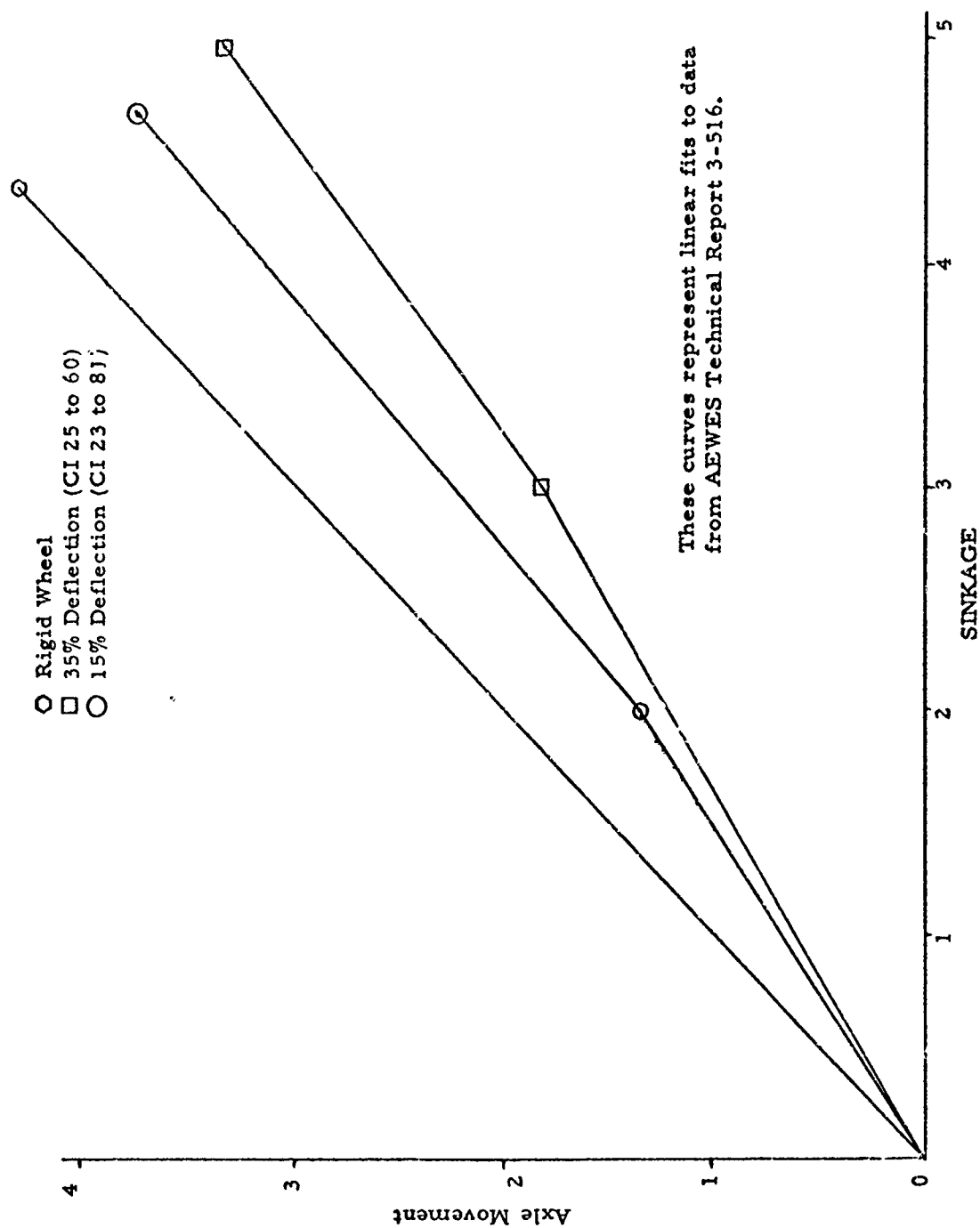


Figure 40. AEWES Data Relating Sinkage to Axle Movement.

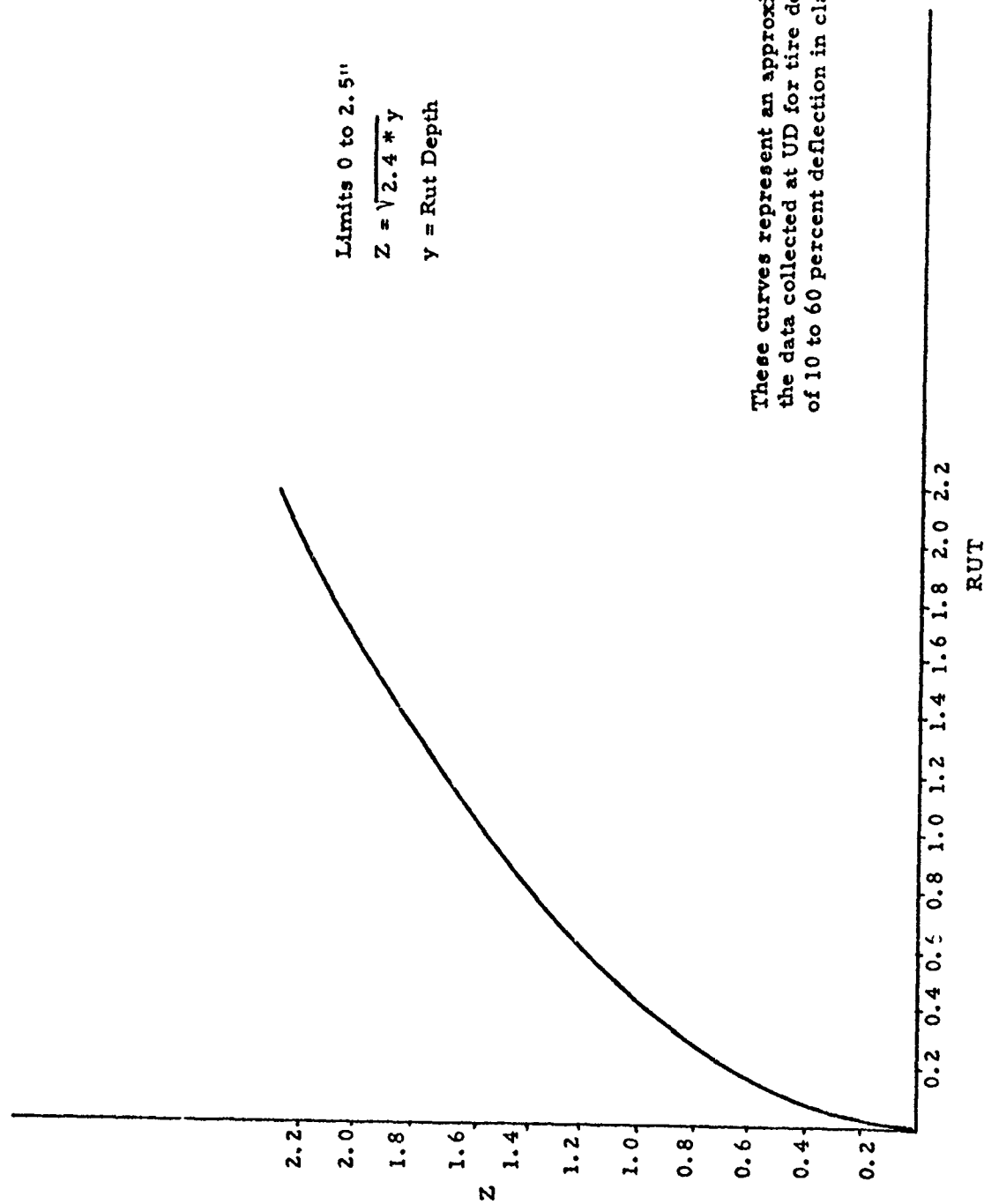


Figure 41. Relation Between Instantaneous Sinkage, Z, and Rut Depth -UD Data.

	<u>Measured Data</u>	<u>Calculated Data</u>
Z	(None)	0.75
Z _A	0.48	0.50
Z _R	0.097	0.21
$\frac{R}{P}$	0.080	0.157

The sinkage calculated does agree with the axle movement, but generates drag that is too high and a rut depth that is too high.

The "linear" portion of the axle movement occurs over the range of 3 to 10 passes. In this area the average drag is 73.9 pounds and average applied load is 758.6 pounds. The nomographic solutions for drag and sinkage using a P/CI of 16.6 are:

$$Z = 0.43$$

$$R/P = 0.095$$

Using a similar approach as before, the calculated axle movement would be 0.29 inches and rut depth would be 0.0775.

Therefore:

	<u>Measured Data</u>	<u>Calculated Data</u>
Z	(None)	0.43
Z _A	0.48	0.29
Z _R	0.097	0.0775
$\frac{R}{P}$	0.080	0.095

The measured data are those collected for a first pass which had an applied vertical force greater than desired. The mean test value for vertical force was about 760 pounds but the first pass was conducted at 800 pounds. The calculated column indicates what would have happened if the "correct" mean value had been used for the first pass.

The calculated sinkage cannot be validated with measured data because there is none. The axle motion similarly cannot be compared with but does indicate that theoretically the measurement would have been less than that observed and more nearly that measurement on the second pass. The calculated rut depth 0.080 is more closely related to the measured 0.097, and calculated drag would be 72.1 pounds for a very close correlation.

Therefore, the first sample of data indicate that first pass calculations of rut depth and drag do approximate those measured and that the drag over the ten passes does not change appreciably. Similar procedures were used for all four single wheel multipass tests and the results are tabulated below.

Test Series Number	Rut Depths			Mean Loads		$\frac{\bar{P}}{CI}$	First Pass Calculated			
	1st	5th	10th	P	D		Z _A	Z	Z _R	D
A74-0001-3	0.10	0.52	0.98	760	74	16.6	0.52	0.78	0.08	84
A74-0002-3	0.31	1.41	2.36	1060	160	22.8	0.75	0.50	0.23	159
A74-0003-3*	0.11	0.34	0.60	1170	82	22.4	0.41	0.27	0.07	82
A74-0010-3*	0.16	0.57	1.22	1050	105	31.4	0.73	0.48	0.22	116
* 8:50-10 Tires										

In all tests it appears that if first pass calculation procedures are used to calculate the drag and rut depth, that the computed and measured will be within reasonable agreement.

The second portion of the analysis was to determine whether or not predictive techniques could be evolved to calculate rut depth as a function of number of passes.

Cumulative rut depth as a function of number of passes is plotted on the figure on the following page. The ordinate reflects the ratio of measured rut depth to first pass calculated rut depth. This was done since we are after relations which can be used to predict based upon first pass calculated values. The curve indicates that there is a spread in the data, and that the rut ratio is highest for the smaller tire. For each tire the ratios decrease with increasing P/CI values.

Various parameter relations were examined to determine a commonality between all tests which could be used to evolve a predictive equation. The result can be expressed as:

$$\frac{Z_{10}}{Z_{RIC}} \cdot \left(\frac{P}{CI} \right) \left(\frac{A}{CI} \right) \left(\frac{Z - Z_r}{Z} \right)_{1C} \cdot \frac{1}{l} = 16.5$$

where: Z_{10} is the 10th pass rut depth

Z_{RIC} is the first pass calculated rut depth

$\frac{P}{CI}$ is the vertical load to cone index ratio

$\frac{A}{CI}$ is the ratio of footprint area to cone in

$\left(\frac{Z - Z_r}{Z} \right)_{1C}$ is the rebound over instantaneous sinkage for the calculated first pass

$\frac{1}{l}$ is the inverse of footprint length.

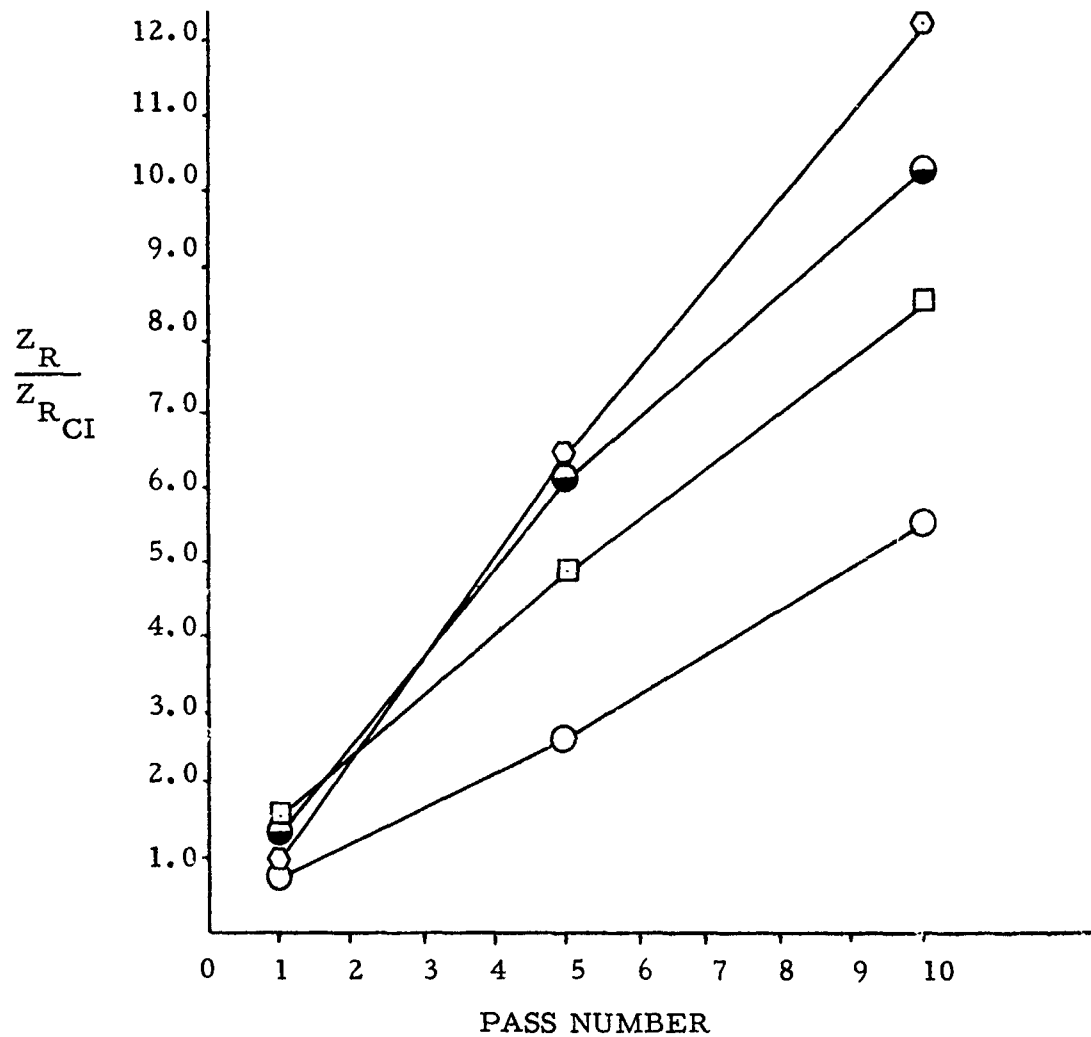


Figure 42. Variation of Cumulative Rut Depth Z_R divided by First Pass Calculated Rut Depth Z_{RCI} .

- 7:00 Tire P/CI = 16.6
- 7:00 Tire P/CI = 22.8
- 8:50 Tire P/CI = 22.4
- 8:50 Tire P/CI = 31.4

Using these relations for the mean tabulated values of \bar{P}/CI and appropriate values of A and l , the computed 10 pass rut depths are:

Test Series Number	Rut Depths	
	Measured	Calculated
A74-0001-3	0.98	0.97
A74-0002-3	2.36	2.46
A74-0003-3	0.60	0.63
A74-0010-3	1.22	1.13

If it is assumed that rut depth increases linearly with number of passes, then the rut depth can be calculated from the expression:

$$Z_N = Z_1 + \left(\frac{Z_{10} - Z_1}{9} \right) (N - 1)$$

where N = the number of the pass

Z_1 is the first pass rut depth

Z_{10} is computed from the above equation.

A more rigorous analysis could be conducted to better fit the data, but it is believed that it is not warranted at the present time. The scatter in the rut depth data as well as the differences between measured axle movement and computed, drag observed and computed, variation in cone index readings, etc., all indicate that for only ten passes, the relation found should be sufficiently accurate. A plot of the calculated data are shown on the following page in comparison with measured.

The results of the analysis indicate that first pass sinkage calculations can be used to compute the rolling drag and cumulative rut depth for rolling tires. The sinkage and drag calculations are from previous relations valid for many tire types and sizes. The cumulative rut data is based upon 7:00-6 and 8:50-10 tires at 35% deflection operation over clay with cone index values of 37 to 55.

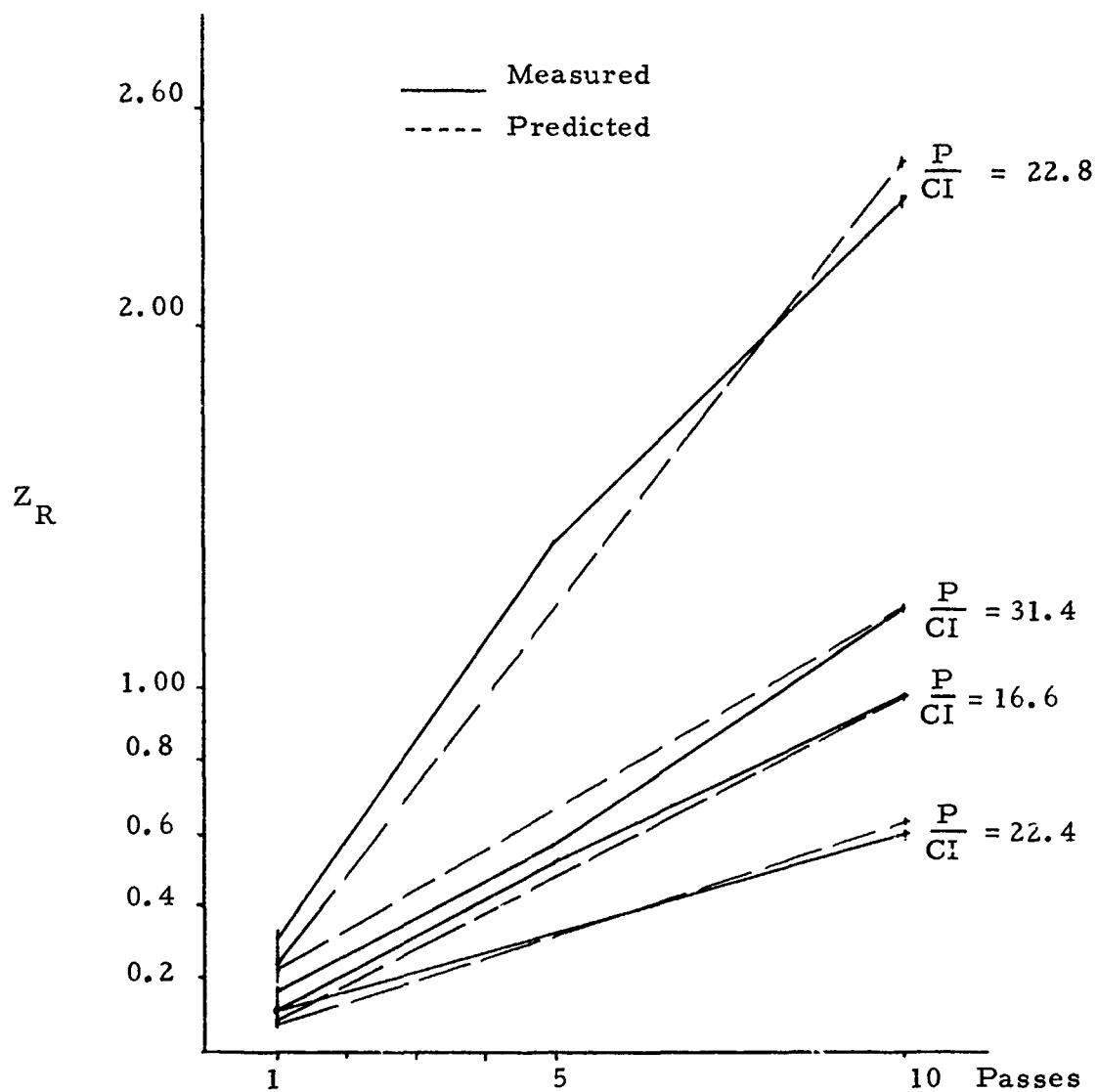


Figure 43. Cumulative Rut Depth Calculated versus Measured for 7:00-6 and 8:50-10 Tires at 35% Deflection with CI Ranges of 37 to 55 in Clay.

D. SINGLE WHEEL, RANDOM BRAKING AND PATH

Test Part 3 of the test matrix called for four tests to be conducted with two tire types, soil strengths and load levels. Sixteen passes were made randomly alternating over three adjacent paths with or without braking.

Preliminary Analysis

Tests identified as series A74-0009-3 were first examined. The preliminary information is shown below.

YEAR	74.	TEST	9.	SOIL	3.			
PASS NO.	DESIRED SLIP %	ACTUAL SLIP %	LOAD LBS	DRAG LBS	AXLE MOVEMENT IN.	AXLE VELOCITY FT/SEC	TORQUE FT-LB	
1.	0.0	2.3	1176.4	-100.3	0.21	10.357	0.0	
2.	35.0	34.0	1183.2	-505.5	0.18	10.351	-349.5	
3.	35.0	33.9	1176.4	-515.4	0.44	10.333	-348.3	
4.	35.0	34.7	1174.9	-522.7	0.13	10.449	-338.4	
5.	0.0	2.1	1163.2	-112.4	0.60	10.347	0.0	
6.	0.0	2.6	1171.3	-106.8	0.74	10.385	0.0	
7.	0.0	5.4	1184.4	-157.7	-0.02	10.350	0.0	
8.	35.0	34.6	1185.4	-565.2	0.31	10.513	-353.2	
9.	0.0	2.8	1164.5	-122.0	0.57	10.435	0.0	
10.	0.0	2.6	1164.7	-122.1	0.80	10.377	0.0	
11.	0.0	3.7	1172.7	-143.6	0.16	10.369	0.0	
12.	35.0	7.0	1173.7	-607.3	0.77	10.466	-388.4	
13.	35.0	7.0	1154.0	-580.4	1.22	10.528	-378.7	
14.	0.0	4.3	1164.0	-164.7	0.05	10.547	0.0	
15.	0.0	3.7	1137.6	-142.9	1.20	10.512	0.0	
16.	35.0	35.2	1170.7	-588.2	0.23	10.564	-328.6	

This was then retabulated in the form shown below.

<u>Pass Number</u>	<u>Path</u>	<u>Braked or Rolling</u>	<u>Axle Movement</u>		
			<u>Path 1</u>	<u>Path 2</u>	<u>Path 3</u>
1	1	R	0.90	-	-
2	2	B	-	0.85	-
3	3	B	-	-	0.81
4	1	B	0.84	-	-
5	1	B	1.43	-	-
6	1	R	1.98	-	-
7	2	R	-	0.78	-
8	2	B	-	1.43	-
9	1	R	2.06	-	-
10	1	R	2.38	-	-
11	3	B	-	-	0.72
12	3	B	-	-	1.45
13	3	R	-	-	2.32
14	2	R	-	1.76	-
15	1	R	1.45	-	-
16	1	B	2.05	-	-

It is interesting to note that the axle movement does not monotonically increase along any one path. Apparently the axle movement over one path increases as the wheel passes directly over the same rut, but decreases if there are intervening passes on adjacent lanes. This suggests that direct application on one lane causes a heaving on the adjacent lane which could or could not vary with the free rolling or braked nature of the pass.

The specific tests series mentioned was examined in detail as discussed in Appendix B. For the first analysis it was assumed that axle movement would be indicative of both instantaneous sinkage and rut depth. This was a gross simplification but was used to determine whether the motion could be predicted or not, could the variation be rationally explained or would this difference in measurements be within measurements and integration error bands.

The approach taken was to assume that the axle movement of one path is the summation of the effects of all prior passes. Also it was assumed that only adjacent lanes would influence one another. Therefore, if the center lane had a direct application of a rolling wheel, the movement would be as shown below where A_R implies applied rolling and N_R near rolling effect.

	Paths			
	1	2	3	Measurement
"Sinkages"	A_R	N_R	N_R	0.90"

Since both lanes 1 and 3 are adjacent, some near rolling effects would be generated. These are defined as N_R . The second pass was a braked pass over the second path and the cumulative motion would be ,

	Paths			
	1	2	3	Measurement
Pass 1	A_R	N_R	N_R	0.90"
Pass 2	N_B	A_B	F_B	0.85"

In this case A_B implies applied braking, N_B , near braking effect, and F_B for braking. Notice that the measured axle movement is only for the lane of directly applied load.

If there are near and far fields effects for rolling and braking that are constants, (fixed applied load, cone index and slip), then it would theoretically be possible to sum the total sinkage down to any particular pass and calculate what the measurement should be. There are 16 passes made and six unknowns. It should be possible to evaluate the constants.

This process was followed in the detailed analysis. Additional work conducted had shown that far field effects were very small indeed and consequently only near field effects were evaluated. Starting with the first pass and sequentially proceeding down the tests generating simultaneous equations, it was found that there weren't any constant values. It was found, however, that there were trends which could be established to explain the data.

For the 7:00-6 tire rolling over clay with a cone index of approximately 43, making passes separated by one tire width, the following could be used to predict axle motion

$$Z_A = \sum_{1}^n Z_R + \sum_{1}^m Z_B + \sum_{1}^k N_R + \sum_{1}^l N_B$$

where	$Z_{R1} = 0.89$	$Z_{B1} = 0.89$	$N_R = -0.06$
	$Z_{R2} = 0.55$	$Z_{B2} = 0.58$	$N_B = -0.47$
	$Z_{R3} = 0.32$	$Z_{B3} = 0.66$	

The coefficients infer that there is some predictable pattern but that the true nature is not well defined. It appears that the first pass creates more sinkage than successive passes, and that successive sinkages may or may not decrease depending upon rolling or braking. It also infers that rolling or braking on an adjacent path provides a decrease in rut depth. Near braking of -0.47 indicates that a braked pass raises the rut by approximately one half of the directly applied rut depth.

Detailed Analysis

There were four test series conducted using single wheel alternating paths and braking. Each test had available cumulative rut depth profile data over the lane just tested. Similarly each test had available the integrated motion observed for the same test. The profile data was collected over 14 stations and averaged to generate an average rut depth. These data were plotted for each test as shown in Figures 44, 45, 46, and 47.

In the figures each pass is identified as to whether it was braked or rolling. Also, the plot makes clear those passes made specifically over the middle path which is the path of interest. The first thing noticeable is that rut depth and axle movement are indeed approximately equal. Secondly, in order for the rut depths to vary as shown it quickly becomes apparent that the indirect application must indeed create a heaving as previously suspected. If the first pass is direct rolling and the second and third indirect braking, then how can the cumulative rut depth at the end of the fourth pass be approximately equal to the rut depth at the end of this first pass? If the direct braking causes a rut depth of $3/4$ inch, as indicated by the first and fifth pass, then the rut depth at the end of the third pass would have to be near the original ground level. Hence two indirect braked passes did raise the soil the equivalent of one direct rolling pass.

At this point there are many approaches possible but all theoretical possibilities are not practical. For example, it is possible to evaluate the change of rut depth as a function of number of the pass or number of the braked pass only, or rolling pass only, and generate a change in rut as a function of several parameters. However, the amount of data available doesn't permit this type of rigorous approach. The first rolling pass generates 0.9 inch rut, the second creates a change of 0.3 inches, and the third, 0.3 inches. Was this an initial step with subsequent rut increases at constant values? Or did the accuracy of the measurements and integrations generate observations of a geometric series such as 0.9 inch, 0.54

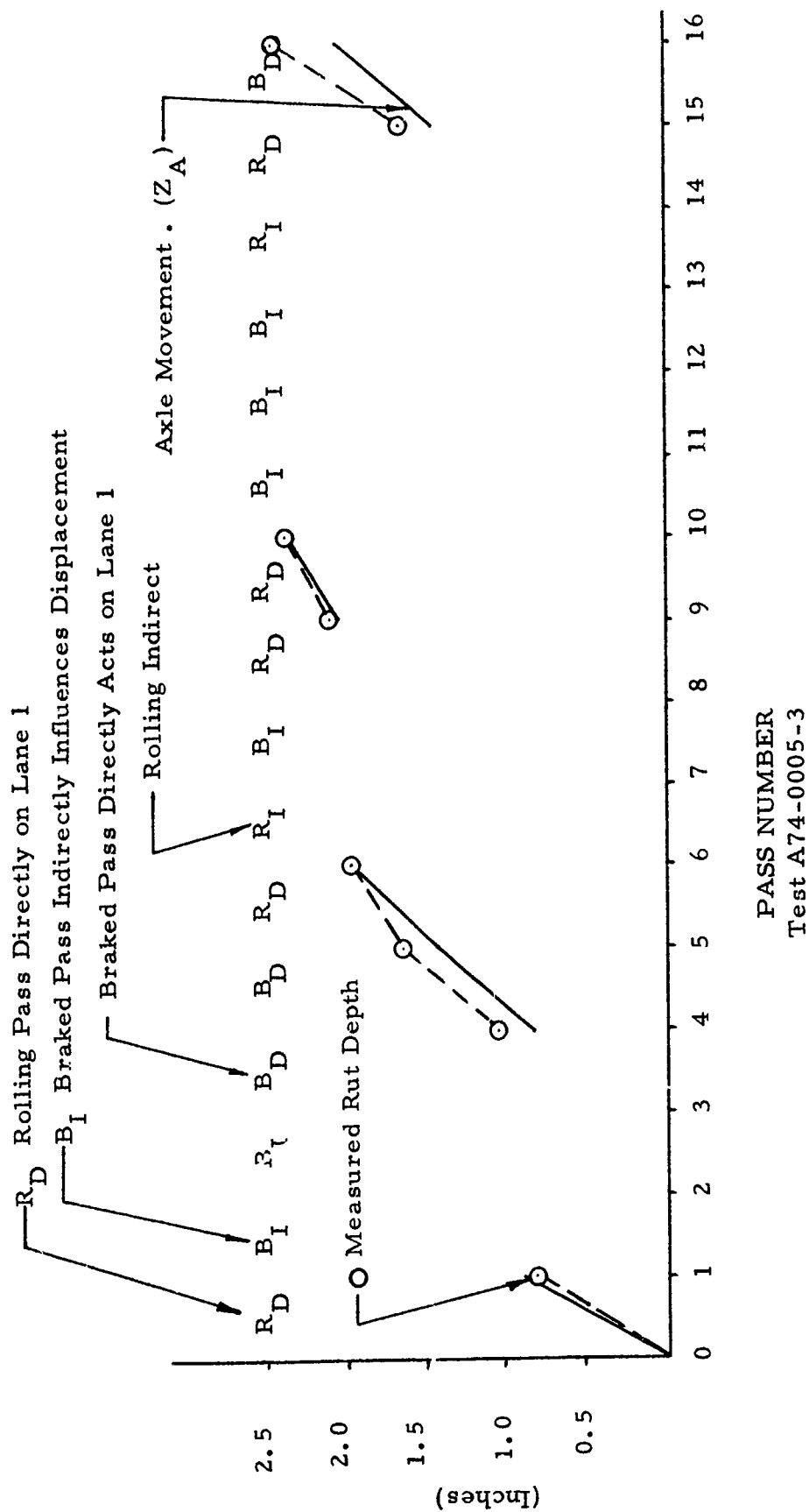


Figure 44. Deformation History of Center Lane (Path # 1) Tire Passed Over Path # 1 on Passes 1, 4, 5, 6, 9, 10, 15, 16; Hence, Z_A are Available.

Test A-740004-3
7:00-6 Aircraft Tire
Towed and Braked

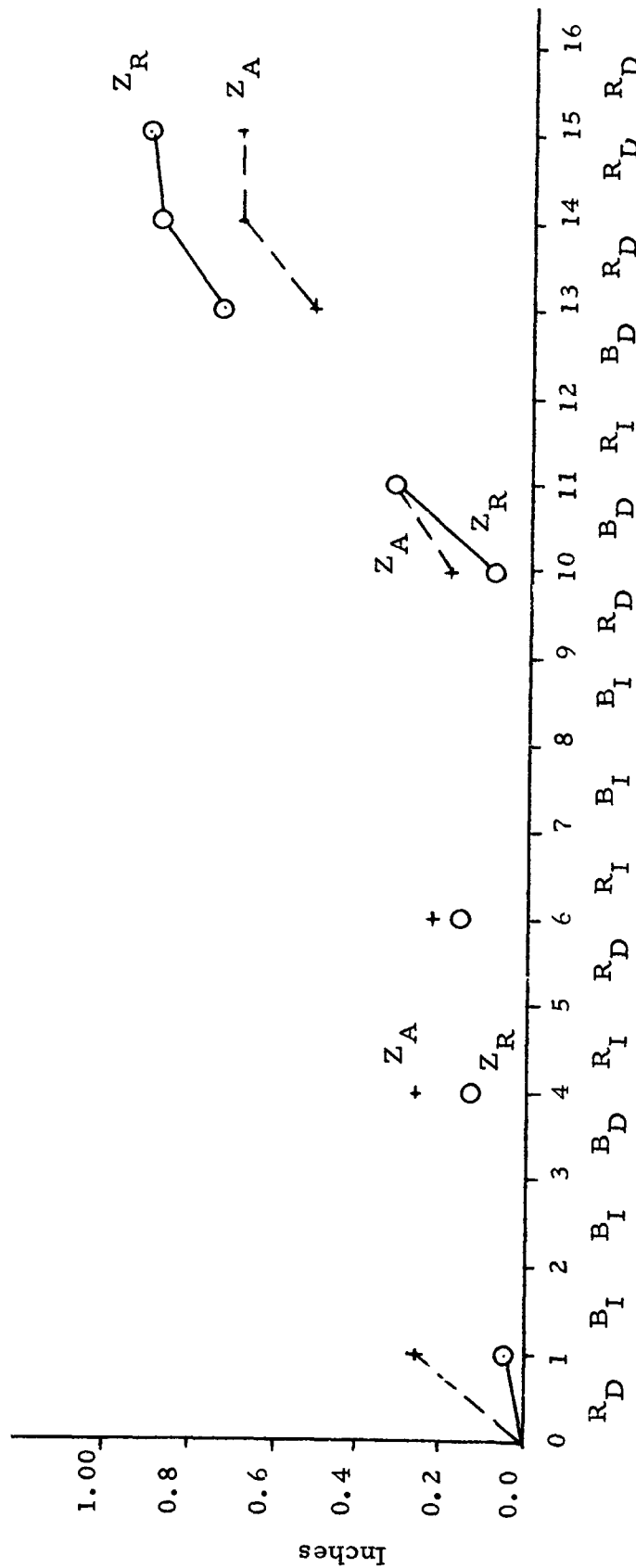


Figure 45. Cumulative Rut Depth and Axle Motion Versus Number of Passes for Center Lane.

Test A-74-0008-3
8:50-10 Aircraft Tire
Towed and Braked

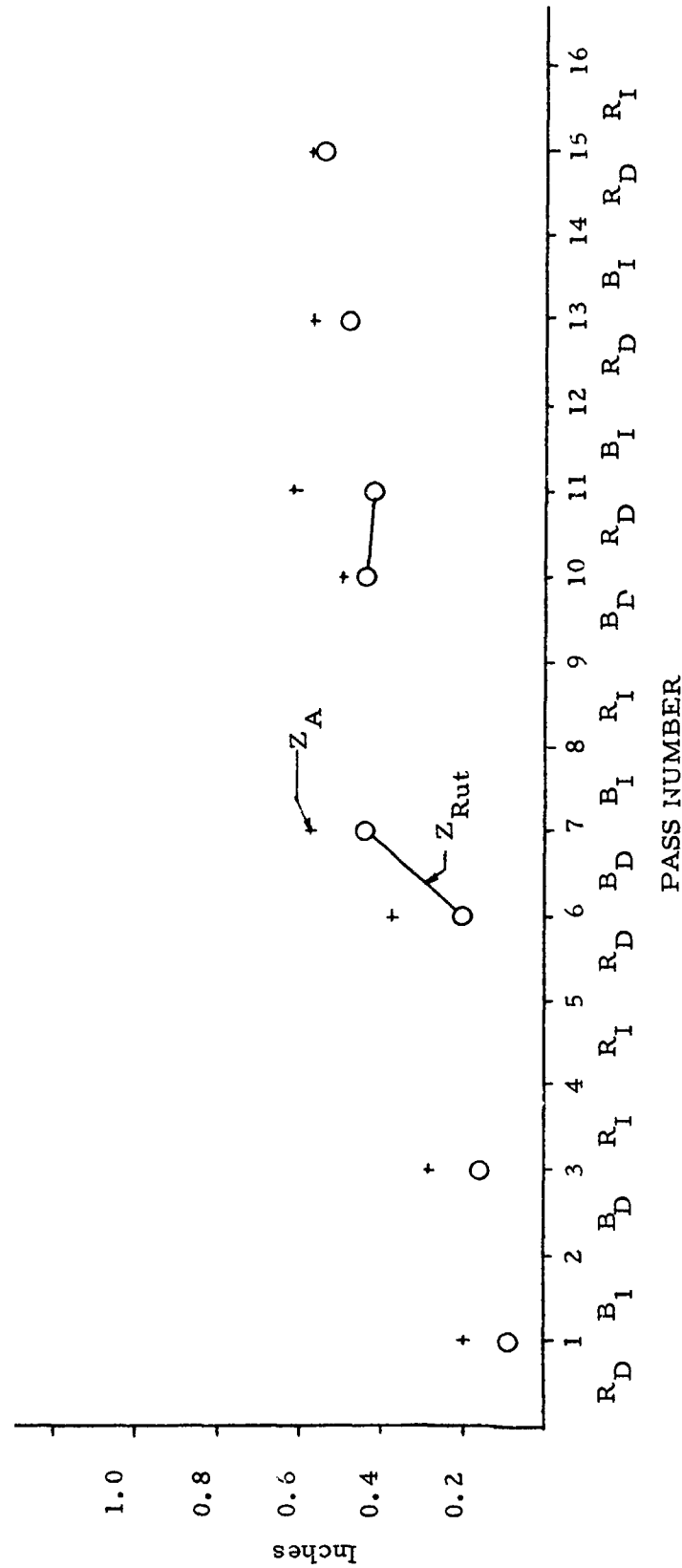


Figure 46. Cumulative Rut Depth and Axle Motion Versus Number of Passes for Center Lane.

Test A-74-0009-3
8:50-10 Aircraft Tire
Towed and Braked

R_D - Direct Rolling
 R_I - Indirect Rolling
 B_D - Braked Direct
 B_I - Indirect Braking

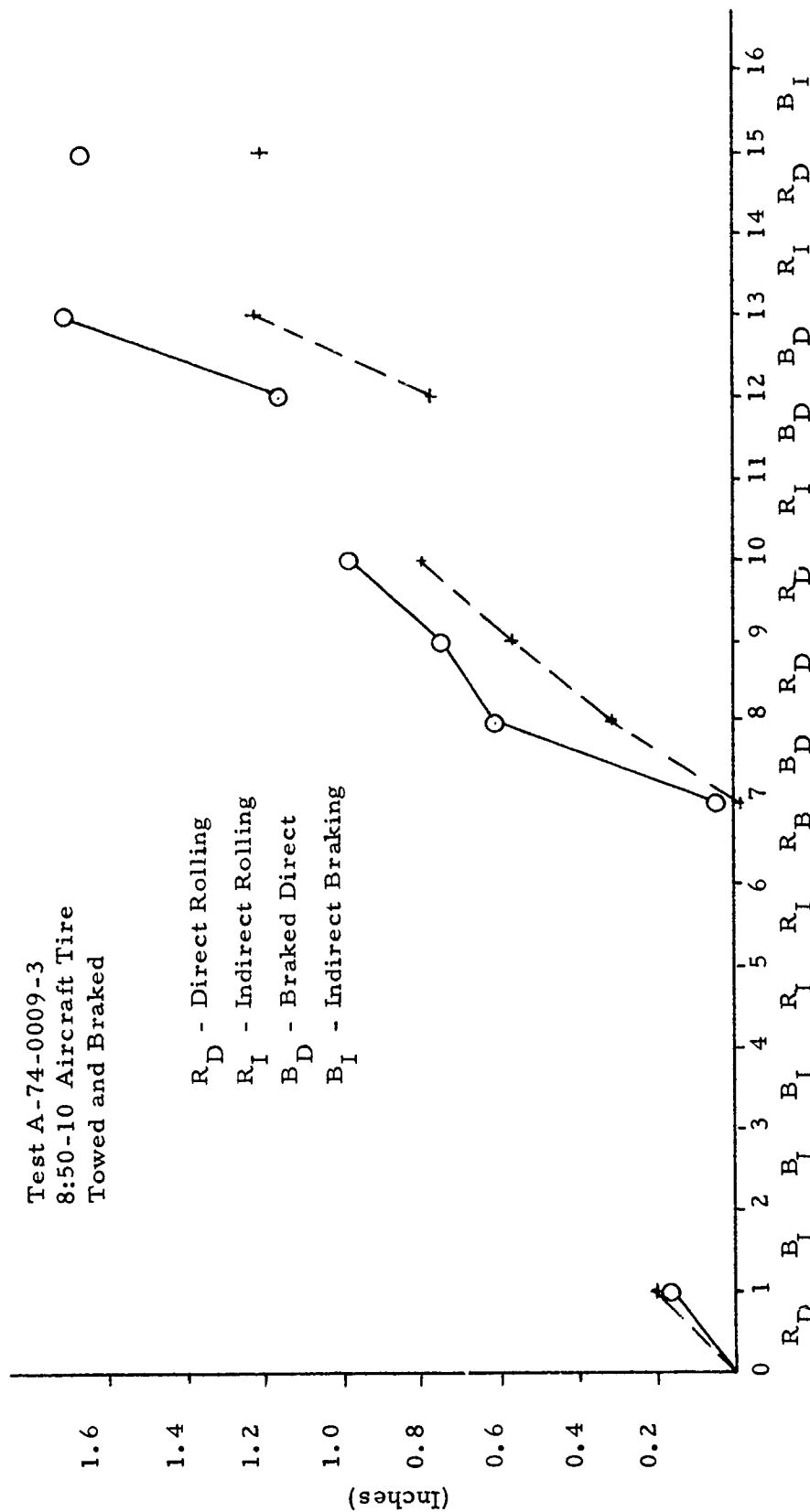


Figure 47. Cumulative Rut Depth and Axle Motion Versus Number of Passes for Center Lane.

inch, and 0.324 inch? With the limited data and referring back to the single wheel free rolling data, it seemed reasonable to assume that the first pass does create a unique rut, and that all subsequent changes are constants independent of the number of the pass. If a direct rolling rut is developed on the tenth pass, the change in rut depth will be the same as for the second pass. The braked rut increment will be a different value, but have that same value for all braked passes.

For the data of Figure 44 the coefficients for direct and indirect rolling and braking are

R_D	R_I	B_D	B_I
+0.25	+0.00	+0.75	- 0.35

where R_D is rolling direct
 R_I is rolling indirect
 B_D is braked indirect
 B_I is braked indirect.

Using these numbers the predictive cumulative rut depth for lane one would have been as shown in Figure 48. Similar procedures were used to develop coefficients for each test series. The values are shown in the following section where they are used in the predictive analysis.

E. MULTIPASS PREDICTIVE PROCEDURES

It was originally desired to have a computer routine which would permit prediction of multipass effects based upon test data. Due to delays in obtaining the data, it was not possible to generate the digital routine, but it was possible to evolve the predictive equations for the data that were available.

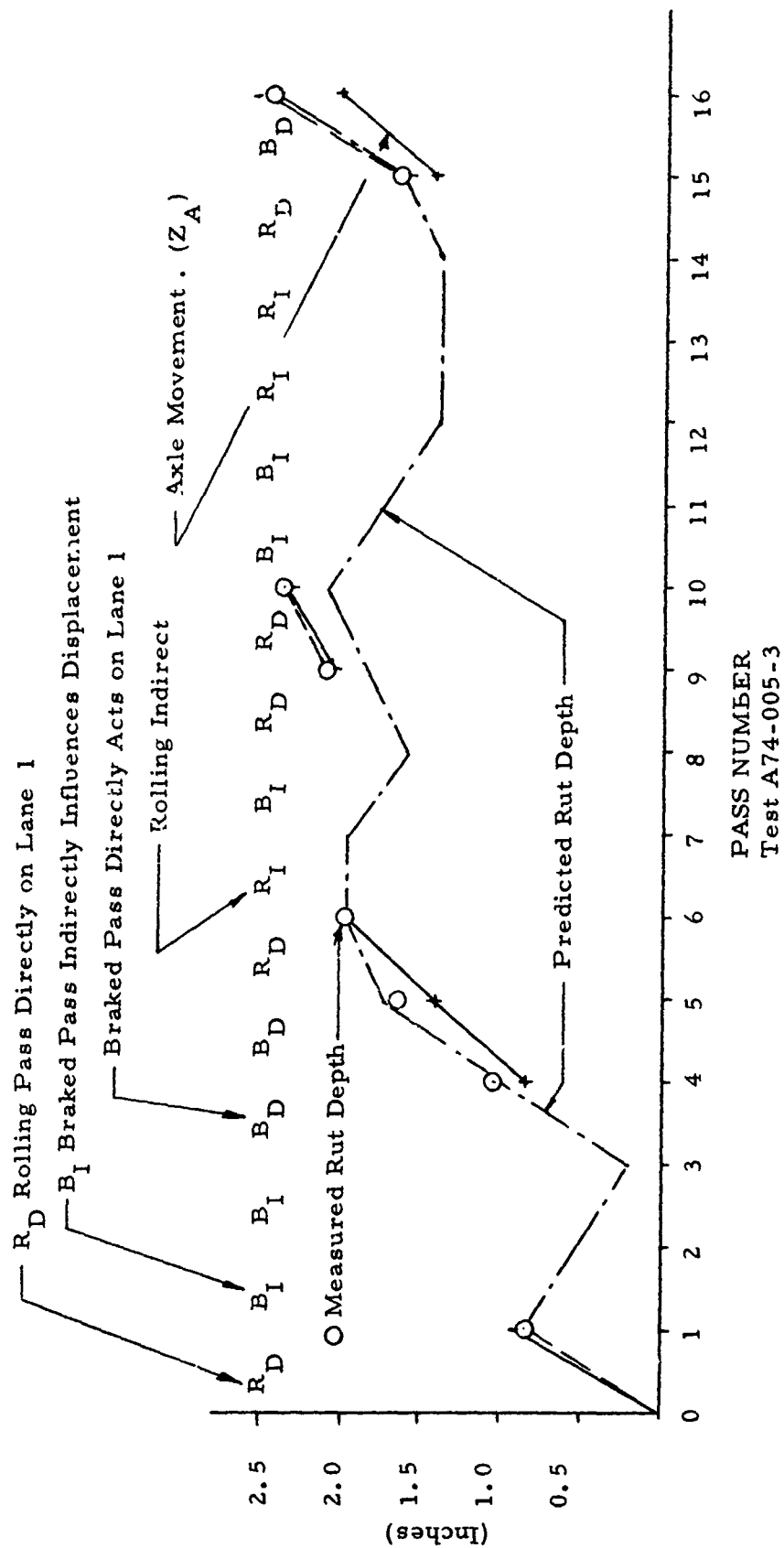


Figure 48. Deformation History of Center Lane (Path #1). Tire Passed Over Path #1 on Passes 1, 4, 5, 6, 9, 10, 15, 16; Hence, Z_A Available Rut Depth Versus Predicted Using Coefficients of page 85.

Previous sections indicated the results of tests conducted to determine the performance of a single wheel passing over a soil surface for: (1) multipass passes over the same path while free rolling, and (2) multiple passes over alternating paths while randomly braked. The data discussed in the following section does not reflect the additional data collected at the University of Dayton which may extend the applicability of the predictive equations.

Through analysis of the data, it has been shown possible to predict cumulative rut depth and drag as a function of the time history of multipass operation. If the tire passes over the same path, or an adjacent path, and rolls or is braked, it is possible to accumulate the effects of the passes. The steps are as follows.

- 1) Calculate first pass sinkage and drag as found using existing techniques.
- 2) Calculate the braked drag using existing techniques.
- 3) Calculate first pass rut depth.
- 4) Calculate incremental rut depth changes for rolling passes.
- 5) Calculate incremental rut depth changes due to direct braking or indirect rolling and braking.
- 6) Define history of multipasses.
- 7) Calculate cumulative effects.

F. DISCUSSION

Calculation of First Pass Sinkage and Drag

For a given tire with known applied load, the sinkage and drag are calculated by the equations:

$$\frac{Z}{l} = 0.11 + 0.33 (\alpha/CI) \text{ for } \frac{\alpha}{CI} \text{ in the ranges of 0.6 to 0.7.}$$

$$\frac{Z}{l} = -0.03 + 0.19 (\alpha/CI) \text{ for } \frac{\alpha}{CI} \text{ in the ranges of 0.2 to 0.6}$$

$$\text{and } \frac{R}{P} = 0.18 + 3.23 (Z/D)$$

The equations for Z/l are specifically for cohesive soil only. This is consistent with all other data discussed in this report.

The calculations can be accomplished either using the above equations or the nomogram which is available.

Calculation of Braked Drag

Braked drag is calculated by first finding the rolling tire sinkage and drag using the equations above. The ratio of fully braked sinkage to rolling sinkage is estimated to be 3.0. Therefore,

$$\frac{Z_{\max}}{Z} = 3.0$$

$$\text{and } Z_B = Z_{\max} \left(\frac{S}{100} \right)^{1/3}$$

where S is the slip desired.

The values of Z_B and S are then substituted into

$$\frac{R_B}{P} = 0.018 + 3.23 \left(\frac{Z_B}{D} \right) + 0.09 \frac{Cl. D^2}{P} \cdot \left(\frac{Z_B}{D} \right)^{1/2} \left(\frac{S}{100} \right)^{1/3}$$

First Pass Rut Depth

Previous AEWES and UD test results had shown that it was possible to relate axle motion, instantaneous sinkage and rut depth by the following expressions.

$$Z_A = 2/3 Z \quad Z < 3.0 \text{ inches}$$

$$\text{and } Z^2 = 2.4 Z_{\text{rut}} \quad Z_{\text{rut}} < 2.5 \text{ inches}$$

The first expression is a linear fit to the curve of Z_A versus Z for a tire having 35% deflection as reported in AEWES TR No. 3-516 by Smith and Frietag. The second expression is quadratic fit to rebound test results measured at UD with limits of 2.5 inches rut depth.

From the most recent test program it was found that the curves had to be modified in order to match measured axle motions and rut depths. The modifications require that:

$$Z = 0.55 + 1.09 Z_R \quad Z > 1.1''$$

$$Z^2 = 2.4 Z_R \quad Z < 1.1''$$

Therefore, if first pass sinkage is known, the rut depth can be calculated. The equation was found using the axle motion equation

$$Z_A = 2/3 Z$$

since instantaneous sinkage is not a measured parameter. It was found that computed instantaneous sinkage, Z , generates axle motions and rut depths which agree with those measured for the first pass.

Incremental Rut Depth - Rolling

The free rolling multipass data indicated that it was possible to calculate cumulative rut depth based upon first pass data. Specifically,

$$Z_{R10} = \frac{16.5 Z_{RI} \ell}{\left(\frac{P}{CI}\right) \cdot \frac{A}{CI} \left(\frac{Z_1 - Z_{R1}}{Z_1}\right)}$$

The tenth pass rut depth Z_{R10} is a function of the first pass rut depth Z_{R1} , and the other first pass parameters;

Z_1 = instantaneous first pass sinkage

$\frac{P}{M}$ = vertical force over cone index

$\frac{A}{CI}$ = foot print area over cone index

ℓ = foot print length

The variation observed in all tests was approximately linear and hence the rut depth of an n th pass is:

$$Z_{Rn} = Z_{R1} + \left(\frac{Z_{R10} - Z_{R1}}{9}\right) (n-1)$$

Incremental Rut Depth - Direct and Indirect

Data were collected for tests conducted on three adjacent paths. Rut depths were examined and plots made to determine the history of a particular path as a function of direct, load applied to the path, and indirect, load applied to the adjacent path, passes. It is assumed that adjacent lanes are influenced but that a separation of two lanes, two tire widths, generates negligible effect.

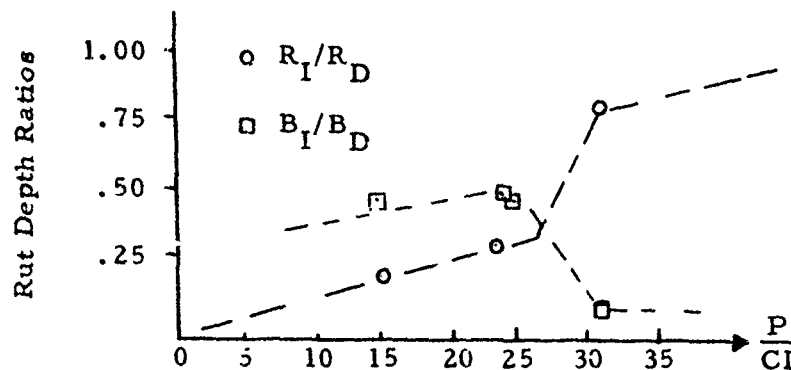
Rut depth per pass for the tests conducted can be tabulated as shown below.

Test Number	R_D	R_I	B_D	B_I	P	P/CI
A-0004-3	0.10	-0.02	0.11	-0.05	750	15
A-0005-3	0.25	-0.00	0.75	-0.35	1060	25
A-0008-3	0.06	-0.02	0.24	-0.12	1150	24
A-0009-3	0.10	-0.08	0.28	-0.02	1160	31

The terms R_D and R_I are the rut depth added per pass to direct rolling and indirect rolling. The terms B_D and B_I are for braked response.

The data were collected for one slip value and there was no apparent means of correlating the slip to the incremental rut depth values. It appears as though the direct braking does create a rut depth change proportional to braked sinkages, about 3 to 1, for the low load to cone index ratio. However, the one test at a low load for the same slip generates braked rut and rolling rut of the same magnitude. Therefore, until tests are conducted at a different value of slip, it will be necessary to remember that the braked incremental rut depth is directly related to 35 percent slip.

For computational purposes, a graph has been constructed to provide a guideline for analysis.



Define Multipass History

It is necessary to list the passes in order as they occur. The history would be of the form:

Pass	Type	Path
1	Rolling	1
2	Braked	2
3	Braked	3
4	Rolling	5
5	Braked	4
6	Braked	3
7	Braked	1
:		5
		5
n	Braked	:

The rolling path effects are reasonably well defined, but it must be remembered that the braked effects are valid only for 35 percent slip. It is assumed that the paths are multiples of tire width so that path 1 is directly down the middle of the runway and all others are offset by an integer multiple of the tire width distance.

Calculate Cumulative Effects

Cumulative rut depth is calculated by generating a running total of the effects that exist on each path. It is necessary to do this because although over 100 passes the cumulative results may be acceptable, the rut depth at any intermediate pass may not be. This is true because indirect effects apparently raise the soil and reduce the rut. Consequently, many direct passes over one lane could generate a rut that exceeded the criteria at the tenth pass, but the indirect effects of the 11th and 12th pass would make a 12 pass analysis appear acceptable if we were only concerned with the cumulative value and not running totals.

The final step is to tabulate the incremental effects with each pass. The running total would appear as shown in Figure 49.

G. SUMMARY

A procedure has been described to calculate the effects of multipass on soil surfaces. The data used restricts the analysis to the following:

- 1) Cohesive soil
- 2) Braked drag of 35 percent slip
- 3) Rut depths of approximately three inches.

Additionally, the following intuitive restriction is necessary. The data indicated that indeed the soil of an adjacent lane can be raised above its original surface by a small amount. It is not believed that this can exceed a very small amount. If calculations indicate that the indirect effects want to raise the soil level above the original ground level, the original value should be used. Cumulative depression is reasonable, cumulative "heaving" above ground level is not.

I. Input Data

Tire Type 7:00-6
 Deflection 35%
 Contact Area 43.4"
 Footprint Length 9.0"

II. First Pass Data

Rolling Sinkage $Z = 0.85$ Rolling Rut Depth 0.32
 Braked Sinkage $Z_B = 1.79$ Braked Rut Depth 1.16

III. Incremental Rut Depth Data

Incremental Rolling Rut Depth $= 0.30 = R_D$

Incremental Braked Rut Depth $= 0.90 = B_D$

Incremental Rut Ratios

$$\frac{R_I}{R_B} = 0.25$$

$$\frac{B_I}{B_D} = 0.50$$

$$R_I = 0.08$$

$$B_I = 0.45$$

IV. Multipass History - Incremental Ruts

Pass No.	Zone No.	Zones				
		4	2	1	3	5
1	1 R	-	-0.08	0.32	-0.08	-
2	2 B	-0.58	1.16	-0.58	-	-
3	5 R	-	-	-	-0.08	0.32
4	4 R	0.32	-0.08	-	-	-
5	3 B	-	-	-0.58	1.16	-0.58
6	3 R	-	-	-0.08	0.30	-0.08
7	2 R	-0.08	0.30	-0.08	-	-
		Cumulative Ruts				
1		-	-0.08	0.32	-0.08	-
2		-0.58	1.08	-0.26	-0.08	-
3		-0.58	1.08	-0.26	-0.16	0.32
4		-0.26	1.00	-0.26	-0.16	0.32
5		-0.26	1.00	-0.84	1.00	-0.26
6		-0.26	1.00	-0.92	1.30	-0.34
7		-0.34	1.30	-1.00	1.30	-0.34

Comments:

First Pass on 1
 First Pass on 2
 First Pass on 5
 First Pass on 4
 First Pass on 3

Figure 49. Sample Cumulative Rut Calculations.

SECTION IV

STATIC STARTUP FORCE ANALYSIS

A. INTRODUCTION

Another aspect of tire/soil interaction is that of the difference between start-up forces and rolling drag forces for a given tire in a particular soil. It has been recognized that the difference does exist, but no quantitative means of predicting this is available. Consequently, existing data were examined to determine how well it could be predicted using rolling tire prediction parameters.

B. DATA AVAILABLE

The sources for start-up force data are listed in Table I on the following page. These were selected because they were the only single wheel tests conducted where initial drawbar pull data existed along with peak rolling forces and average rolling force. All tests were conducted in a heavy clay soil (buckshot).

C. DATA PRESENTATION

The primary concern of previous efforts has been the development of rolling or braked drag ratios that could be predicted based upon tire/soil parameter combinations. Similarly, then, static start-up drag ratios should also be calculated for the same tire/soil parameter combinations if possible. Consequently, the static start-up drag ratio is defined as $\frac{R_S}{P}$, where R_S is the start-up drag force and P the applied single wheel vertical load. It was assumed that just as rolling drag was dependent upon the ratio of applied stress to cone index (α/CI), so should the static start-up drag.

Figure 50 presents all of the data available for the 25.00 x 28, 30 ply tire. Two curves are shown for both free rolling drag ratio and start-up drag ratio since both first pass and twentieth pass data were available. The start-up ratios show considerable scatter and the free rolling values appeared to be low. Magnitudes of the free rolling drag ratio were computed using the

TABLE I
DATA SOURCES

Reference Report	Tire Type	Inflation Pressure	Rated CBR	Applied Vertical Load (lbs)
AFFDL-TR-66-43 Part III	56x16, 24 Ply	100 psi	9.5	35,000
AFFDL-TR-66-43 Part VII	25x28, 30 Ply	50 psi	12.0	35,000
	25x28, 30 Ply	100 psi	12.0	60,000
AFFDL-TR-66-43 Part VIII	56x16, 32 Ply	100 psi	9.2	25,000
	25x28, 30 Ply	100 psi	7.8	25,000
	17x16, 12 Ply	100 psi	7.8	25,000
	34x9.9, 14 Ply	100 psi	8.4	25,000
AFFDL-TR-66-43 Part IX	25x28, 30 Ply	25 psi	3.9	25,000
	25 x 28, 30 Ply	40 psi	4.7	25,000
	25x28, 30 Ply	60 psi	4.6	25,000
	25x28, 30 Ply	80 psi	5.0	25,000
	*25x28, 30 Ply	100 psi	3.9	25,000
AFFDL-TR-66-43 Part X	25x28, 30 Ply	50 psi	4.7	35,000

* This test was not used since lane trafficked had been used before although "essentially undamaged".

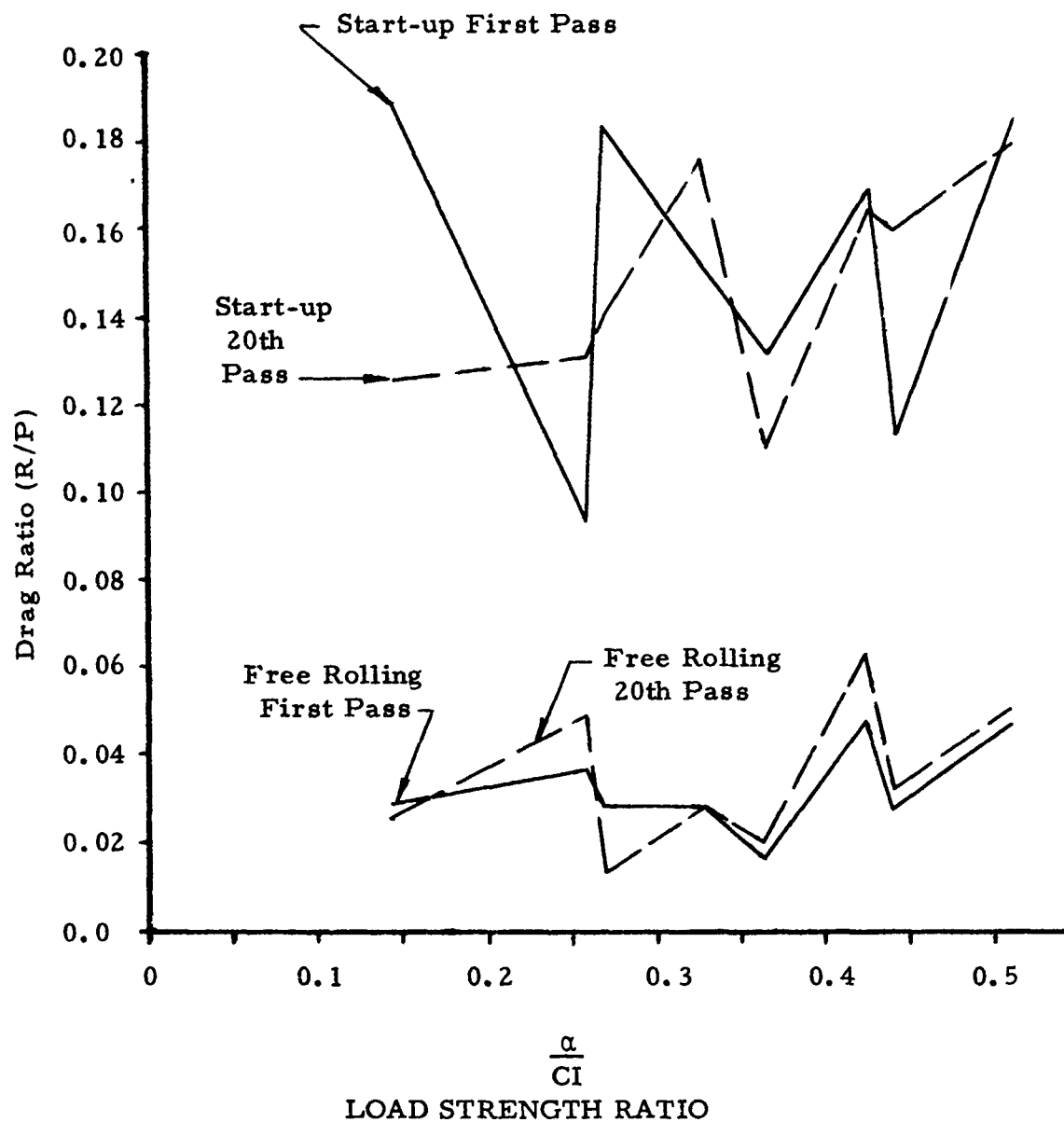


Figure 50. Drag Ratio Comparisons versus Load Strength Ratio.

available predictive equations and plotted as shown on Figure 51. The load strength ratios (α / CI) were calculated using the contact areas given in the referenced reports for the particular tire at the given tire pressure. Since there was such a significant difference between measured and calculated, the peak rolling forces were plotted as also shown. The results of examining the "peak" rolling and "average" rolling ratios is that it is apparent that the current predictive equations reflect the average force ratios for the two.

The start-up force ratio can be approximated by using the slope of the calculated rolling drag ratio and adding an intercept magnitude of 0.1. Therefore:

$$\frac{R_S}{P} = \frac{R}{P} + 0.1$$

is the gross approximation of the data.

It is possible to conduct further analysis on the data but it is not believed to be justified. The data points seem to be functions of cone index, applied load and tire pressure although plotted against α / CI which contains the same parameters. If only a given applied load and cone index is examined there are four data points that can be used. These indicate, Figure 52, that there may be a tendency to follow the linear approximation, or that there may be a curve in the response observed.

The linear plot could be an approximation because of the data scatter. The curve can also be justified. At the lower α / CI values the tire is soft relative to the soil. If the tire becomes softer, it ultimately approaches a flat tire which indeed has a large start-up force. At the higher α / CI value the tire has greater stiffness than the soil and in the limit acts as a thin sharp tire sinking deeply into a soft soil. Both extremes could suggest that there is some optimum value of applied force, tire pressure and soil index

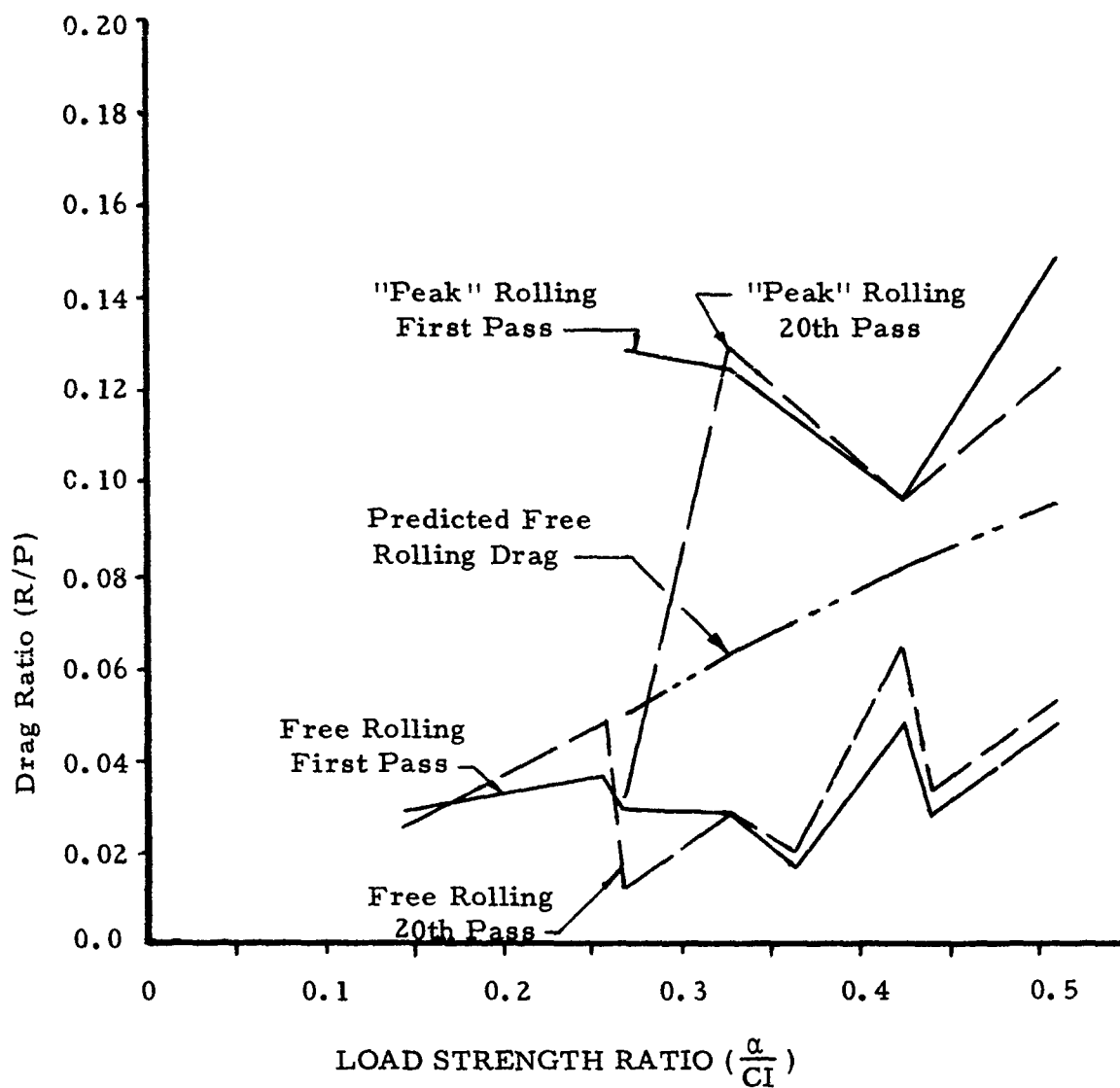


Figure 51. "Peak" Rolling and Free Rolling Drag Ratio versus Load Strength Ratio.

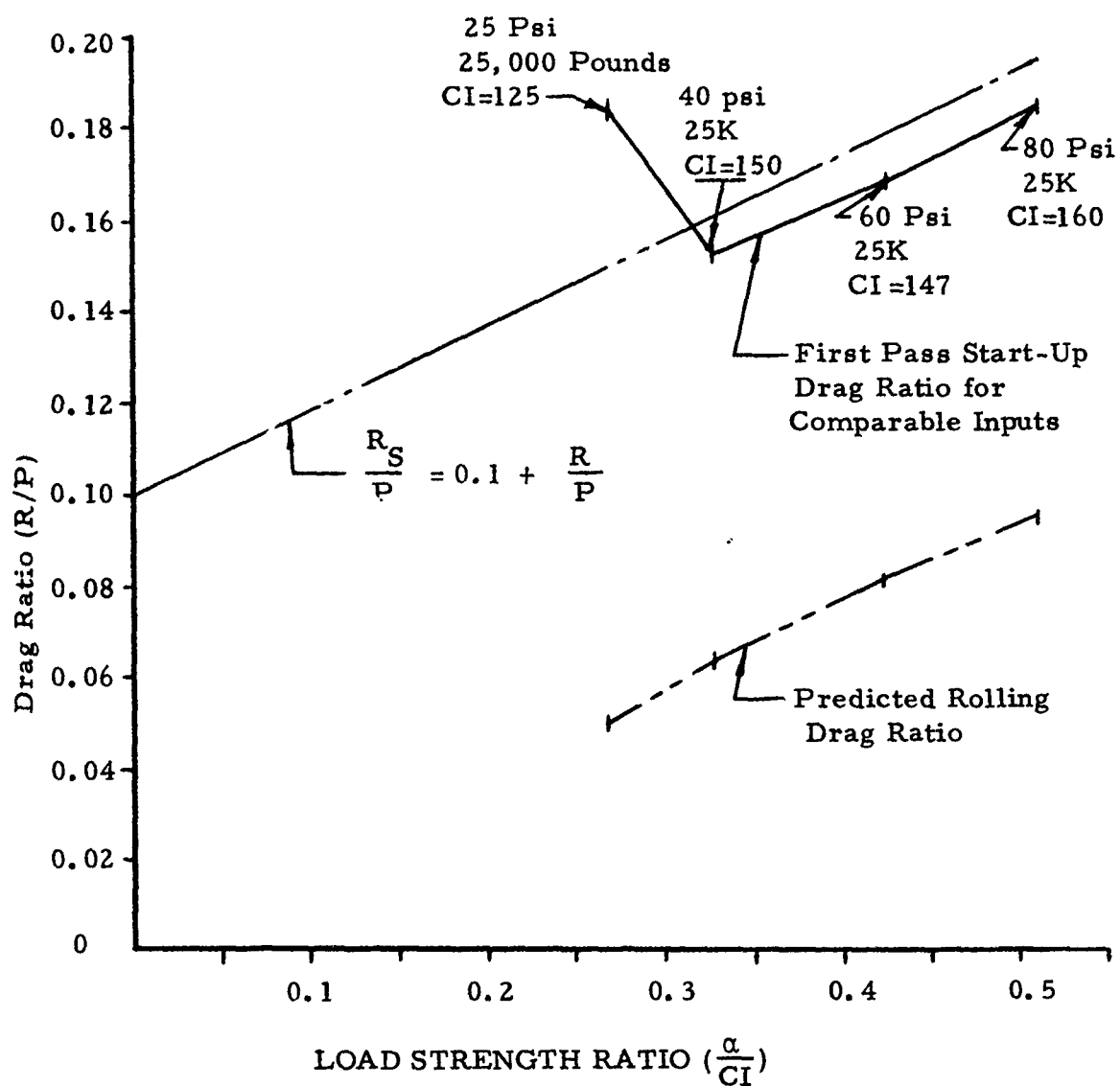


Figure 52. Start-Up Predicted Drag Ratio versus Comparable Measured Data.

to minimize start-up drag. However, the data are too limited to find the true nature of the start-up approximation.

Other attempts were made to isolate the effects of tire pressure for a given cone index, applied force for a given pressure, and other combinations of parameters. However, the data are too limited for any rigorous analysis.

D. SUMMARY

The data examined indicate that the start-up drag force is greater than the measured or predicted rolling drag force for any given load strength ratio. The number of data points available and the number of parameters to be isolated are not compatible in terms of finding exact relations. The trend of start-up drag can be seen, but how it can be more exactly predicted cannot be determined. For preliminary criteria, if necessary, the start-up drag ratio is:

$$\frac{R_S}{P} = \frac{R}{P} + 0.1$$

recognizing that this was found from tests conducted in buckshot clay with the pressures of 25 to 100 psi, vertical forces of 25,000 to 60,000 pounds, and soil strengths of CBR 3.9 to CBR 12.0.

SECTION V

TIRE/SOIL ROUGHNESS INTERACTION STUDIES

A. INTRODUCTION

Another area of the research effort to be considered was the investigation of surface roughness effects upon tire and landing gear loads. There have been many research efforts directed toward solving the problem of tire and soil interaction with roughness present. Unfortunately, there have only been a few analyses where flexible tires, soft soil and roughness have all been considered simultaneously. The purpose of the analytical representation selected to compute such an interaction, was that it should reflect tire deflection, soil compression, drawbar pull or driving torque, surface slip and the nature of the soil, whether cohesive or cohesionless.

There have been other representations similar to that described, but it is believed that the current model has greater flexibility and potential capability to predict the desired response.

B. BACKGROUND

The tire as it rolls through the soil deforms and depresses the soil. At the interface between the two, shear and normal forces act to create an equilibrium between horizontal, vertical and angular forces and inertial accelerations. The problem classically has been to evolve a set of equations that predicts evaluation of the forces at the interface which will generate the measured forces at the wheel hub and the soil instantaneous sinkage and subsequent rut depth. The problem is further complicated if we permit the tire to roll over large obstacles which cause localized forces and deformations significantly different from what would be called "steady-state rolling".

The equations that have been used to present the tire/soil response can be best explained by using an analytical model. The model consists of several elements selected to best duplicate the tire and soil without being excessively complicated.

The tire is represented by a series of rotating spring mass-damper systems. Figure 53 shows a tire segment which represents a nine-degree portion of the tire. The wheel hub is the attachment point for all radial segments, and is the location of the application of all vehicle inputs. That is, at the hub we have the vehicle initial vertical and horizontal motions and forces. The tire "tread" is represented by a mass which is separated from the hub by an elastic and viscous element. Usually these are linearly elastic elements, but for the computer routine evolved, this is not mandatory. The values of the stiffness, damping and mass are inputs to the program.

At the tire inertial element is shown the soil element. The analytical representation was selected because it was desirable to have damped inertial response, the top elements, and some representation of permanent deformation, the lower element. It is known that the drag force of the tire has a peak at some speed and then drops off. The model used permits this to occur while allowing a calculation of both instantaneous sinkage and rut depth.

As shown, the figure indicates one tire segment pushing down upon one soil element. In order to have a more valid representation of the tire, a series of these segments are used. Figure 54 indicates 11 elements used to represent the lower portion of the tire. These rotate at an angular velocity and translate forward as dictated by the velocities of the hub. As the wheel "rolls", each tire segment contacts a soil element and compresses it. If at the surface we have a normal and tangential force, it is possible to write the equation of equilibrium as shown in Figure 55.

The free body diagram indicates that a moment is applied at the hub. This can be either positive or negative depending upon whether or not the tire is torque driven or braked. Each tire segment contributes to the summation of forces and moments as it rotates from a starting position through an arc of 90 degrees.

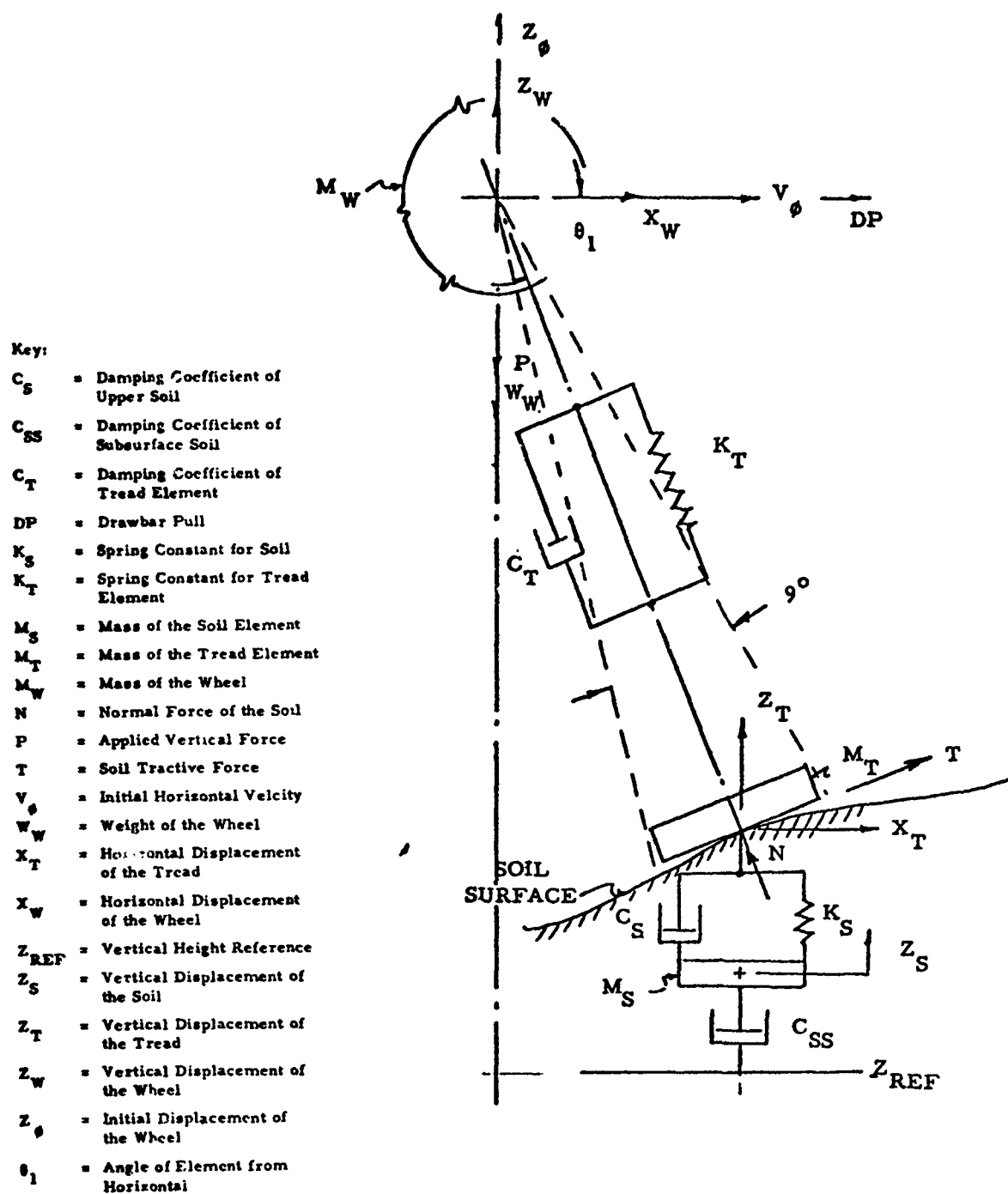


Figure 53. Tire/Soil/Roughness Model.

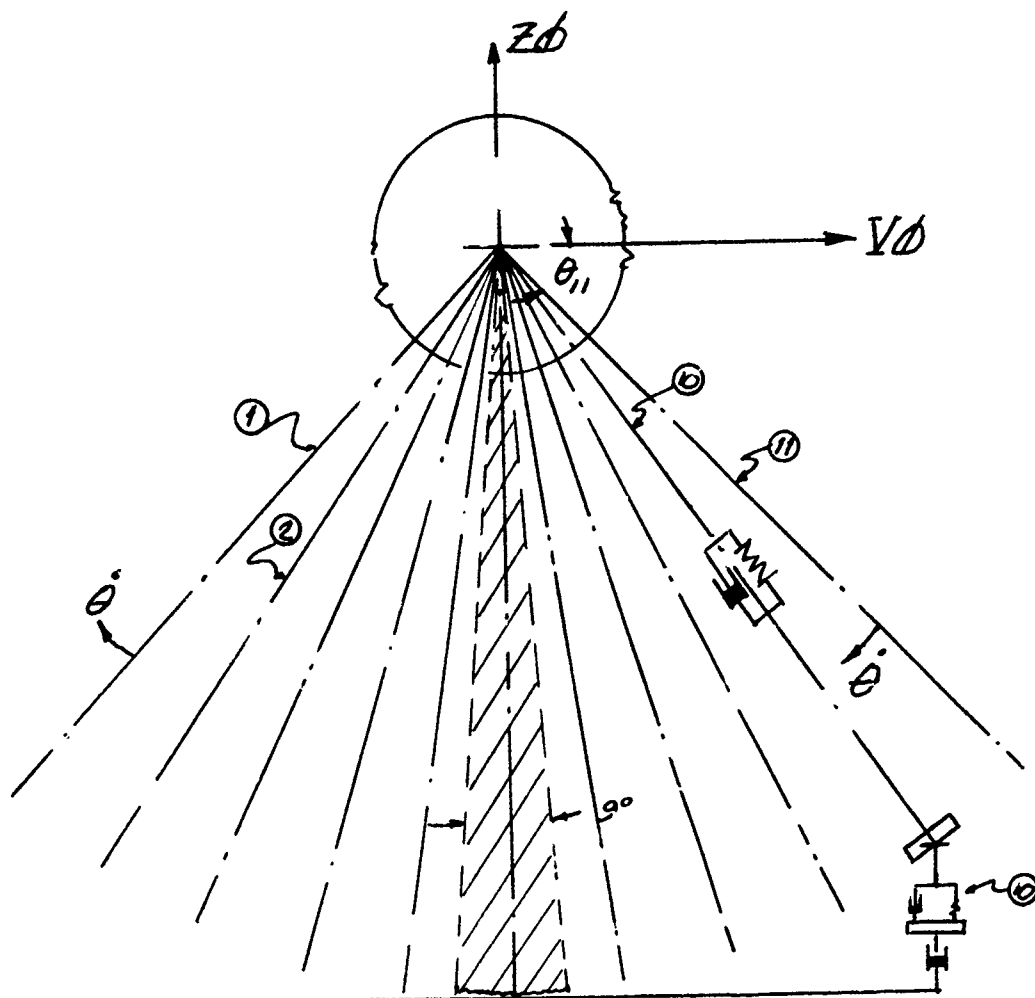
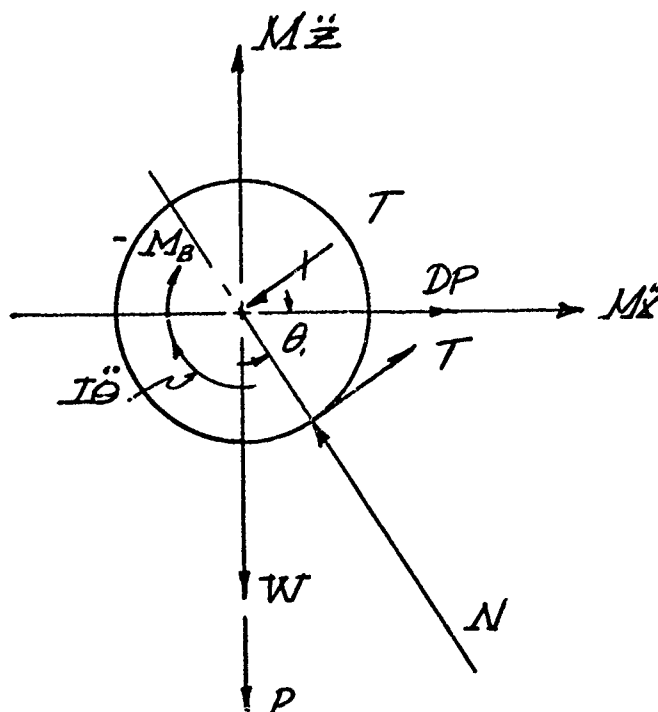


Figure 54. Schematic of Eleven Elements Rotating at Angular Velocity θ .



Key:

- DP = Drawbar Pull
- I = Mass Moment of Inertia of the Wheel and Tire
- M_B = Braking Torque
- M = Mass of Wheel and Tire
- N = Soil Normal Force
- P = Applied Vertical Force
- T = Soil Tractive Force
- W = Total Weight
- \ddot{X} = Horizontal Acceleration
- \ddot{Z} = Vertical Acceleration
- θ_1 = Angle of One Element
- $\ddot{\theta}$ = Angular Acceleration

Figure 55. Free Body Diagram of Complete Wheel.

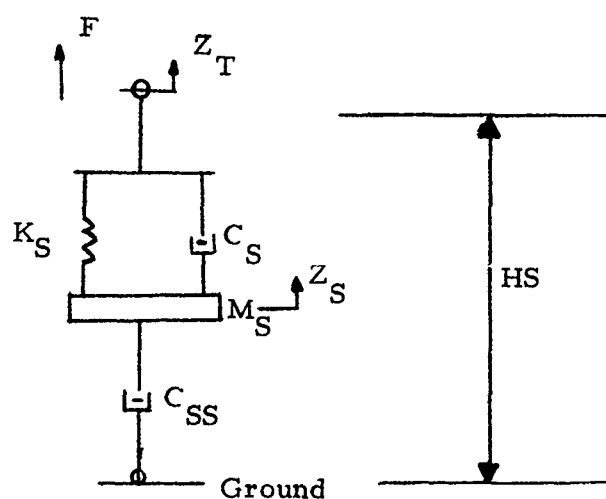
The soil surface is represented by a series of line segments defined by vertical position as functions of displacements along the "runway". The points are input into the program as ordered pairs.

The calculation of resulting tire/soil forces is made by following the position of the tire "tread" and determining where and when the intersection of tire and soil contour begins. When this occurs, the integration of the differential equations begins and the motion of the hub results. The outputs from the program are hub motions and forces, tire/soil interface forces, instantaneous sinkage as well as rut depth prediction.

The Soil Element

The soil is modeled by having a spring-mass-damper system resting on top of a viscous element. This configuration was chosen because of its capability to produce a "resonant" force. Additionally, the two dependent parameter model permits instantaneous sinkage as well as rut depth prediction.

The model is shown below with a positive applied force.



The applied force, F , is developed at the tire tread interface. The upper stiffness and damping elements are K_S and C_S , respectively. The soil mass, that beneath the tire tread, is M_S , and the "subsoil" damping is characterized by C_{SS} . The soil motion is all referenced to an inertial ground.

At the applied force,

$$\Sigma F = Ma = M\ddot{Z}_T$$

since no mass is present

$$\Sigma F = 0$$

$$\therefore F_1 + K_S(Z_S - Z_T) + C_S(\dot{Z}_S - \dot{Z}_T) = 0$$

or,

$$F_1 = K_S(Z_T - Z_S) + C_S(\dot{Z}_T - \dot{Z}_S).$$

The force supplied by the tire equals the resistance developed by the "upper" soil.

For the "soil" element,

$$M_S\ddot{Z}_S = K_S(Z_T - Z_S) + C_S(\dot{Z}_T - \dot{Z}_S) - C_{SS}\dot{Z}_S$$

or,

$$M_S\ddot{Z}_S = F_1 - C_{SS}\dot{Z}_S.$$

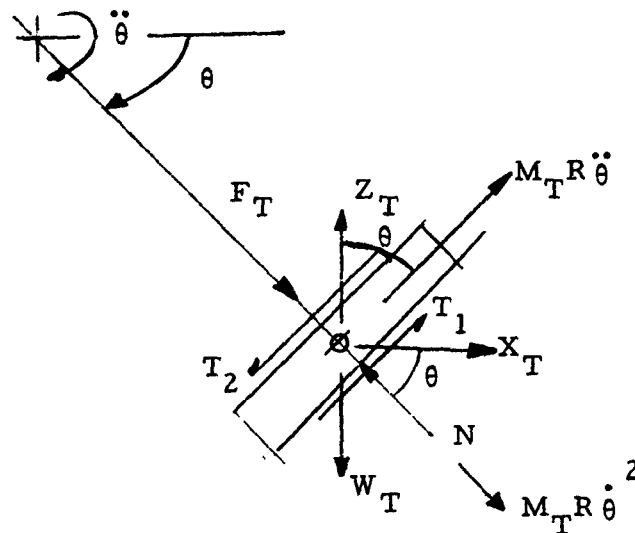
These are the equations necessary to define the response of the soil. The only remaining aspect is that a logical control must be added such that the force at the tire tread cannot be a tensile force. The soil cannot pull the tread. When the force gets to zero, all soil forced response must stop and transient response follow.

The soil response starts whenever the tread contacts the soil. At small angles of tire impact, when θ is small, the model is intuitively unrealistic since it is likely that a cohesionless soil would be pushed out of the way rather than compressed. However, in order for the equations of soil and tread to be consistent, the same action/reaction force and displacements for both, it is necessary to model the interaction as though only compression occurs.

Later it will be shown that the normal force component that acts on the tire will be used to calculate the frictional forces developed.

Tire Tread

A portion of the tire is represented by the tire "tread" at the interface between tire and soil.



The tread is acted upon by the soil, a normal and frictional force, the inertial effects of the rotation, and the elasticity and damping of the tire. The forces are shown with the tire accelerating positively. Summing forces in the vertical direction,

$$\Sigma F_V = M_T \ddot{Z}_T$$

$$M_T \ddot{Z}_T = N \sin \theta + T_1 \cos \theta - T_2 \cos \theta + M_T R \ddot{\theta} \cos \theta - M_T R \dot{\theta}^2 \sin \theta - F_T \sin \theta - W_T$$

It is assumed that the traction across the tread is transferred directly without any moment. Therefore $T_1 = T_2$ and the equation becomes

$$M_T \ddot{Z}_T = N \sin \theta + M_T R \ddot{\theta} \cos \theta - M_T R \dot{\theta}^2 \sin \theta - F_T \sin \theta - W_T.$$

The forces due to the angular motion of the wheel can also be eliminated since they are internally accounted for. That is, the centrifugal force of the element is balanced by a component of the tire reaction F_T . A similar component exists on the other side of the wheel hub, and hence the net effect upon wheel response is negligible. The component due to angular acceleration is accounted for in that no net force on hub is created and the moment generated is contained within the product of the mass moment of inertia of the entire wheel multiplied by the wheel angular acceleration. Therefore, the tread equation reduces to

$$M_T \ddot{Z}_T = N \sin \theta - F_T \sin \theta - W_T.$$

The normal force, N , is the normal of the soil force F_{S1} , hence

$$N_1 = F_{S1} \sin \theta \text{ in magnitude.}$$

However, since F_{S1} was derived for a positive displacement of the soil and the force acting upon the tire is equal and opposite to that acting on the soil, $N_1 = -F_{S1} \sin \theta$, is the correct equation for the free body of the tread.

At the surface of the tire a frictional force is developed which is carried into the elastic side wall. The equation used for this was:

$$T = A_Z (\sigma \tan \phi - C) \mu (s)$$

where T is the frictional forces in pounds

A_Z is the tread area, square inches

σ is the normal stress, pounds/square inch

$\tan \phi$ is the angle of internal soil friction, radians

C is the soil cohesion, pounds/square inch.

$\mu (s)$ is the cube root of the slip.

The equation was developed in Reference 3 and provides a means of calculating the surface force as a function of both soil properties, and local slip.

The area of the tread is calculated assuming that each tread segment represents nine degrees of arc. This, with the tire diameter and section width, is sufficient to calculate a tread area. Specifically, for nine degrees,

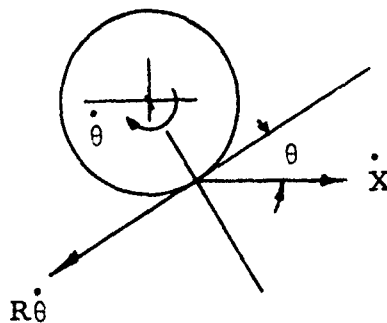
$$A_Z = B_T (.15708) RW$$

where B_T is the section width, and RW is the tire radius.

Slip is defined as

$$SLIP = \frac{V_w - V_a}{V_w}$$

where V_w is the peripheral speed of the wheel, and V_a is the horizontal speed. However, for the portion of the tire which is touching a slope, the slip must be redefined to account for the components along the slope.



Slip is now the difference between peripheral speed and the component of the horizontal speed divided by the peripheral speed

$$SLIP = \frac{R\dot{\theta} - \dot{X} \sin \theta}{R\dot{\theta}}$$

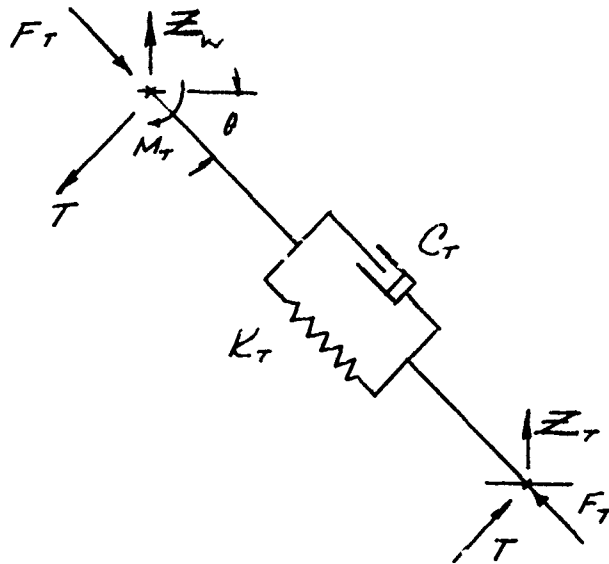
This reverts to the original definition for tangency at the bottom of the wheel.

If the peripheral speed is greater than the translational component, the slip is positive as a powered wheel, whereas negative slip infers braking.

The frictional force, T , originally defined in the tire tread free body is shown as a positive force upward. This is consistent with a positive slip. If the peripheral velocity exceeds the translational component, slip is positive, the wheel slips over the soil and a friction force is developed that acts to retard the motion in a positive direction.

Tire Elastic-Viscous Element

The tire "side" wall is an elastic and viscous element in parallel.



It is assumed that the friction force, T , can be carried by the bending stiffness of the side wall element without deformation. Therefore, T is balanced by T and M_T at the top of the element, the wheel hub. The element is an axial force element and the force is:

$$F_T = K_T (\delta_T - \delta_W) + C_T (\dot{\delta}_T - \dot{\delta}_W)$$

where K_T is the stiffness in pounds/inch

C_T is the damping in pounds/inch/second

δ_T is the axial deformation at the tire tread

δ_W is the axial deformation of the hub.

Since

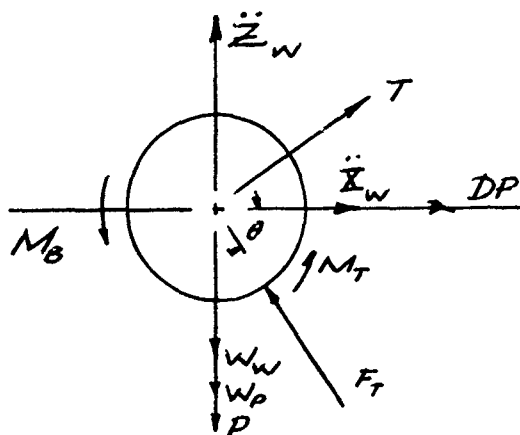
$$Z_T = \delta_T \sin \theta, \text{ and}$$

$$Z_W = \delta_W \sin \theta$$

$$F_T = (K_T (Z_T - Z_W) + C_T (\dot{Z}_T - \dot{Z}_W)) / \sin \theta .$$

Wheel Hub

The free body diagram for the wheel hub is shown below.



where DP is the drawbar pull,

W_W is the weight of the payload

W_P is the weight of the payload

M_B is an applied torque (positive or negative)

P is an applied vertical force.

The equations of motion are:

$$(M_P + M_W) \ddot{Z}_W = T \cos \theta + F_T \sin \theta - W_W - P - W_P$$

$$(M_P + M_W) \ddot{X}_W = T \sin \theta - F_T \cos \theta + DP$$

$$I_W \ddot{\theta} = -M_T - M_B .$$

The only variable not previously defined is M_T . This is the moment generated by the friction at the soil and carried through the side wall. It is therefore,

$$M_T = T \cdot r$$

where

$$r = R_W + \delta_W - \delta_T,$$

the undeformed radius R_W , plus the extension of the hub, minus compression at the tread. Since

$$\delta_W = Z_W / \sin \theta, \quad \delta_T = Z_T / \sin \theta,$$

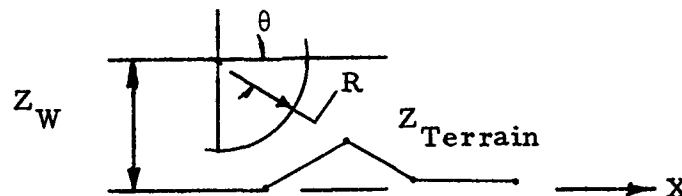
then

$$r = R_W + (Z_W - Z_T) / \sin \theta.$$

Logical Controls

The equations developed are necessary to calculate the force and moment response of a soft tire as it compresses a soft soil. However, the equations reflect the response as though at some initial time tire and soil are touching with known initial conditions. This is not true in that we wish to have a tire element rotate until it touches the soil, and then the response is calculated for whatever conditions existed at that moment.

Recognition of tire-soil impact is accomplished by computing the difference in elevation between the tread and soil at any particular time.



C. ROLLING TIRE COMPUTER PROGRAM AND SAMPLE RESULTS

The equations evolved were programmed using the MIMIC computer program detailed in Reference 19. A complete listing of the program is shown in Appendix B. Many comment cards have been included in the printout to indicate the appropriate steps being taken for each block of cards.

A sample run was made using the following input conditions.

Initial horizontal velocity	240. inches per second
Initial vertical velocity	0. inches per second
Initial vertical applied force	0. pounds
Drawbar pull	500. pounds
Braking moment	0. inch pounds
Payload weight	500. pounds
Wheel weight	500. pounds
Wheel height above ground reference	30. inches
Tire radius	25. inches
Wheel moment of inertia	500. pound-inch -seconds square
Tire segment weight	5. pounds
Tire Segment stiffness	500. pounds
Tire segment damping	5. pounds per inch per second
Tire width	20. inches
Weight of soil segment	20. pounds
Soil segment stiffness	2000. pounds per inch
Soil segment damping	0. pounds per inch per second
Subsoil damping	20. pounds per inch per second
Height of soil above reference	6.5 inches
Soil cohesion	1. pound per square inch
Internal friction angle	0.016 radian

The numbers used are generally indicative of realistic values although some of them are strictly estimates. The soil model characteristics are not known since we do not know how a soil "segment" reacts. This doesn't, however, eliminate the use of real world value for cohesion and integral friction at the tire tread/soil interface. Consequently, those values are for a low strength clay soil.

The computed drag and slip are shown on Figure 56. The pilots indicate that in free falling for one-tenth of a second, transient response is still present after 0.65 seconds of motion. Assuming that steady state drag will be about 100 pounds, the drag ratio would be 0.1. The sinkage computed for the same impact is approximately 2 inches for a 50-inch diameter wheel. Therefore, $Z/D = 0.04$ and this corresponds to a rolling drag ratio of 0.17 for CBR 6 soil. Consequently the drag is at least the right order of magnitude for a rather hypothetical wheel.

The computation shown required approximately five minutes of computer time using a CDC 6600 series computer. If the routine had been run long enough for a steady state solution and then a "roughness" introduced, it is apparent that significant computer time would be required. Additional study is required to more thoroughly evaluate the model and establish whether or not sufficiently accurate results can be established with a single representation.

D. ROUGHNESS INTERACTION STUDIES SUMMARY

A computer program has been developed which is designed to calculate the effects of soil surface roughness upon the sinkage and drag of a pneumatic tire. The program has the capability to utilize true soil properties and realistic tire and wheel characteristics and applied loads, and surface roughness. The one aspect remaining to be solved is that of defining the analytical characteristics of soil and tire stiffness and damping. The program was developed in order to use as input existing test data for rolling

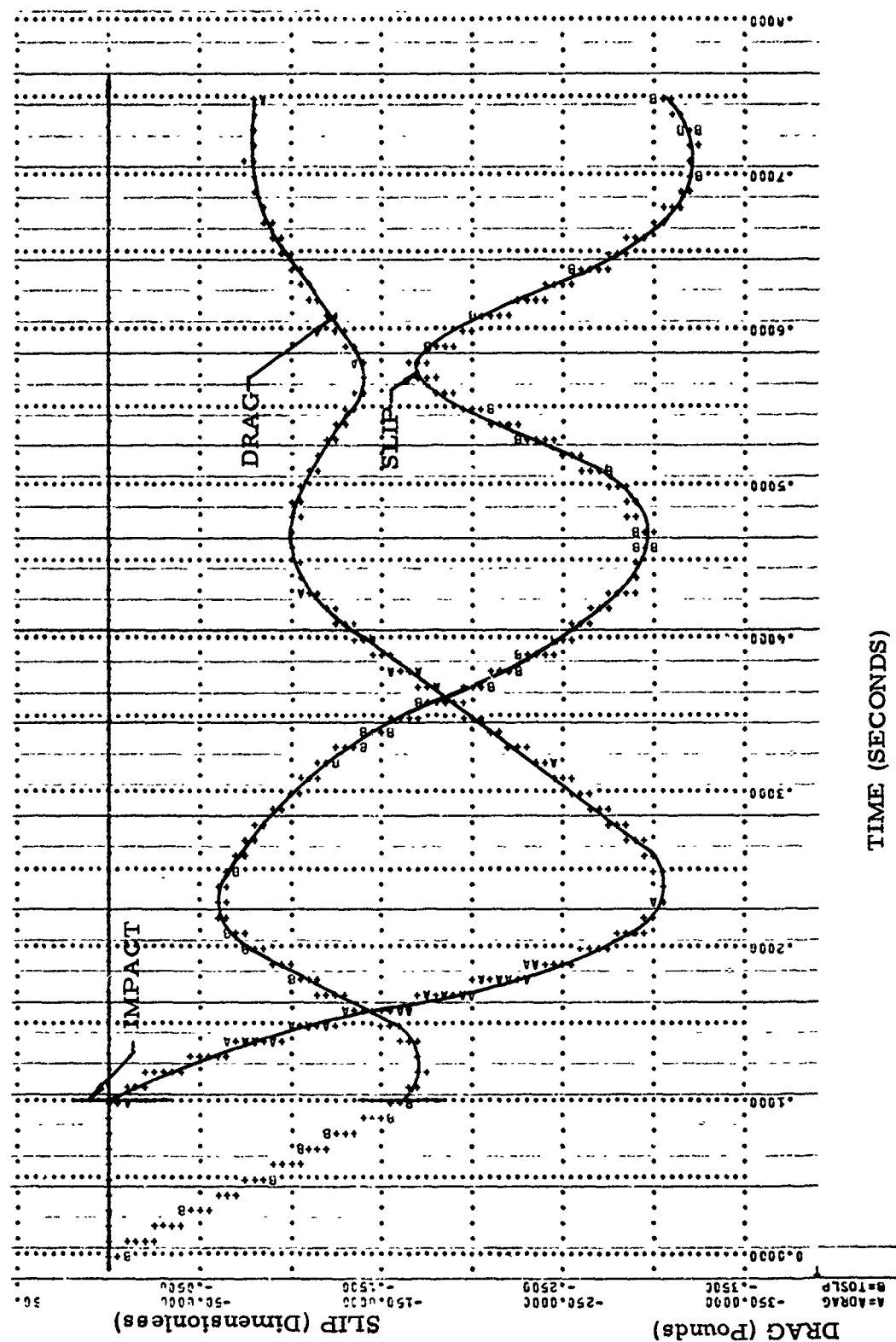


Figure 56. Transient Response of Theoretical Soft Tire in Soft Soil.

tires. Since the test data would reflect the input and outputs for given soils and tires, the model coefficients would be adjusted to match the measured output of drag, instantaneous sinkage and rut depth. The program was developed to the point of generating the desired outputs, but it was not possible to conclude the effort with test data which are available. Hopefully, in the future such steps will be taken.

SECTION VI
ADDITIONAL EFFORT IN TIRE/SOIL INTERACTION

A. TRAINING SESSION - SHORT COURSE ON LANDING GEAR/SOIL INTERACTION AND FLOTATION SYSTEM DESIGN

A short course on landing gear/soil interaction and flotation design was held at the University of Dayton on September 18 and 19, 1974. The course was designed to disseminate the latest information available on landing gear/soil interaction phenomena and associated aircraft design and operation criteria for soil runways to government and industry personnel. A total of 21 persons, representing airframe manufacturers, aircraft tire manufacturers, governmental agencies, and one university were present.

Three volumes of material were provided to all participants along with video tape explanations and workshop problem sessions. The areas discussed were:

- Aircraft tire/soil sinkage and drag performance
- Multiwheel sinkage and drag performance
- High speed sinkage and drag performance
- Braked tire sinkage and drag performance
- Turning performance on soils
- Takeoff and landing performance on soils

A complete set of instructional materials can be obtained for the cost of reproduction upon request to:

Dr. David C. Kraft
Dean of Engineering
University of Dayton
Dayton, Ohio 45469

SECTION VII

DEVELOPMENT OF A FULL-SCALE TEST PROGRAM

A. INTRODUCTION

The following proposed test plan outlines a series of tests to be conducted using a full-scale aircraft operating on a soil runway. The type of aircraft is not specified, but the parameters to be controlled and measured should be applicable to any aircraft having a medium transport classification.

B. PURPOSE

Significant advances have been made in the last several years in the area of predicting tire/soil response of aircraft tires while free rolling, turning, or being braked. The majority of the data has been the results of tests conducted in laboratories using loads and tires that are not those seen in operational conditions. Although the prediction equations are based upon particular tire/soil parameters which correlate with a great amount of data collected for many tire types and sizes and several soil types and strengths; still it remains to conduct full-scale tests.

The tests proposed are concerned with the taxi and turning aspects of ground maneuvering. Turning is a function of free rolling drag, braked drag and side forces developed on both nose wheel and main gear. Since the side forces are functions of the zero steering angle forces, it is necessary to measure "taxi" loads first, before proceeding on to the turning maneuver.

The accomplishment of the proposed tests would accomplish several objectives:

- 1) Permit comparison of measured forces on full-scale wheel assemblies under operational loads, with predicted values for free rolling and braked wheels.

- 2) Permit comparisons of measured and calculated rut depths for free rolling and braked, zero steering angle, wheel assemblies.
- 3) Provide guidance in updating the existing routines so that additional parameters that are significant can be isolated and incorporated.

C. TEST PROGRAM

There are many ways of establishing the test matrix for a particular test program. The most direct approach for this program is to consider the various means of performing over the ground maneuvers. Specifically, there are three ways to maneuver over the ground at low airspeeds. These are: 1) differential engine thrust, 2) differential braking, and 3) nose wheel steering. These can be tabulated as shown below.

Brakes	Thrust (Symmetrical)		Thrust (Unsymmetrical)	
	Trail	Steering	Trail	Steering
None	1	3	2	4
Symmetrical	5	7	6	8
Differential	9	11	10	12

This suggests the hierarchy of testing required to accurately isolate the many variables present. For example, block number 1; symmetrical thrust, no steering and no brake, is a description of a free-rolling taxi maneuver. If a vehicle were taxiing at constant thrust and velocity under these conditions, any measurements taken on the landing gear mounts would be indicative of free rolling drag as modified by any multiwheel effects. Therefore, for the particular wheel and tire configuration, load distribution and soil, it is possible to compare the forces developed with predicted values from existing equations.

The next added complexity could then be that of braking as listed in block number 5. Symmetrical braking of the main gear does not cause any turning (theoretically) but does cause increased drag loads as a function of wheel slip. No turn angle or steering angles would be introduced and it would be possible to collect data for braked wheel response.

All other cells of the table do introduce some turning and hence generate a turn angle for all wheel assemblies. The question is how to best conduct the testing to minimize any multiple parameter effects and maximize the effects of particular parameters. The next test block would therefore be number 3 which introduces nosewheel steering as the means of turning.

By using only nose wheel steering with free rolling wheels and constant thrust, the vehicle has to reach an equilibrium condition where there will be a specific turn angle for each wheel assembly as dictated by the free rolling side and drag forces. Additionally, at that condition a turned sinkage and rut depth will be generated. The effects of thrust and braking have been eliminated.

The next higher order of complexity would be possible testing with symmetrical braking as identified by cell number 7. By adding symmetrical braking it is possible to establish the effects of braked slip at a turn angle. The effects of combined braking and turning on tire sinkage and drag are not known. Since the previous test series was to be conducted at a turned condition with no braking, it should be possible to estimate how the sinkage and drag are related with braking.

This completes the testing required in that any other combination of thrust, braking or steering does not introduce a new environment for the wheel. It can either be straight ahead rolling, turned rolling, or braked with and without a turn angle. The four test series outlined provide data for all of these combinations. Any additional testing would certainly be beneficial in better defining the effects of thrust and braking upon overall vehicle response, but would not, theoretically, alter the interaction effects already evaluated.

Further refinement of the test program is possible when we consider the number of significant parameters and the possible variations. These are:

<u>Parameter</u>	<u>Variations</u>	<u>Number</u>
Gross Weight	Design gross weight and max gross weight.	2
Taxi Speed	Minimum and maximum of Region II (5 to 20 kts)	2
Tire Deflection	Operational value only (32%)	1
Soil Type	Clay or Sand	2
Thrust	Symmetrical as required for constant speed.	1
Steering	Trail position, 20, 40 and 60°.	4
Brakes	Symmetrical, 15, 30, and 45 percent slip.	4

The steering values of 20, 40 and 60° were selected based upon known criteria for C-130E turning. The braked slip values are established to investigate minimum braking, an intermediate value which theoretically generated a braked drag ratio of 50% and a maximum value which should approach the 0.8 drag ratio required by specification.

Using the above values generates the following number of tests .

Control Variables	Test Type				
	1	5	3	7	Σ
Gross Weight	2*	2	2	2	
Taxi Speed	2	2	2	2	
Soil Type	2	2	2	2	
Thrust	As Required →				
Steering	1	1	3	3	
Brakes	1	3	1	3	
Product	8	24	24	72	128

* Number of variations.

Therefore, 128 separate passes would be required. Realistically this implies that at one test site 64 taxi tests would be required in order to cover a spectrum of operational conditions.

Test Matrix

The test matrix for one testing site would be as shown.

TABLE II
TEST SITE "A" (SOIL I)

Test Number	Gross Weight	Velocity (Kts)	Steering (Degrees)	Braked (% slip)	Objectives
101	W ₁	5	Trail	None	Verify
102	W ₂	5	Trail	None	Free Rolling
103	W ₁	20	Trail	None	Drag and Sinkage
104	W ₂	20	Trail	None	Prediction Techniques - With no Turning
501	W ₁	5	Trail	15	Verify
502	W ₁	5	Trail	30	Braked Rolling
503	W ₁	5	Trail	45	Response
504	W ₁	20	Trail	15	Prediction
505	W ₁	20	Trail	30	Techniques
506	W ₁	20	Trail	45	With no
507	W ₂	5	Trail	15	Turning
508	W ₂	5	Trail	30	

TABLE II (Continued)

Test Number	Gross Weight (lbs)	Velocity (Kts)	Steering (Degrees)	Braked (% Slip)	Objectives
509	W ₂	5	Trail	45	
510	W ₂	20	Trail	15	
511	W ₂	20	Trail	30	
512	W ₂	20	Trail	45	
301	W ₁	5	20	None	Establish
302	W ₁	5	40	None	Effects of
303	W ₁	5	60	None	Turn Angle
304	W ₁	20	20	None	on
305	W ₁	20	40	None	Free Rolling
306	W ₁	20	60	None	Wheels
307	W ₂	5	20	None	
308	W ₂	5	40	None	
309	W ₂	5	60	None	
310	W ₂	20	20	None	
311	W ₂	20	40	None	
312	W ₂	20	60	None	
701	W ₁	5	20	15	Establish
702	W ₁	5	20	30	Effects of
703	W ₁	5	20	45	Turn Angle
704	W ₁	5	40	15	on

TABLE II (Continued)

Test Number	Gross Weight (lbs)	Velocity (Kts)	Steering (Degrees)	Braked (% Slip)	Objectives
705	W ₁	5	40	30	Braked Wheels
706	W ₁	5	40	45	
707	W ₁	5	60	15	
708	W ₁	5	60	30	
709	W ₁	5	60	45	
710	W ₁	20	20	15	
711	W ₁	20	20	30	
712	W ₁	20	20	45	
713	W ₁	20	40	15	
714	W ₁	20	40	30	
715	W ₁	20	40	45	
716	W ₁	20	60	15	
717	W ₁	20	60	30	
718	W ₁	20	60	45	
719	W ₂	5	20	15	
720	W ₂	5	20	30	
721	W ₂	5	20	45	
722	W ₂	5	40	15	
723	W ₂	5	40	30	
724	W ₂	5	40	45	
725	W ₂	5	60	15	

TABLE II (Concluded)

Test Number	Gross Weight (lbs)	Velocity (Kts)	Steering (Degrees)	Braked (% Slip)	Objectives
726	W_2	5	60	30	
727	W_2	5	60	45	
728	W_2	20	20	15	
729	W_2	20	20	30	
730	W_2	20	20	45	
731	W_2	20	40	15	
732	W_2	20	40	30	
733	W_2	20	40	45	
734	W_2	20	60	15	
735	W_2	20	60	30	
736	W_2	20	60	45	

The matrix evolved was generated assuming that gross weight changes would be most difficult to achieve during testing, and braking and steering the least difficult. As a variation of parameters the matrix is correct, but operationally it would seem more realistic to run all tests of one gross weight first, then modify it to the other value. Hence, at one site, all gross weight W_1 tests would be conducted first for all configurations of velocity, steering and braking, and then all W_2 tests conducted. The tests would then be reduced to two 32 test series at the one site. Thirty-two tests are possible without significant pretest preparation assuming the taxi area does not need preparation between tests and that the gross weight does not change significantly during the time required.

Measurements Required

The measurements required can be classified as aircraft data, landing gear data, tire data, soil characteristics, controls and response data.

The aircraft parameters with computer related symbols are:

Gross Weight	(W)
Mass Moment of Inertia about the Vertical Axis	(I_{zz})
Taxi Velocity	(V_o)
Ground Level to Thrust Line	(UE)
Engine Spacing	(EE)
Ground Level to Forward c. g.	(U)

Landing gear parameters are:

Nose gear c. g. to forward c. g.	(L)
Nose gear c. g. to Average c. g.	(AL)
Nose gear c. g. to aft c. g.	(LL)
Nose gear c. g. to main c. g.	(F)
Main gear c. g. to forward c. g.	(M)
Main gear c. g. to average c. g.	(AVM)
Spacing between main gear	(E)
Twin spacing of nose gear	SN
Twin spacing of main gear	SM
Tandem spacing of main tires	SM

Tire Data

Nose tire type	
Nose tire deflection	DE
Nose tire diameter	DN
Nose tire flange diameter	DFN
Total number of nose tires	NN

Main tire type	
Main tire deflection	DEM
Main tire diameter	DM
Main tire flange diameter	DFM
Total number of main tires	NM
Number of tire per side	N1
Number of tires in tandem	NM1
Number of tires in twin configuration	NN1

Soil Data

Soil classification	NTYP
Soil strength by cone index reading	CI

Controls Data

Braked slip as a function of time	SL
Nose wheel steering angle as a function of time	BETA

Response Data

Nose wheel drag	RN
Nose wheel side force	SFN
Nose wheel torque	TMN
Nose wheel steering angle	BP
Nose wheel vertical force	PN
Nose wheel rut depth	ZR1
Left wheel drag	RML
Left wheel side force	SFML
Left wheel torque	TMML
Left wheel vertical force	PMR
Left wheel rut depth	ZR2
Right wheel drag	RMR

Right wheel side force	SFMR
Right wheel torque	TMMR
Right wheel vertical force	PML
Right wheel rut depth	ZR2
Vehicle side acceleration versus time	ACVS
Vehicle thrust versus time	THRT
Path over the ground versus time	

All of the above are in pounds and inches except for velocity which is currently in knots and side acceleration which is in "g" units.

Some of the desired measurements will come from manufacturers data and can be compiled before any tests occur. The tests which will have to be measured by transducer or direct measurement are:

- Gross weight
- Taxi velocity
- Soils data
- Controls data
- All response data

Specific Measurement Requirements

The following items are discussed in order to establish the range of values that can be anticipated and possible means of collecting the data.

Gross Weight

Gross weight has to be found whether as a particular number indicative of calculated values from a weights and balance handbook, or as a summation of vertical forces measured at each landing gear mount. The gross weight can be obtained from strain gage data on the struts, pressures within the struts, or however it can be easily measured.

Soils Data

It is desirable to have tests run on clay type soil and granular type soil. The strength is determined by cone penetration tests and it could be that the strength may dictate the gross weight ranges to be used. The nomograph of Figure 39 will be used to establish the combination of gross weight and soil strength which is reasonable. Standard bulk soil sample tests for each site are necessary for classification purposes. For the range of steering angles and velocities assumed, it is realistic to require cone index data to be collected at approximately 250 foot intervals. This would generate about 4 readings along the path for the 20 knot, 20° turn.

Taxi Velocity

The velocity of the vehicle over the ground should be established for the entire test as a function of time. There are several means of achieving this available. One would be direct measurement of wheel motion but this would be subject to the problems of inherent slip, wheel differential in turns, surface roughness and dynamic response. Another means would be optical tracking as by a phototheodolite. This means suffers from having to differentiate displacement measurements as well as tracking the true center of gravity. However, the optical tracking is suggested as the primary means since the path over the ground is also desired.

Controls Data

Braked wheel slip and nose wheel steering as functions of time are required. Wheel slip specifically, is difficult to measure. Consequently it will be necessary to instead measure brake pressure, braking torque or whatever may be available to infer wheel slip. Nose wheel steering should be taken from a nose wheel indicator if possible. It is understood that some steering devices have built-in limiting devices which do not permit severe control motions. Therefore, any measurements at the control wheel could be out-of-phase and measurement should be taken at the wheel or mount as indicative of response not control.

Response Data

All landing gear struts should be instrumented for vertical force, drag force, side forces and torque. If individual wheel measurements could be taken this would also be greatly desirable. The specific force levels for each will have to be based upon existing criteria limits unless sufficient data is available ahead of time to compute theoretical values. Side and drag force ratios of one-half can be assumed and a coefficient of friction of 0.8 assumed to calculate generated torque.

Rut depths should be measured at each cone index location and at those points where significant changes can be observed due to steering or braking changes. Because of the many possible trajectories it will be necessary to take measurements across the ruts assuming that the terrain at two to three landing gear widths was unaffected by the passage of the gear. Surveying equipment will be necessary to establish the location of the measurements.

Vehicle side acceleration measurements can be collected using an accelerometer with one half "g" range mounted at or near the center of gravity of the vehicle and aligned with the lateral axis of the vehicle. Longitudinal measurements should also be taken to establish when an equilibrium condition is achieved.

Engine thrust is required if data are available to relate the thrust to cockpit lever displacement. If position measurements would be recorded as function of time. If it is not possible, tachometer readings should be recorded or engine output thrust values if possible.

Additional Comments

It is extremely desirable to utilize the existing computer program to study some of the selected variations for the particular vehicle selected. By doing that it is possible to establish force levels anticipated and more importantly trajectories. It is desired to conduct the test for "first pass" data collection. This infers that it is possible to conduct tests that do not cross over the paths of one another. Otherwise surface preparation would possibly be required after each test. By examining the trajectories ahead of time it may be possible to establish not only a time hierarchy but a spatial hierarchy.

Test Facility

Where the tests can be conducted is not known at the present time.

Data Reduction

It is assumed that the majority of the response and controls data would be collected using on-board recorders generating hard copy oscillogram records. The number of channels required indicate probably two recorder time synchronized to provide a valid time base.

The data channels can be manually examined to determine where equilibrium conditions exists as seen in longitudinal acceleration, lateral acceleration drag force, side force and vehicle velocity. These locations are then reduced using the proper calibration factors and tabulated in the same manner as shown on the computer printout shown in Figure 57. When this type of display it is then possible to return to the equations contained within the computer program and determine how computed forces and sinkages compare with measured. Ideally it would be desirable to have the data reduction conducted by a data acquisition system similar to that used at AEWES for tire tests. The system uses a computer to establish the mean values of the parameters and print them out for "equilibrium" conditions.

AIRCRAFT PARAMETERS

Gross Weight	GW = 133000.0 Lbs.
Initial Ground Vel.	V0 = 5.0 Knots

TIRE DATA --

NOSE

MAIN

Tire Deflection (%)	DE = 35.00	DEM = 35.00
Tire Diameter (In.)	DN = 38.00	DM = 55.20
Flange Diam. (In.)	DFN = 18.50	DFM = 24.00
Total No. of Tires	NN = 2	NM = 4
No. of Tires/Bogie		N1 = 2
No. of Tires--Tandem		NM1 = 2
No. of Tires --Twin		NN1 = 0
Tire Type	Type 3	Type 3

TIRE AND C.G. DISTANCES -- (IN INCHES)

Nose Gear C.G. to FWD C.G.	L = 346.30
Nose Gear C.G. to AVE C.G.	AL = 358.80
Nose Gear C.G. to AFT C.G.	LL = 371.30
Nose Gear C.G. to Main Gear C.G.	F = 388.00
Main Gear C.G. to FWD C.G.	M = 41.70
Main Gear C.G. to AVE C.G.	AVM = 29.20
Ground Level to FWD C.G.	U = 150.00
Ground Level to Engine	UE = 153.00
Between C.G.'s of Left & Right Main	E = 172.00
Twin Spacing of Nose Tires	SN = 22.00
Twin Spacing of Main Tires	SM = 0.00
Tandem Spacing of Main Tires	SNM = 60.00

SOIL PARAMETERS

Cone Index	CI = 192.00
Soil Type	NTYP = 1

ENGINE PARAMETER

Thrust Differential PE =	1.00
--------------------------	------

Figure 57. Master Program Input Requirements.
(Typed Facsimile for Clarity.)

Should this not be possible, manual techniques can be used since there would only be 64 tests at one site.

The reduction of the phototheodolite data cannot be discussed until more is known about the type of system available (if that system is used).

Technical Order and Specification Development

As mentioned previously, it is very advantageous to conduct preliminary analyses for the assumed vehicle configuration for several of the more severe maneuvers. These may indicate that force ratio will be excessive and that the braking, steering or velocity should be reduced. This in effect is generating a set of criteria for a technical order which will be verified or modified by test. Similarly, the forces developed may indicate that the specifications currently used can be modified in that the force ratios for wheel assemblies or the total vehicle are not realistic unless additional parameters are included in the specification. That is, the current specification does not mention turning velocity, yet velocity is an important parameter if side force is to be limited while conducting a minimum radius turn. Additionally, even if the turn can be accomplished, the ruts developed may not be acceptable because of the required mission of the unprepared airfield.

Preliminary technical orders and military specification modifications can be evolved prior to testing and updated after the test results have been evaluated.

SECTION VIII

MASTER PREDICTIVE COMPUTER PROGRAM

The Master Predictive Computer Program is composed of four previously developed computer programs; TAKEOFF, LANDING (TAKE-OFF modified for landing aircraft), TURNING, and DPEAC (aircraft passes capability). Any one of the programs or any combination of the four programs can be run for a given set of data, and as many data sets as are required can be used. A data set consists of the values of the program option variables and the input values necessary for the particular program(s) to run.

The program option variables are IOPT1, IOPT2, IOPT3, and IOPT4 which correspond respectively to the TAKEOFF, LANDING, TURNING, and DPEAC programs. By setting the appropriate option variable equal to an integer 1 (one) for TAKEOFF, TURNING, and DPEAC and equal to an integer 2 (two) for LANDING the designated program(s) will be executed. If a program is not to be run, an integer other than those mentioned above must be supplied as input.

DASET, the number of data sets to be run, is the first variable read. Next to the program option variables (IOPT1, IOPT2, IOPT3, IOPT4) are read followed by the variables common to all four programs. The rest of the variables read in are specific to particular programs as illustrated in Figure 58.

All of the variables used in the master program have been previously used and defined in the TAKEOFF, TURNING, and DPEAC programs except for the following:

THMAX - maximum aircraft thrust

VOL - initial velocity for LANDING

VTOL - dummy takeoff velocity variable in LANDING (VTOL must have a greater value than VOL for LANDING to run)

AOL - initial acceleration for LANDING

SOL - initial runway distance for LANDING

VO3 - initial velocity for TURNING (VO in original TURNING)

DT3 - time increment for TURNING (DT in original TURNING)

An example of the data cards required to run the master predictive program is shown in Figure 59 for the C-130E aircraft. The program option variables in this example (data card number 2) have been supplied with values to run all four programs. As an illustration of using combinations of the programs, the program option variables data card shown beneath the data set has values which will run only TAKEOFF and LANDING.

The outputs generated by the selected routines are identical to those previously discussed. That is, the turning portion provides output as seen in Figure 56, and the number of passes are presented in Reference 20. The main purpose of developing the master program was to generate one program which would use the same variables in essentially three different digital routines. This aspect was accomplished but the outputs were not modified to have a "standardized" appearance.

133000.	1	2	1	1					
35.	38.	55.2	12.38	19.6	35.				
60.0	18.5	24.	388.	22.	0.				
	2	2	3	3	0	.	2		
	2	1							
0.1	0.	180.	1745.	2.395	0.05				
1.	41.7	2.6	0.	10200.					
	3	4							
	-20.	0.	200.						
10200.	10200.	10200.							
3.	188.	0.	0.						
188.	200.	0.	0.						
0.									
346.3	371.3	41.7	150.	172.					4
3.0	6.0	9.0	12.0	15.0	18.0	20.0	20.0	20.0	20.0
20.0	20.0	20.0	20.0	20.0	20.0	20.0	20.0	20.0	20.0
20.0	20.0	20.0	20.0	20.0	20.0	20.0	20.0	20.0	20.0
20.0	20.0	20.0	20.0	20.0	20.0	20.0	18.0	12.0	6.0
0.0	0.0	0.0	0.0	0.0	0.0	0.0	0.0	0.0	0.0
0.0	0.0	0.0	0.0	0.0	0.0	0.0	0.0	0.0	0.0
0.0	0.0	0.0	0.0	0.0	0.0	0.0	0.0	0.0	0.0
3500000.	20.	0.5	153.						

Program Option Variable Data Card For
Running Takeoff and Landing

1	2	0	0
---	---	---	---

Figure 59. Input Data Cards for Master Program.
(Typed Facsimile for Clarity)

SECTION IX
APPLICATION TO CURRENT SPECIFICATIONS

A. TURNING

Military Specification MIL-A-008862A , Airplane Strength and Rigidity, Landing and Ground Handling Loads, contains the definition of a turn and formula to be used to establish turning loads. Under paragraph 3.3.2 Turning the turn is to be achieved by:

- a) Unsymmetrical thrust or nose wheel steering
- b) Unsymmetrical thrust or nose wheel steering with symmetrical braking, and
- c) Differential braking.

The parameters that generate a turn are the braking, differential thrust or nose wheel steering. If we tabulate the various values these parameters can have, there are twelve combinations. For example

Brakes	Thrust (Symmetrical)		Thrust (Unsymmetrical)	
	Trail	Steering	Trail	Steering
None	1	3	2	4
Symmetrical	5	7	6	8
Differential	9	11	10	12

Cells 1 and 5 are trivial combinations since either no brakes or symmetrical brakes with a trailing nose wheel and symmetrical thrust, will not turn the vehicle.

If we consider turns achieved by only one control parameter, there are three possibilities. Cells 2, 3, and 9 are for a turn generated by thrust alone, steering alone, and differential braking respectively.

Two control parameter turns are those of cells, 4, 6, 7, 10, and 11. These are asymmetrical thrust with nose wheel steering and symmetrical brakes, nose wheel steering with symmetrical brakes, differential braking with asymmetrical thrust and with nose wheel steering. Symmetrical brakes introduces a unique turning condition because they influence the vertical forces at the landing gear by changing the pitching moment. Therefore, even though symmetrical braking does not change the direction of the aircraft, its combination with other parameters changes the turning response. All three parameters are used in cells 8 and 12 where differential thrust, nose wheel steering, and symmetrical and differential braking are possible.

Current specifications, as listed above, consider only cells 2, 3, 6, 7, and 9. Combining these with the trivial cells and eliminating these from the total, there are five conditions not covered by the current specifications. These are:

- Asymmetrical thrust with steering
- Asymmetrical thrust with steering and symmetrical brakes
- Asymmetrical thrust with unsymmetrical brakes
- Differential braking with steering
- Differential braking with steering and unsymmetrical thrust

From the table it is apparent that those not currently specified are those of the most extreme maneuvering inputs, those with the greater number of control parameters. From very limited data, it appears that these conditions would be those that would create the smallest operational turning radius and would therefore be very desirable maneuvers for aircraft operating in forward areas. The data presented in Section III indicate that for a particular set of input conditions to a C-130E, the minimum field width could be reduced by 20 percent by using differential braking with nosewheel steering. The thrust required to overcome the

braked drag is nearly all of the thrust available and therefore in this case differential thrust would not even be possible. Therefore, it appears that while some of the combinations are at least theoretically possible, they may not in fact be practically possible. Nonetheless, there are additional turning maneuver operations which could conceivably be considered for inclusion into the specification.

Under Paragraph 4.6 Turning, of the standard, several formulas are given for calculating the loads for outside and inside gear based upon vertical load factor, N_Z , side load factor, N_s , and weight distribution based upon the geometry of the landing gear. This is consistent with assuming that the vehicle is in a steady state turn where side forces balance the inertial response and the vertical forces are generated by inertial response and rolling moment.

From previous discussions, it is apparent that rolling drag can become very large. Therefore, it is not necessarily realistic to ignore the effects of rolling drag developed in soils. The specification indicates that for bare soil fields, each unbraked wheel shall have a drag reaction of 0.2 times the vertical reaction. If this is observed, then it is only reasonable to have a forward load factor, N_L , which would be used to calculate an additional contribution to the vertical forces on each landing gear. The current specified value of 0.8 times the vertical reaction for lateral load (drag and side force resultant) seems reasonable. The drag ratio at that level would add significantly to the nose wheel loads.

The specified side load ratio of 0.5 for both vehicle and any wheel seems reasonable for vehicle and main gear based upon very limited data. The C130E example indicates that the vehicle side force ratio can only be approached at high taxi speeds where the turning radius becomes very large. Hence, considering the desire to keep taxi speeds down and turn in a reasonable space, the vehicle side force ratio is probably consistent with other turn parameters.

The side force ratio as applied to any one wheel may be more suspect. The first two specified means of turning are with nose wheel steering. Test data indicates that the limiting value may be exceeded depending upon the turn angle and sinkage. Additionally, the peak side force on the nose wheel may occur because of the steering rate, not the steering angle. Therefore, it appears that the nose wheel may require a special analysis to predict its maximum loading condition. Either that or retaining the present maximum side force ratio will require that steering rate and forward velocity be examined to calculate their effects. This is necessary since the turn angle is dictated both by the steering rate and the forward velocity.

Present turning specifications do not reflect all possible configurations of turning mechanisms possible. The equations available do provide realistic load factors for vehicle side force, but do not reflect the pitching moment due to drag and thrust. Nosewheel steering can provide unique loading conditions due to steering rate and forward velocity and these factors should be mentioned. Additionally, with current equations and nomograms available for the solution of sinkage and drag, it is possible to obtain better estimates of rolling and braked drag rather than assuming two distinct values. Lastly, because of the effects of speed, not only for drag but upon turning rate, velocity should be introduced in order to call attention to its presence.

B. MULTIPASS

The Design Handbook, AFSC DM-21, under Design Notes 4C2, Un-surfaced Airfields, lists a method to be used in evaluating relative ground flotation performance. The procedure enables calculation of the permissible number of passes an aircraft can make over heavy clay soil prior to the formation of a three-inch rut. The procedure is restricted to one soil type and one soil failure criteria. Data collected from this program indicate that rut depth can be predicted as a function of soil type and strength, and

number of passes. The data are currently restricted to a limited number of passes, but it is indicative that the depth can be predicted since the three-inch rut may not be limiting for large diameter tires.

Since the prediction of rut depth relies upon first pass sinkage and rut, it is possible that additional nomograms or equations could be included in the multipass analysis currently used. The technique requires the calculation of tire contact area and single wheel load. The solution of first pass sinkage and rut depth then only requires knowledge of soil type and strength. With this as a starting point, rut depth for a given number of passes in the same path, or adjacent paths could be determined. In this manner, it is possible to determine an allowable number of passes for a variable rut depth. If it can be shown that the permissible rut depth is dictated by limiting drag or structural interference, then the number of passes would be dictated by tire size and deflection, soil properties, and the particular vehicle geometry, not a selected rut depth.

A revised means of calculating allowable passes would be:

- (1) Establish maximum permissible rut depth based upon landing gear physical configuration, external stores, or vehicle consideration such as wheel well doors.
- (2) Establish maximum permissible rut depth based upon structural strength restrictions or drag restriction determined by thrust available.
- (3) Select maximum permissible rut depth from the above information.
- (4) For the specific landing gear, tire, soil and vehicle weight distribution, calculate the number of passes possible. This can assume multiple passes in the same lanes or a specific distribution and time phasing between passes. Braking could be included.

In summary, multipass design criteria can be updated so that the appropriate specifications would require the allowable number of passes to be found based upon new predictive equations. These would reflect soil strength and type, and the time history of the passes made.

C. TAKEOFF AND LANDING

Takeoff and landing performance on unprepared runways is specified in terms of rolling or braked drag. Rolling drag is assumed to be 0.2 times the vertical reaction while braked drag is 0.8 times the vertical reaction. These can be altered to easily reflect all influencing parameters except forward velocity. There are nomograms which permit calculation of rolling drag as a function of tire, soil and single wheel load. Hence, the rolling drag coefficient for the particular vehicle could be evaluated using specified procedures, rather than having specified values for all aircraft. Similarly, the results of the rolling drag analysis can be used in braked drag equations to determine the effect of braking upon landing rollout.

Of particular significance in calculating braked rollout would be the evaluation of braked rut depth. The braked rut is greater than the free rolling and the performance of multiple landings and takeoffs could be severely restricted unless this is recognized. Consequently, any landing and take-off specification should reflect not only the drag ratio analysis, but rut depth generation as it influences multipass operations.

SECTION X

CONCLUSIONS AND RECOMMENDATIONS

A. CONCLUSIONS

The reported results of the past years research have generated the following conclusions.

Turned Tire Phenomena

1. Drag, sinkage and rut depth increase with turn angle. The increases are greater in cohesionless soils than in cohesive soils for a given load and soil strength.
2. The lateral load ratio can and in some cases will exceed one-half where the turn angle becomes large.
3. Pneumatic trail is negative (behind the tire axis) and decreases with turn angle in cohesive soil. Pneumatic trail is positive and increases with turn angle for cohesionless soil. Therefore, the trail generates a stable condition in cohesive soil and unstable in the cohesionless.
4. Realistic results are generated by an analytical model of a turning aircraft using predictive equations from tire test data.
5. Computed turning results indicate that current specified nose wheel steering angles generate turn angles greater than those used in the laboratory tests. Additionally, load strength ratio limits were exceeded.
6. A limited parametric study indicates that the optimum means of turning, considering force ratios only, is nose wheel steering only, nose wheel steering with engine thrust differential, and differential braking last. If an extremely tight turn is required, only an analysis considering the vehicle configuration can determine the best balance of steering, braking, and thrust.

Multipass Response

1. Rut depth generated by a single rolling tire passing over the same path in cohesive soil, can be calculated by a linear change from the first pass rut depth for approximately twenty passes not exceeding a three-inch cumulative rut depth.
2. Drag forces measured on the same single free rolling wheel passing over the same path do not significantly increase in a cohesive soil.
3. A single wheel which alternates path and braking generates a rut depth which can be calculated using superposition of constant coefficient effects all related to first pass sinkage and rut depth.

Start-Up Forces

1. The limited data examined indicate that the start-up drag force ratio can be approximated as a function of the first pass free rolling drag ratio.
2. The data indicate that there is a trend which follows the load strength ratio, α / CI , but there are other effects more directly related to total force and cone index alone which are not yet defined.

Roughness Effects

It is possible to model the soft tire/soft soil response using lumped parameter elements as well as soil properties. The computational time may be excessive for a "real world" simulation.

B. RECOMMENDATIONS

Turned Tire Phenomena

1. Additional tests are desired for tires operating at greater turn angles with and without braking. It is not known how the braked

drag is influenced by the sinkage created by the turn angle. This effect can be significant as shown by the computed results.

2. Full-scale testing of an instrumented vehicle as developed in the Test Plan of Section VII is necessary to validate the digital program developed from tire test results.

Multipass Response

1. All results generated during this research effort were for cohesive soils. Therefore, the next step required is that of conducting another test series using a cohesionless soil for similar test parameter ranges.
2. The direct and indirect rolling and braking, rut depth coefficients exhibit an apparent reversal at a particular value of P/CI . Tests should be conducted over that range to validate the limited data available.

Start-Up Forces

1. A test series should be conducted to isolate the effects of time, tire pressure, load strength ratio, and total force upon start-up force.

Roughness Effects

1. The lumped parameter values for the computer model should be established for several tire configurations using existing test data. There are test results available to establish tire coefficients, rolling tires on rigid surfaces, and to establish soil coefficients, rigid tires on soft soils. After these have been developed, selected "roughness" configurations can be studied.

APPENDIX A

CHARACTERISTICS OF AIRCRAFT USED FOR TURNING
PARAMETRIC STUDY

AIRCRAFT PARAMETERS

GROSS WEIGHT GW = 133000.0 LBS.
INITIAL GROUND VEL. V0 = 5.0 KNOTS

TIRE DATA--	NOSE	MAIN
TIRE DEFLECTION(%)	DE = 35.00	DEM = 35.00
TIRE DIAMETER (IN.)	DN = 38.00	DM = 55.20
FLANGE DIAM. (IN.)	DFN = 18.50	DFM = 24.00
TOTAL NO. OF TIRES	NN = 2	NM = 4
NO. OF TIRES/BOGIE		N1 = 2
NO. OF TIRES--TANDEM		NM1 = 2
NO. OF TIRES--TWIN		NN1 = 0
TIRE TYPE	TYPE 3	TYPE 3

TIRE AND C.G. DISTANCES--(IN INCHES)

NOSE GEAR C.G. TO FWD C.G.	L = 346.30
NOSE GEAR C.G. TO AVE C.G.	AL = 358.80
NOSE GEAR C.G. TO AFT C.G.	LL = 371.30
NOSE GEAR C.G. TO MAIN GEAR C.G.	F = 388.00
MAIN GEAR C.G. TO FWD C.G.	M = 41.70
MAIN GEAR C.G. TO AVE C.G.	AVM = 29.20
GROUND LEVEL TO FWD C.G.	U = 150.00
GROUND LEVEL TO ENGINE	UE = 153.00
BETWEEN C.G.'S OF LEFT & RIGHT MAIN	E = 172.00
TWIN SPACING OF NOSE TIRES	SN = 22.00
TWIN SPACING OF MAIN TIRES	SM = 0.00
TANDEM SPACING OF MAIN TIRES	SNM = 60.00

SOIL PARAMETERS

CONE INDEX CI= 192.00
SOIL TYPE NTYP= 1

ENGINE PARAMETER

THRUST DIFFERENTIAL PE= 1.00

C-130 Configuration Vehicle Characteristics

AIRCRAFT PARAMETERS			
GROSS WEIGHT	GW =	3100.0	LBS.
INITIAL GROUND VEL.	VO =	5.0	KNOTS
TIRE DATA--		NOSE	MAIN
TIRE DEFLECTION(%)	DE =	32.0	DEM = 32.00
TIRE DIAMETER (IN.)	DN =	23.73	DM = 34.55
FLANGE DIAM. (IN.)	DFN =	11.81	DFM = 18.75
TOTAL NO. OF TIRES	NN =	1	NM = 2
NO. OF TIRES/BOGIE			N1 = 1
NO. OF TIRES--TANDEM			NM1 = 0
NO. OF TIRES--TWIN			NN1 = 0
TIRE TYPE		TYPE 7	TYPE 7
TIRE AND C.G. DISTANCES--(IN INCHES)			
NOSE GEAR C.G. TO FWD C.G.		L =	184.70
NOSE GEAR C.G. TO AVE C.G.		AL =	188.25
NOSE GEAR C.G. TO AFT C.G.		LL =	191.79
NOSE GEAR C.G. TO MAIN GEAR C.G.		F =	212.79
MAIN GEAR C.G. TO FWD C.G.		M =	21.00
MAIN GEAR C.G. TO AVE C.G.		AVM =	24.55
GROUND LEVEL TO FWD C.G.		U =	89.10
GROUND LEVEL TO ENGINE		UE =	113.40
BETWEEN C.G.'S OF LEFT & RIGHT MAIN		E =	206.86
TWIN SPACING OF NOSE TIRES		SN =	0.00
TWIN SPACING OF MAIN TIRES		SM =	0.00
TANDEM SPACING OF MAIN TIRES		SNM =	0.00
SOIL PARAMETERS			
CONE INDEX	CI =	192.00	
SOIL TYPE	NTYP =	1	
ENGINE PARAMETER			
THRUST DIFFERENTIAL	PE =	1.00	

Attack Vehicle Characteristics

AIRCRAFT PARAMETERS

GROSS WEIGHT GW = 216000.0 LBS.
INITIAL GROUND VEL. VG = 5.0 KNOTS

TIRE DATA--

NOSE

MAIN

TIRE DEFLECTION(%)	DE = 32.00	DEM = 32.00
TIRE DIAMETER (IN.)	DN = 40.00	DM = 40.00
FLANGE DIAM. (IN.)	DFN = 19.50	DFM = 19.50
TOTAL NO. OF TIRES	NN = 2	NM = 8
NO. OF TIRES/BOGIE		N1 = 4
NO. OF TIRES--TANDEM		NM1 = 4
NO. OF TIRES--TWIN		NN1 = 4
TIRE TYPE	TYPE**	TYPE 7

TIRE AND C.G. DISTANCES--(IN INCHES)

NOSE GEAR C.G. TO FWD C.G.	L = 427.80
NOSE GEAR C.G. TO AVE C.G.	AL = 449.20
NOSE GEAR C.G. TO AFT C.G.	LL = 452.60
NOSE GEAR C.G. TO MAIN GEAR C.G.	F = 487.00
MAIN GEAR C.G. TO FWD C.G.	M = 59.20
MAIN GEAR C.G. TO AVE C.G.	AVM = 46.80
GROUND LEVEL TO FWD C.G.	U = 176.00
GROUND LEVEL TO ENGINE	UE = 241.00
BETWEEN C.G.'S OF LEFT & RIGHT MAIN	E = 223.00
TWIN SPACING OF NOSE TIRES	SN = 31.00
TWIN SPACING OF MAIN TIRES	SM = 60.00
TANDEM SPACING OF MAIN TIRES	SNM = 35.00

SOIL PARAMETERS

CONE INDEX CI= 192.00
SOIL TYPE NTYP= 1

ENGINE PARAMETER

THRUST DIFFERENTIAL PF= 1.00

Advanced Transport Characteristics

APPENDIX B

PROGRAM LISTING FOR ROLLING TIRE ON SOFT SOIL

NIMC SOURCE-LANGUAGE PROGRAM
 VERSION 1 10/01/68 MOD LEVEL C001

```

1  SOFT TIRE ROLLING ON A SOFT SURFACE
   CON(VO,ZO,P,OP,MB,WP)
   CON(HM,HM,RW,IN)
   CON(HT,KT,CT,BT)
   CON(HS,XS,CS,CSS,HS)
   CON(COHS,IFS)

2  CALCULATE NEEDED CONSTANTS
   MT  MT/386.
   HM  HM/386.
   HP  HP/386.
   HS  HS/386.
   OM  VO/RW
   AZ  BT*.1571*RW

3  CALCULATE ACCELERATION OF WHEEL HUB VERTICALLY
   ZDZW1 (-P+TSUM+FSUM)/(HM+MP)-386.

31  CALCULATE SUM OF TANGENTIAL FORCES
   TSUM  TSUM1+TSUM2+TSUM3
   TSUM1 T1*COS(TH1)+T2*COS(TH2)+T3*COS(TH3)+T4*COS(TH4)
   TSUM2 T5*COS(TH5)+T6*COS(TH6)+T7*COS(TH7)+T8*COS(TH8)
   TSUM3 T9*COS(TH9)+T10*COS(TH10)

32  CALCULATE SUM OF SPOKE FORCES
   FSUM  FVT1*SIN(TH1)+FVT2*SIN(TH2)+FVT3*SIN(TH3)+FSUM1
   FSUM1 FVT4*SIN(TH4)+FVT5*SIN(TH5)+FVT6*SIN(TH6)+FSUM2
   FSUM2 FVT10*SIN(TH10)

33  TANGENTIAL FORCE PERMITTED AFTER IMPACT
   T1  LSW(GO,T1,0.)
   T2  LSW(GO2,T2,0.)
   T3  LSW(GO3,T3,0.)
   T4  LSW(GO4,T4,0.)
   T5  LSW(GO5,T5,0.)
   T6  LSW(GO6,T6,0.)
   T7  LSW(GO7,T7,0.)
   T8  LSW(GO8,T8,0.)
   T9  LSW(GO9,T9,0.)
   T10 LSW(GO10,T10,0.)

34  RELATIVE VELOCITY DICTATES SIGN OF T
   T10 FSW(RVEL,-T10,0.,T10)
   T20 FSW(RVEL2,-T20,0.,T20)
   T30 FSW(RVEL3,-T30,0.,T30)
   T40 FSW(RVEL4,-T40,0.,T40)
   T50 FSW(RVEL5,-T50,0.,T50)
   T60 FSW(RVEL6,-T60,0.,T60)
   T70 FSW(RVEL7,-T70,0.,T70)
   T80 FSW(RVEL8,-T80,0.,T80)
   T90 FSW(RVEL9,-T90,0.,T90)
   T100 FSW(RVEL10,-T100,0.,T100)

35  RELATIVE VELOCITY AT SPOKE SURFACE
   RVEL R*10TH1-10XW*SIN(TH1)
   RVEL2 R2*10TH1-10XW*SIN(TH2)
   RVEL3 R3*10TH1-10XW*SIN(TH3)
   RVEL4 R4*10TH1-10XW*SIN(TH4)
   RVEL5 R5*10TH1-10XW*SIN(TH5)
   RVEL6 R6*10TH1-10XW*SIN(TH6)
   RVEL7 R7*10TH1-10XW*SIN(TH7)
   RVEL8 R8*10TH1-10XW*SIN(TH8)
   RVEL9 R9*10TH1-10XW*SIN(TH9)
   RVEL10 R10*10TH1-10XW*SIN(TH10)

36  MAGNITUDE OF FRICTIONAL FORCE T
   T1A (AZ*COHS*N1*IFS)*MUSL
  
```

```

T2A (AZ*COM5+N2*IFS)*MUSL2
T3A (AZ*COM5+N3*IFS)*MUSL3
T4A (AZ*COM5+N4*IFS)*MUSL4
T5A (AZ*COM5+N5*IFS)*MUSL5
T6A (AZ*COM5+N6*IFS)*MUSL6
T7A (AZ*COM5+N7*IFS)*MUSL7
T8A (AZ*COM5+N8*IFS)*MUSL8
T9A (AZ*COM5+N9*IFS)*MUSL9
T10A (AZ*COM5+N10*IFS)*MUSL10
37 CUBE ROOT OF SLIP
MUSL EXP(0.333,SLIP)
MUSL2 EXP(0.333,SLIP2)
MUSL3 EXP(0.333,SLIP3)
MUSL4 EXP(0.333,SLIP4)
MUSL5 EXP(0.333,SLIP5)
MUSL6 EXP(0.333,SLIP6)
MUSL7 EXP(0.333,SLIP7)
MUSL8 EXP(0.333,SLIP8)
MUSL9 EXP(0.333,SLIP9)
MUSL10 EXP(0.333,SLIP10)
38 SLIP IS RELATIVE VELOCITY OVER R OMEGA
SLIP ABS(RVEL/(10TH1*R))
SLIP2 ABS(RVEL2/(10TH1*R2))
SLIP3 ABS(RVEL3/(10TH1*R3))
SLIP4 ABS(RVEL4/(10TH1*R4))
SLIP5 ABS(RVEL5/(10TH1*R5))
SLIP6 ABS(RVEL6/(10TH1*R6))
SLIP7 ABS(RVEL7/(10TH1*R7))
SLIP8 ABS(RVEL8/(10TH1*R8))
SLIP9 ABS(RVEL9/(10TH1*R9))
SLIP10 ABS(RVEL10/(10TH1*R10))
39 FORCES IN THE SPOKE
FVT1 (KT*(ZT1-ZW1)+CT*(10ZT1-10ZW1))/SIN(TH1)
FVT2 (KT*(ZT2-ZW2)+CT*(10ZT2-10ZW2))/SIN(TH2)
FVT3 (KT*(ZT3-ZW3)+CT*(10ZT3-10ZW3))/SIN(TH3)
FVT4 (KT*(ZT4-ZW4)+CT*(10ZT4-10ZW4))/SIN(TH4)
FVT5 (KT*(ZT5-ZW5)+CT*(10ZT5-10ZW5))/SIN(TH5)
FVT6 (KT*(ZT6-ZW6)+CT*(10ZT6-10ZW6))/SIN(TH6)
FVT7 (KT*(ZT7-ZW7)+CT*(10ZT7-10ZW7))/SIN(TH7)
FVT8 (KT*(ZT8-ZW8)+CT*(10ZT8-10ZW8))/SIN(TH8)
FVT9 (KT*(ZT9-ZW9)+CT*(10ZT9-10ZW9))/SIN(TH9)
FVT10 (KT*(ZT10-ZW10)+CT*(10ZT10-10ZW10))/SIN(TH10)
4 CALCULATE HUB RELATIVE VELOCITY
41 SPOKE VELOCITIES AFTER IMPACT
10ZW1 LSW(G0,10ZW1B,0.)
10ZW2 LSW(G02,10ZW2B,0.)
10ZW3 LSW(G03,10ZW3B,0.)
10ZW4 LSW(G04,10ZW4B,0.)
10ZW5 LSW(G05,10ZW5B,0.)
10ZW6 LSW(G06,10ZW6B,0.)
10ZW7 LSW(G07,10ZW7B,0.)
10ZW8 LSW(G08,10ZW8B,0.)
10ZW9 LSW(G09,10ZW9B,0.)
10ZW10 LSW(G010,10ZW10B,0.)
42 INTEGRATE ACCELERATIONS AFTER IMPACT
10ZW1B INT(20ZW1,W1,TRUE,G01)
10ZW2B INT(20ZW1,W2,TRUE,G02)
10ZW3B INT(20ZW1,W3,TRUE,G03)
10ZW4B INT(20ZW1,W4,TRUE,G04)
10ZW5B INT(20ZW1,W5,TRUE,G05)
10ZW6B INT(20ZW1,W6,TRUE,G06)
10ZW7B INT(20ZW1,W7,TRUE,G07)
10ZW8B INT(20ZW1,W8,TRUE,G08)
10ZW9B INT(20ZW1,W9,TRUE,G09)
10ZW10B INT(20ZW1,W10,TRUE,G010)
43 TRACK AND STORE INERTIAL VELOCITY

```

```

W1      TAS(10ZW1A,IN1,0.)
W2      TAS(10ZW1A,IN2,0.)
W3      TAS(10ZW1A,IN3,0.)
W4      TAS(10ZW1A,IN4,0.)
W5      TAS(10ZW1A,IN5,0.)
W6      TAS(10ZW1A,IN6,0.)
W7      TAS(10ZW1A,IN7,0.)
W8      TAS(10ZW1A,IN8,0.)
W9      TAS(10ZW1A,IN9,0.)
W10     TAS(10ZW1A,IN10,0.)
10ZW1A  INT(20ZW1,Z0)
----- 44 ----- CALCULATE SPOKE DISPLACEMENT AFTER IMPACT
ZW1     INT(10ZW1,0.,TRUE,G01)
ZW2     INT(10ZW2,0.,TRUE,G02)
ZW3     INT(10ZW3,0.,TRUE,G03)
ZW4     INT(10ZW4,0.,TRUE,G04)
ZW5     INT(10ZW5,0.,TRUE,G05)
ZW6     INT(10ZW6,0.,TRUE,G06)
ZW7     INT(10ZW7,0.,TRUE,G07)
ZW8     INT(10ZW8,0.,TRUE,G08)
ZW9     INT(10ZW9,0.,TRUE,G09)
ZW10    INT(10ZW10,0.,TRUE,G010)
ZW1A    INT(10ZW1A,0.)
----- 5 ----- CALCULATE ACCELERATION OF TIRE TREAD
20ZT1   (-FVT1-FS1)/MT-386.
20ZT2   (-FVT2-FS2)/MT-386.
20ZT3   (-FVT3-FS3)/MT-386.
20ZT4   (-FVT4-FS4)/MT-386.
20ZT5   (-FVT5-FS5)/MT-386.
20ZT6   (-FVT6-FS6)/MT-386.
20ZT7   (-FVT7-FS7)/MT-386.
20ZT8   (-FVT8-FS8)/MT-386.
20ZT9   (-FVT9-FS9)/MT-386.
20ZT10  (-FVT10-FS10)/MT-386.
51      TREAD VELOCITIES AFTER IMPACT
10ZT1   LSW(G01,10ZT13,0.)
10ZT2   LSW(G02,10ZT28,0.)
10ZT3   LSW(G03,10ZT38,0.)
10ZT4   LSW(G04,10ZT48,0.)
10ZT5   LSW(G05,10ZT58,0.)
10ZT6   LSW(G06,10ZT68,0.)
10ZT7   LSW(G07,10ZT78,0.)
10ZT8   LSW(G08,10ZT88,0.)
10ZT9   LSW(G09,10ZT98,0.)
10ZT10  LSW(G010,10ZT108,0.)
----- 52 ----- INTEGRATE ACCELERATIONS AFTER IMPACT
10ZT18  INT(20ZT1,Z1,TRUE,G01)
10ZT28  INT(20ZT2,Z2,TRUE,G02)
10ZT38  INT(20ZT3,Z3,TRUE,G03)
10ZT48  INT(20ZT4,Z4,TRUE,G04)
10ZT58  INT(20ZT5,Z5,TRUE,G05)
10ZT68  INT(20ZT6,Z6,TRUE,G06)
10ZT78  INT(20ZT7,Z7,TRUE,G07)
10ZT88  INT(20ZT8,Z8,TRUE,G08)
10ZT98  INT(20ZT9,Z9,TRUE,G09)
10ZT108 INT(20ZT10,Z10,TRUE,G010)
----- 53 ----- TRACK AND STORE STORES AT IMPACT
Z1      TAS(VT1,IN1,0.)
Z2      TAS(VT2,IN2,0.)
Z3      TAS(VT3,IN3,0.)
Z4      TAS(VT4,IN4,0.)
Z5      TAS(VT5,IN5,0.)
Z6      TAS(VT6,IN6,0.)
Z7      TAS(VT7,IN7,0.)
Z8      TAS(VT8,IN8,0.)
Z9      TAS(VT9,IN9,0.)

```

```

54  Z10  TAS(VT1),IN10,0.)
    INITIAL IMPACT VELOCITY OF SPOKE
    VT1  10ZW1A-RW*10TH1*COS(TH1)
    VT2  10ZW1A-RW*10TH1*COS(TH2)
    VT3  10ZW1A-RW*10TH1*COS(TH3)
    VT4  10ZW1A-RW*10TH1*COS(TH4)
    VT5  10ZW1A-RW*10TH1*COS(TH5)
    VT6  10ZW1A-RW*10TH1*COS(TH6)
    VT7  10ZW1A-RW*10TH1*COS(TH7)
    VT8  10ZW1A-RW*10TH1*COS(TH8)
    VT9  10ZW1A-RW*10TH1*COS(TH9)
    VT10 10ZW1A-RW*10TH1*COS(TH10)
    IN1  LSW(GO,FALSE,TRUE)
    IN2  LSW(GO2,FALSE,TRUE)
    IN3  LSW(GO3,FALSE,TRUE)
    IN4  LSW(GO4,FALSE,TRUE)
    IN5  LSW(GO5,FALSE,TRUE)
    IN6  LSW(GO6,FALSE,TRUE)
    IN7  LSW(GO7,FALSE,TRUE)
    IN8  LSW(GO8,FALSE,TRUE)
    IN9  LSW(GO9,FALSE,TRUE)
    IN10 LSW(GO10,FALSE,TRUE)
56  TREAD DISPLACEMENT AFTER IMPACT
    ZT1  INT(10ZT1,J.,TRUE,G01)
    ZT2  INT(10ZT2,J.,TRUE,G02)
    ZT3  INT(10ZT3,J.,TRUE,G03)
    ZT4  INT(10ZT4,J.,TRUE,G04)
    ZT5  INT(10ZT5,J.,TRUE,G05)
    ZT6  INT(10ZT6,J.,TRUE,G06)
    ZT7  INT(10ZT7,J.,TRUE,G07)
    ZT8  INT(10ZT8,J.,TRUE,G08)
    ZT9  INT(10ZT9,J.,TRUE,G09)
    ZT10 INT(10ZT10,J.,TRUE,G010)
57  NORMAL FORCES ON TREADS
    N1  -FS1*SIN(TH1)
    N2  -FS2*SIN(TH2)
    N3  -FS3*SIN(TH3)
    N4  -FS4*SIN(TH4)
    N5  -FS5*SIN(TH5)
    N6  -FS6*SIN(TH6)
    N7  -FS7*SIN(TH7)
    N8  -FS8*SIN(TH8)
    N9  -FS9*SIN(TH9)
    N10 -FS10*SIN(TH10)
6  CALCULATE ACCELERATION OF SOIL MASS
    20ZS1 (FS1-CSS*10ZS1)/MS
    20ZS2 (FS2-CSS*10ZS2)/MS
    20ZS3 (FS3-CSS*10ZS3)/MS
    20ZS4 (FS4-CSS*10ZS4)/MS
    20ZS5 (FS5-CSS*10ZS5)/MS
    20ZS6 (FS6-CSS*10ZS6)/MS
    20ZS7 (FS7-CSS*10ZS7)/MS
    20ZS8 (FS8-CSS*10ZS8)/MS
    20ZS9 (FS9-CSS*10ZS9)/MS
    20ZS10 (FS10-CSS*10ZS10)/MS
61  SOIL FORCE MUST BE COMPRESSIVE
    FS1  FSW(FS1A,FS1A,0.,0.)
    FS2  FSW(FS2A,FS2A,0.,0.)
    FS3  FSW(FS3A,FS3A,0.,0.)
    FS4  FSW(FS4A,FS4A,0.,0.)
    FS5  FSW(FS5A,FS5A,0.,0.)
    FS6  FSW(FS6A,FS6A,0.,0.)
    FS7  FSW(FS7A,FS7A,0.,0.)
    FS8  FSW(FS8A,FS8A,0.,0.)
    FS9  FSW(FS9A,FS9A,0.,0.)
    FS10 FSW(FS10A,FS10A,0.,0.)

```

```

62      FORCE ABOVE SOIL MASS
FS1A    (KS*(ZT1-ZS1)+CS*(10ZT1-10ZS1))
FS2A    (KS*(ZT2-ZS2)+CS*(10ZT2-10ZS2))
FS3A    (KS*(ZT3-ZS3)+CS*(10ZT3-10ZS3))
FS4A    (KS*(ZT4-ZS4)+CS*(10ZT4-10ZS4))
FS5A    (KS*(ZT5-ZS5)+CS*(10ZT5-10ZS5))
FS6A    (KS*(ZT6-ZS6)+CS*(10ZT6-10ZS6))
FS7A    (KS*(ZT7-ZS7)+CS*(10ZT7-10ZS7))
FS8A    (KS*(ZT8-ZS8)+CS*(10ZT8-10ZS8))
FS9A    (KS*(ZT9-ZS9)+CS*(10ZT9-10ZS9))
FS10A   (KS*(ZT10-ZS10)+CS*(10ZT10-10ZS10))
7       CALCULATE SOIL VELOCITY AND DISPLACEMENT
10ZS1   INT(20ZS1,0.,TRUE,G0)
10ZS2   INT(20ZS2,0.,TRUE,G02)
10ZS3   INT(20ZS3,0.,TRUE,G03)
10ZS4   INT(20ZS4,0.,TRUE,G04)
10ZS5   INT(20ZS5,0.,TRUE,G05)
10ZS6   INT(20ZS6,0.,TRUE,G06)
10ZS7   INT(20ZS7,0.,TRUE,G07)
10ZS8   INT(20ZS8,0.,TRUE,G08)
10ZS9   INT(20ZS9,0.,TRUE,G09)
10ZS10  INT(20ZS10,0.,TRUE,G010)
71      ESTABLISH WHEN IMPACT OCCURS
THW     ZW1A+H4
DIFF1   (THW-RW*SIN(TH1))-HS
DIFF2   (THW-RW*SIN(TH2))-HS
DIFF3   (THW-RW*SIN(TH3))-HS
DIFF4   (THW-RW*SIN(TH4))-HS
DIFF5   (THW-RW*SIN(TH5))-HS
DIFF6   (THW-RW*SIN(TH6))-HS
DIFF7   (THW-RW*SIN(TH7))-HS
DIFF8   (THW-RW*SIN(TH8))-HS
DIFF9   (THW-RW*SIN(TH9))-HS
DIFF10  (THW-RW*SIN(TH10))-HS
72      B1 INSURES RESET AT MAX ANGLE
B1      LSW(G0A,1.,-1.)
B2      LSW(G02J,-1.,1.)
B3      LSW(G03J,-1.,1.)
B4      LSW(G04J,-1.,1.)
B5      LSW(G05J,-1.,1.)
B6      LSW(G06J,-1.,1.)
B7      LSW(G07J,-1.,1.)
B8      LSW(G08J,-1.,1.)
B9      LSW(G09J,-1.,1.)
B10     LSW(G010J,-1.,1.)
73      G0 INSURES SPOKE RECOGNIZES IMPACT
G0      FSW(DIFF,TRUE,TRUE,FALSE)
G02     FSW(DIFF2,TRUE,TRUE,FALSE)
G03     FSW(DIFF3,TRUE,TRUE,FALSE)
G04     FSW(DIFF4,TRUE,TRUE,FALSE)
G05     FSW(DIFF5,TRUE,TRUE,FALSE)
G06     FSW(DIFF6,TRUE,TRUE,FALSE)
G07     FSW(DIFF7,TRUE,TRUE,FALSE)
G08     FSW(DIFF8,TRUE,TRUE,FALSE)
G09     FSW(DIFF9,TRUE,TRUE,FALSE)
G010    FSW(DIFF10,TRUE,TRUE,FALSE)
74      SOIL DISPLACEMENT
ZS1     INT(10ZS1,0.,TRUE,G0)
ZS2     INT(10ZS2,0.,TRUE,G02)
ZS3     INT(10ZS3,0.,TRUE,G03)
ZS4     INT(10ZS4,0.,TRUE,G04)
ZS5     INT(10ZS5,0.,TRUE,G05)
ZS6     INT(10ZS6,0.,TRUE,G06)
ZS7     INT(10ZS7,0.,TRUE,G07)
ZS8     INT(10ZS8,0.,TRUE,G08)
ZS9     INT(10ZS9,0.,TRUE,G09)

```

```

      ZS10      INT(10ZS10,0.,TRUE,G010)
8    CALCULATE TIRE ROTATIONAL ACCELERATION
      ZDTH1     (-TOR-49)/IW
91    CALCULATE MOMENTS DUE TO SPOKE FRICTION
      TOR       T1*R+T2*R2+T3*R3+T4*R4+T5*R5+TOR1
      TOR1      T6*R6+T7*R7+T8*R8+T9*R9+T10*R10
82    CALCULATE RADII
      R         RW+(ZM1-ZT1)/SIN(TH1)
      R2        RW+(ZM2-ZT2)/SIN(TH2)
      R3        RW+(ZM3-ZT3)/SIN(TH3)
      R4        RW+(ZM4-ZT4)/SIN(TH4)
      R5        RW+(ZM5-ZT5)/SIN(TH5)
      R6        RW+(ZM6-ZT6)/SIN(TH6)
      R7        RW+(ZM7-ZT7)/SIN(TH7)
      R8        RW+(ZM8-ZT8)/SIN(TH8)
      R9        RW+(ZM9-ZT9)/SIN(TH9)
      R10       RW+(ZM10-ZT10)/SIN(TH10)
      IDTH1     INT(.20TH1,0H)
83    ALL SPOKES START BASED ON TH1
      TH1       INT(10TH1,0.506,TRUE,G0A)
84    TH1 RESETS AT MAX ANGLE
      G0A       FSW(TH1-2.176,TRUE,TRUE,FALSE)
85    ANGLES CAN NOT BE NEGATIVE OR ZERO
      TH2       FSW(TH21,0.636,0.606,TH21)
      TH3       FSW(TH31,0.636,0.606,TH31)
      TH4       FSW(TH41,0.636,0.606,TH41)
      TH5       FSW(TH51,0.606,0.606,TH51)
      TH6       FSW(TH61,0.636,0.606,TH61)
      TH7       FSW(TH71,0.636,0.606,TH71)
      TH8       FSW(TH81,0.636,0.606,TH81)
      TH9       FSW(TH91,0.636,0.606,TH91)
      TH10      FSW(TH101,0.606,0.606,TH101)
96    GET LOGICAL CONTROL AWAY FROM ORIGIN
      G02B1     FSW((T-(1.414))/(OH)),TRUE,TRUE,G02B)
      G03B1     FSW((T-(1.414))/(OH)),TRUE,TRUE,G03B)
      G04B1     FSW((T-(1.414))/(OH)),TRUE,TRUE,G04B)
      G05B1     FSW((T-(1.414))/(OH)),TRUE,TRUE,G05B)
      G06B1     FSW((T-(1.414))/(OH)),TRUE,TRUE,G06B)
      G07B1     FSW((T-(1.414))/(OH)),TRUE,TRUE,G07B)
      G08B1     FSW((T-(1.414))/(OH)),TRUE,TRUE,G08B)
      G09B1     FSW((T-(1.414))/(OH)),TRUE,TRUE,G09B)
      G010B1    FSW((T-(1.414))/(OH)),TRUE,TRUE,G010B)
87    ESTABLISH START FOR OTHER ANGLES
      G02P      FSW(TH1-0.763,FALSE,FALSE,TRUE)
      G03P      FSW(TH1-0.921,FALSE,FALSE,TRUE)
      G04P      FSW(TH1-1.077,FALSE,FALSE,TRUE)
      G05P      FSW(TH1-1.234,FALSE,FALSE,TRUE)
      G06P      FSW(TH1-1.391,FALSE,FALSE,TRUE)
      G07P      FSW(TH1-1.543,FALSE,FALSE,TRUE)
      G08P      FSW(TH1-1.705,FALSE,FALSE,TRUE)
      G09P      FSW(TH1-1.862,FALSE,FALSE,TRUE)
      G010P     FSW(TH1-2.013,FALSE,FALSE,TRUE)
88    EQUATIONS FOR OTHER ANGLES
      TH21      LSW(G02B1,TH1-0.197,TH1+2.019)
      TH31      LSW(G03B1,TH1-0.314,TH1+1.862)
      TH41      LSW(G04B1,TH1-0.471,TH1+1.705)
      TH51      LSW(G05B1,TH1-0.628,TH1+1.548)
      TH61      LSW(G06B1,TH1-0.785,TH1+1.391)
      TH71      LSW(G07B1,TH1-0.942,TH1+1.234)
      TH81      LSW(G08B1,TH1-1.099,TH1+1.077)
      TH91      LSW(G09B1,TH1-1.256,TH1+0.920)
      TH101     LSW(G010B1,TH1-1.413,TH1+0.763)
9    CALCULATE ACCELERATION OF WHEEL HUB HORIZONTALLY
      ZDXH      (OP+TOT*FORCE)/(MM*MP)
91    SUM TANGENTIAL CONTRIBUTIONS
      TOT       T1*SIN(TH1)+T2*SIN(TH2)+T3*SIN(TH3)+T4*SIN(TH4)+TOT1

```



```

TOT1    T5*SIN(TH5)+T6*SIN(TH6)+T7*SIN(TH7)+T8*SIN(TH8)+TOT2
TOT2    T9*SIN(TH9)+T10*SIN(TH10)
92      SUM SPOKE AXIAL CONTRIBUTION
FORCE   FVT1*CCS(TH1)+FVT2*CCS(TH2)+FVT3*CCS(TH3)+FORC1
FORC1    FVT4*CCS(TH4)+FVT5*CCS(TH5)+FVT6*CCS(TH6)+FORC2
FORC2    FVT7*CCS(TH7)+FVT8*CCS(TH8)+FVT9*CCS(TH9)+FORC3
FORC3    FVT10*CCS(TH10)
10XM    INT(20XM,V0)
XM       INT(10XM,J.)
DRAG     (MW+MP)*20XM-OP
ADRAG    (INT(DRAG,J.))/(T+.001)
4        CALCULATE TOTAL SLIP
TOSLP    (RW*10TH1-10XM)/(10TH1*RW)
DTMAX    DTHIN
DTMIN    .0001
DT        .001
          FIN(T,.75)
          PLO(T,ZT1,ZT3,ZT5,ZT7,ZT9)
          PLO(T,ADRAG,TOSLP)
          END

```

REFERENCES

1. Kraft, David C., et al., "Multiwheel Landing Gear-Soils Interaction and Flotation Criteria - Phase III, Part II," AFFDL-TR-71-12, Part II, Air Force Flight Dynamics Laboratory, Wright-Patterson Air Force Base, Ohio, January 1972.
2. Kraft, David C., and Hoppenjans, J. Richard, "Design Procedure for Establishing Aircraft Capability to Operate on Soil Surfaces," AFFDL-TM-71-09-FEM, Air Force Flight Dynamics Laboratory, Wright-Patterson Air Force Base, Ohio, September 1971.
3. Kraft, David C., Luming, Henry, and Hoppenjans, J. Richard, "Multiwheel Landing Gear-Soils Interaction and Flotation Criteria - Phase III, Part I," AFFDL-TR-71-12, Part I, Air Force Flight Dynamics Laboratory, Wright-Patterson Air Force Base, Ohio, May 1971.
4. Kraft, David C., Luming, Henry, and Hoppenjans, J. Richard, "Aircraft Landing Gear-Soils Interaction and Flotation Criteria, Phase II," AFFDL-TR-69-76, Air Force Flight Dynamics Laboratory, Wright-Patterson Air Force Base, Ohio, November 1969.
5. Kraft, David C., "Analytical Landing Gear-Soils Interaction, Phase I," AFFDL-TR-68-88, Air Force Flight Dynamics Laboratory, Wright-Patterson Air Force Base, Ohio, May 1968.
6. Crenshaw, B.M., and Butterworth, C.K., "Aircraft Landing Gear Dynamic Loads from Operation on Clay and Sandy Soil," AFFDL-TR-69-51, Air Force Flight Dynamics Laboratory, Wright-Patterson Air Force Base, Ohio, September 1968.
7. Turnage, G. W., and Brown, D.N., "Prediction of Aircraft Ground Performance by Evaluation of Ground Vehicle Rut Depths," Technical Report - Working Draft Only, U. S. Army Engineers Waterways Experiment Station, Vicksburg, Mississippi, 1973.
8. Richmond, L.D., et al., "Aircraft Dynamic Loads from Substandard Landing Sites," AFFDL-TR-67-145, Air Force Flight Dynamics Laboratory, Wright-Patterson Air Force Base, Ohio, September 1968.
9. Ladd, D., et al., "Aircraft Ground Flotation Investigation," AFFDL-TR-66-43, Air Force Flight Dynamics Laboratory, Wright-Patterson Air Force Base, Ohio, August 1967.

10. Islinger, J. S., Investigation to Determine Criteria for Designing Aircraft Nose Gear Steering Systems, Technical Report WADC-TR-55-34, Wright-Patterson Air Force Base, Ohio, November 1955.
11. Schwanghart, H., "Lateral Forces on Steered Tires in Loose Soil," Journal of Terramechanics, 5/1:9-29 (1968).
12. Taylor, P.A. and Bertwistle, R., "Experimental Studies of Force Systems on Steered Agricultural Tires," Institution of Mechanical Engineers, (London) Automobile Division Proceedings, 181/4:133-148 (1966-1967).
13. Kraft, D.C., "Turned Tire Test Program (AEWES) - Test Report," School of Engineering, University of Dayton, October 1973.
14. Kraft, D.C., and Kahle, D.A., "Preliminary - Turned Tire Test Program Part II - Test Effort," UDRI-TR-73-27, June 1973.
15. Phillips, N.S., Luming, H., Kraft, D.C., "A Digital Program for Calculating Aircraft Turning Response on Cohesive Soil Surfaces," School of Engineering, University of Dayton, May 1974.
16. Hancock, K.G. and Person, P., "Power Steering for Aircraft," Journal Royal Aeronautical Society, July 1952.
17. "A Special Training Program on Landing Gear/Soil Interaction and Flotation System Design," Training Session No. 1, Part II, School of Engineering, University of Dayton, September 1974.
18. Phillips, N.S., "Multipass Tire Test Program (AEWES) - Test Report," School of Engineering, University of Dayton, April 1975.
19. Samson, T.J. and Petersen, H.E., "Mimic Programming Manual," SEG-TR-67-31, July 1967.
20. Kraft, D.C., et al., Design Procedure for Establishing Aircraft Capability to Operate on Soil Surfaces, AFFDL-TR-72-129, December 1972.